

NASA Contractor Report 4021

(NASA-CR-4021) COMPUTATION OF
MULTI-DIMENSIONAL VISCOUS SUPERSONIC FLOW
Final Contractor Report (Scientific Research
Associates, Inc.) 194 p

N87-13406

CSCL 01A

Unclass

H1/02 43671

Computation of Multi-Dimensional Viscous Supersonic Flow

**R. C. Buggeln, Y. N. Kim,
and H. McDonald**

**CONTRACT NAS3-22027
OCTOBER 1986**



NASA Contractor Report 4021

Computation of Multi-Dimensional Viscous Supersonic Flow

**R. C. Buggeln, Y. N. Kim,
and H. McDonald**

*Scientific Research Associates, Inc.
Glastonbury, Connecticut*

Prepared for
Lewis Research Center
under Contract NAS3-22027



National Aeronautics
and Space Administration

**Scientific and Technical
Information Branch**

1986

TABLE OF CONTENTS

	Page
SUMMARY	1
INTRODUCTION	2
LIST OF SYMBOLS	8
ANALYSIS	11
SOLUTION OF THE GOVERNING EQUATIONS	24
TEST CASES	27
DISCUSSION AND CONCLUSIONS	45
USER'S MANUAL	46
REFERENCES	91
FIGURES	94
TABLES	150

PRECEDING PAGE BLANK NOT FILMED

SUMMARY

A method has been developed for two- and three-dimensional computations of viscous supersonic jet flows interacting with an external flow. The approach employs a reduced form of the Navier-Stokes equations which allows solution as an initial-boundary value problem in space, using an efficient noniterative forward marching algorithm. Numerical instability associated with forward marching algorithms for flows with embedded subsonic regions is avoided by approximation of the reduced form of the Navier-Stokes equations in the subsonic regions of the boundary layers. Supersonic and subsonic portions of the flow field are simultaneously calculated by a consistently split linearized block implicit computational algorithm. The results of computations for a series of test cases associated with supersonic jet flow is presented and compared with other calculations for axisymmetric cases. Demonstration calculations indicate that the computational technique has great promise as a tool for calculating a wide range of supersonic flow problems including jet flow. Finally, a User's Manual is presented for the computer code used to perform the calculations.

I. INTRODUCTION

During the past two decades much effort has been expended in developing numerical procedures which can be used as alternatives to solving the full Navier-Stokes equations for certain classes of problems (Ref. 1). These procedures treat a reduced form of the steady state Navier-Stokes equations, often referred to as the 'parabolized Navier-Stokes equations,' as an initial boundary value problem that can be solved by spatial forward marching. The ability to obtain a solution by forward marching the governing equations from an initial streamwise location to some desired downstream location rather than perform a global solution of the governing equations, as is required for the solution of the full Navier-Stokes equations, results in a considerable savings of computational time. Although the amount of savings will depend on the problem considered, the efficiency of the solution procedures and numerous other variables, this savings is the primary motivation for the development of these marching procedures.

To devise a set of governing equations suitable for the spatial forward marching of supersonic flows, three steps must be taken. First, a nominal primary flow direction must be identified. Second, a coordinate system must be constructed with one of its coordinate directions closely aligned with the primary flow direction. Third, all diffusion in the primary flow direction must be neglected. These steps when applied to the steady Navier-Stokes equations produce a set of governing equations which is well posed for the spatial forward marching of supersonic flows (e.g. Ref. 2). The introduction of no slip surfaces into a supersonic flow results in the formation of embedded subsonic regions adjacent to these surfaces. When the set of reduced equations, without further approximation, is forward marched with embedded subsonic regions the governing equations are not well posed and hence the solution procedure may become unstable. Even when the flow in this embedded subsonic region is approximated further and governed by what are essentially the boundary layer equations, an instability can still be encountered. This particular instability, which is often referred to as the branching phenomenon, has been the subject of much research (e.g. Refs. 3-8) and the technique used to suppress this instability is a convenient way to

differentiate between procedures for solving the reduced form of the Navier-Stokes equations for supersonic flow with embedded subsonic regions. In one of the earliest works in this area Garvine (Ref. 3) demonstrated (for a model problem) the existence of exponentially growing (divergent) terms in the spatial development of a solution of a reduced form of the Navier-Stokes equations when applied to the problem of an inviscid supersonic flow interacting with a viscous boundary layer. The author concluded that for this problem the reduced form of the Navier-Stokes equations was improperly set as an initial value problem, because the interaction dynamics contained upstream "elliptic" influence. In the model problem, if the upstream conditions are not precisely set as to cause the divergent terms to be multiplied by zero, the exponentially growing terms will cause the streamwise pressure gradient terms to grow exponentially large resulting in unrestrained acceleration or deceleration of the flow. In general it is not possible to pick the upstream conditions to negate the exponentially growing modes, hence several investigators have attempted to suppress the unstable (or branching) behavior by further modification of the reduced form of the Navier-Stokes equations for supersonic flows with embedded subsonic regions.

Much of the early work on the solution of the reduced form of the Navier-Stokes equations is based on the work of Rudman and Rubin (Ref. 4). Rudman and Rubin solved the equations for the hypersonic flow over slender bodies with sharp leading edges. Based on a order of magnitude analysis they demonstrated that for this class of problems the streamwise pressure gradient term was negligible when compared with the inertia and viscous terms of the streamwise momentum equation. Neglecting the streamwise pressure gradient term together with all streamwise diffusion results in a reduced form of the Navier-Stokes equations that is well posed for spatial forward marching even with embedded subsonic regions and branching was not observed in their calculations. Although this approach does yield a set of equations that is well posed for spatial forward marching, the assumption of negligible streamwise pressure gradient limits the class of flows which can be considered. In a later work Lubard and Helliwell (Ref. 5) proposed a method for preventing branching that involved explicit spatially lagged evaluation of the streamwise pressure gradient term. When marching from the i^{th} to the $i+1^{\text{st}}$ streamwise station all streamwise terms (See Fig. 1), except the streamwise pressure gradient, are evaluated by a backward difference. The

streamwise pressure gradient term is approximated by differencing the streamwise pressure gradient at prior known spatial locations, i.e. at the $i-1^{\text{st}}$ and i^{th} station (hence the terminology explicit evaluation). The above authors found that in addition to the frequently encountered problem of instability associated with exceeding some marching direction step size, a further instability is encountered when the step size is reduced below some limit. By examining the eigenvalues of a model set of equations (Ref. 9) they were able to develop a criterion for this minimum step size. (Numerical experimentation with their computer code demonstrated reasonable correlation with their criterion). Numerous flow fields have been successfully predicted using this method (mainly for cone flow) by the authors of Ref. 5 and others (Refs. 10-12), and in these cases evidently the restriction on the minimum marching step size was not a problem in allowing sufficiently accurate results to be obtained. However, the restriction on minimum marching step size is, in principle, not a desirable feature, since it does prevent arbitrary mesh refinement, and thereby the assurance that an accurate unique solution has been obtained. In at least one case (Ref. 9) this minimum step size restriction prevented the authors from successfully obtaining a solution. In a later technique developed by Rakich, Vigneron, and Agarwal (Ref. 6) a variant of the technique of Lubard and Helliwell was used to prevent branching. In this particular variant the streamwise pressure gradient term is approximated by an implicit backward difference in the supersonic portion of the flow. However, in the subsonic region only that portion of the streamwise pressure gradient term that can be included without causing branching is evaluated implicitly. The results of a stability analysis similar to that of Ref. 9 also produces a restriction on the minimum allowable step size. When that portion of the subsonic pressure gradient which could not be evaluated implicitly is evaluated explicitly by a lagged technique similar to Lubard and Helliwell, Rakich et al noted that the scheme became unstable. Thus, in order to achieve stability this technique neglected the explicit portion of the streamwise pressure gradient term in the subsonic region, and implicitly took into account only that portion of the term that can be stably computed. Schiff and Steger (Ref. 7) treat the subsonic streamwise pressure

gradient term by what the authors term either a first- or second-order streamwise extrapolation technique in the subsonic regions. The first order technique is equivalent to setting the streamwise pressure gradient term equal to zero in the subsonic region while the second order technique is equivalent to the explicit evaluation of the streamwise pressure term (as was done by Lubard and Helliwell). As with the two previously discussed techniques, these authors also report a restriction on the minimum marching step size that they may take and still retain a stable calculation. Lin and Rubin (Ref. 8) have developed a global relaxation procedure for solving the reduced form of the Navier-Stokes equations. This technique was primarily developed for application to cases where upstream influence is strong. To obtain the upstream influence with the reduced form of the Navier-Stokes equations requires a global iteration or relaxation procedure. The above authors do this by approximating the streamwise pressure gradient term by a forward difference. When marching the solution from the i^{th} to the $i+1^{\text{st}}$ station the pressure gradient term is evaluated in terms of the pressure at the $i+1^{\text{st}}$ and $i+2^{\text{nd}}$ station (the $i+1^{\text{st}}$ station is the implicit station; all other streamwise derivatives are backward differenced between $i+1$ and i). Initially the (unknown) pressure at the $i+2^{\text{nd}}$ station is guessed; during subsequent global iterations the previously calculated value is used. Global iteration of the governing equations is continued until the solution converges. Lin and Rubin report that convergence is typically obtained in five to ten iterations for cases with small streamwise pressure gradients (cases run to date have been limited to flow over cones). The authors also report that there is no minimum marching step size requirement with their approach.

The purpose of the present investigation is to develop an efficient numerical procedure for the solution of the two and three-dimensional reduced form of the Navier-Stokes equations for high Reynolds number internal flow. The study is limited to cases where the incoming flow is supersonic and the flow inside the internal flow device is, in the mean, supersonic. The existence of embedded subsonic regions adjacent to the surfaces of the internal flow devices is to be accounted for as part of the analysis. Because of the complexity of the physical processes occurring in internal flow devices and, especially in three dimensions, the large number of grid

points required (and hence computer time) to accurately resolve these processes, it was decided that a technique that solves the full Navier-Stokes equations would be used only if no suitable alternative could be found.

The physics of supersonic internal flow devices is characterized by the formation of shock waves, the growth of boundary layers, and the interaction of these phenomena. Many of the above internal flow phenomena are turbulent and have associated with them large streamwise pressure gradients, e.g., a high Reynolds number incident shock wave-boundary layer interaction. It is to be expected that in regions of such an interaction one would desire to take a small streamwise marching step to accurately resolve the phenomenon. In particular, it might prove necessary to resolve the turbulent boundary layer viscous sublayer (large cross flows can occur in this region) and take marching steps of this order. Reviewing the existing methods for Refs. 4-8 causes one to be concerned that techniques having such a minimum step size might not permit sufficient resolution of the large gradients expected. The method of Rudman and Rubin presumes that the streamwise pressure gradient is small in comparison with the inertia and viscous terms. For the cases they considered this is a valid assumption. This is not the case for a shock wave-boundary layer interaction in moderately supersonic flow. The methods of Refs. 5-7 all make an attempt to consider the effect of the streamwise pressure gradient in the embedded subsonic regions. However, they give only an approximate treatment to this possibly dominant term and all of those methods have a minimum marching step size limitation which, in many cases of interest in this study, may not either allow for an accurate or in some cases even a minimally acceptable solution. Subsequently, it will be demonstrated that for a case with a large streamwise pressure gradient the minimum step size size limitation of the order of magnitude found in Ref. 9 was insufficient to accurately resolve the phenomenon. Here we seek a noniterative approach with a consequent reduction in computer cost relative to either the global iteration approach to solving the reduced form of the Navier-Stokes equations or solution of the full Navier-Stokes equation. Further as a prerequisite, we require that there exist no numerical limitation on the minimum marching step and it is desired to keep to a minimum any approximation to the streamwise pressure gradient term.

In view of the above, it was decided to develop a numerical procedure for the solution of the reduced form of the Navier-Stokes equations, with special emphasis to be placed upon application to internal flow devices. The remainder of this report will describe that effort. It will consist of (1) a discussion of the analysis used in the study, (2) a discussion of the solution of the governing equations, (3) the results of a series of test cases run to demonstrate the applicability of the analysis and to exercise and to validate the resulting computer code and (4) a user's manual for the computer code, termed PEPSIS.

LIST OF SYMBOLS

A	Square Matrix of coefficients
B	Constant of proportionality
C	Constant of proportionality
C_H	Nondimensional heat transfer coefficient
C_p	Specific heat
D	Column vector whose elements are spatial differential operators
D:D	Second invariant of the mean flow rate of deformation tensor
H	Column vector associated with marching direction terms
J	Jacobian
L	Linear differential operator
M	Mach number
P	Static pressure
Pr	Prandtl number
Re	Reynolds number
S	Source term, distance from the leading edge
T	Static temperature
U	Streamwise velocity component
V	Transverse velocity component
W	Spanwise velocity component
X	Distance from leading edge
\vec{v}	Velocity
\mathcal{D}	Damping coefficient
h	Metric coefficient, enthalpy
l_m	Mixing length

\hat{n}	Unit vector normal
q	Heat transfer
w	Velocity component
x	Coordinate direction
y	Distance from a surface
y^+	Nondimensional distance from a surface

GREEK SYMBOLS

α	Yaw angle
γ	Ratio of specific heats
δ_b	Boundary layer thickness
η	Blasius similarity parameter
κ	von Karman constant
μ	Viscosity
ρ	Density
τ	Viscous stress tensor
∇	Nabla operator
Δx	Marching direction step size

Subscripts

i	i^{th} direction
j	j^{th} direction
l	Laminar
n	Normal direction
w	Wall
R	Reduced
S	Sonic line

Subscripts (Continued)

T Turbuent, tangential direction
0 Stagnation condition
1 Streamwise direction
2 Cross plane direction
3 Cross plane direction
 ∞ Free stream condition

Superscripts

i i^{th} streamwise station
T Transpose

II. ANALYSIS

Governing Equations:

The fluid dynamic conservation laws of mass, momentum and energy respectively can be written in nondimensional operator form as

$$\nabla \cdot \rho \vec{V} = 0 \quad (1)$$

$$\nabla \cdot (\rho \vec{V} \vec{V}) + \nabla P - \frac{\nabla \cdot \tau}{Re} = 0 \quad (2)$$

and

$$\nabla \cdot (\rho h_0 \vec{V}) - \nabla \cdot \left[\frac{C_p}{Re} \left(\frac{\mu_L}{Pr_L} + \frac{\mu_T}{Pr_T} \right) \nabla T \right] - \nabla \cdot \frac{(\tau \cdot \vec{V})}{Re} = 0 \quad (3)$$

This form of the governing equations, often referred to as the full Navier-Stokes equations, requires several auxilliary relationships and models before these equations can be solved. In this study, the stagnation enthalpy, h_0 , is related to the static temperature, T , and the velocity, \vec{V} , through the relationship (assuming constant specific heat)

$$h_0 = C_p T + \frac{\vec{V} \cdot \vec{V}}{2} \quad (4)$$

while the temperature, T , pressure, P , and density, ρ , are related by means of the calorically perfect gas equation of state

$$P = \frac{\gamma-1}{\gamma} C_p \rho T \quad (5)$$

The stress tensor, τ , is modelled by the relationship

$$\tau = \mu (\nabla \vec{V} + \nabla \vec{V}^T) - \frac{2}{3} \mu \nabla \cdot \vec{V} \quad (6)$$

where the superscript T refers to the transpose of the tensor. The components of the velocity vector, \vec{V} , are interpreted as the mass weighted

mean velocity components and ρ , P and T are the ensemble-averaged density pressure and temperature (Ref. 13). Hence, these equations can be applied to both laminar and turbulent flows if the effective viscosity, μ , is interpreted as the sum of the laminar and turbulent, μ_t , viscosities, i.e.,

$$\mu = \mu_l + \mu_t \quad (7)$$

It is assumed that the laminar viscosity can be computed from Sutherland's law, and that the laminar and turbulent Prandtl numbers, Pr_l and Pr_t are constant. For this study, an algebraic mixing length turbulence model of the form

$$\mu_t = Re \rho l_m^2 \sqrt{D:D} \quad (8)$$

was used where l_m is the algebraic mixing length and $D:D$ is the second invariant of the mean flow rate of deformation tensor (Ref. 14). In this study, the mixing length of McDonald and Camarata (Ref. 15) was used.

$$l_m = 0.09 \delta_b \tanh[\kappa \tilde{y}/(0.09 \delta_b)] D \quad (9)$$

Where δ_b is the local boundary layer thickness, κ is the von Karman constant, \tilde{y} is the distance to the nearest wall, and D is the sublayer damping term of van Driest (Ref. 16).

To obtain what is often referred to as the reduced form or the 'parabolized' form of the Navier-Stokes equations involves approximation of the diffusion terms (both stress and Fourier heat conduction) of Eqs. (2), (3) and (6). This approximation neglects all derivatives of the stress tensor and the Fourier heat conduction terms in a selected 'marching' or 'streamwise' direction. In addition, all streamwise derivatives of the velocity components of the stress tensor are neglected. For example, in a general orthogonal coordinate system the principle and shear stress components can be expressed respectively as

$$\tau_{ii} = 2\mu \left(\frac{1}{h_i} \frac{\partial w_i}{\partial x_i} + \sum_{j=1}^3 \frac{w_j}{h_i h_j} \frac{\partial h_i}{\partial x_j} \right) - \frac{2}{3} \frac{\mu}{J} \sum_{j=1}^3 \frac{\partial}{\partial x_j} \left(\frac{J}{h_j} w_j \right) \quad (10)$$

and

$$\tau_{ij} = \mu \left[\frac{h_j}{h_i} \frac{\partial}{\partial x_j} \left(\frac{w_i}{h_j} \right) + \frac{h_i}{h_j} \frac{\partial}{\partial x_j} \left(\frac{w_i}{h_i} \right) \right] \quad (11)$$

where

$$J = h_1 h_2 h_3 \quad (12)$$

1 refers to the streamwise direction and 2 and 3 refer to the cross plane directions, w_i refers to the velocity component in the i^{th} direction and h_i refers to the metric in the i^{th} direction. The approximation neglects all direction 1 derivatives of velocity components in Eqs (10) and (11). Thus, for example, τ_{11} and τ_{13} are approximated by

$$\tau_{11} \cong 2\mu \left(\frac{w_2}{h_1 h_2} \frac{\partial h_1}{\partial x_2} + \frac{w_3}{h_3 h_1} \frac{\partial h_1}{\partial x_3} \right) - \frac{2}{3} \frac{\mu}{J} \left[\frac{\partial}{\partial x_2} \left(\frac{J}{h_2} w_2 \right) + \frac{\partial}{\partial x_3} \left(\frac{J}{h_3} w_3 \right) \right] \quad (13)$$

and

$$\tau_{13} \cong \mu \frac{h_1}{h_3} \frac{\partial}{\partial x_3} \left(\frac{w_1}{h_1} \right) \quad (14)$$

Application of the approximations needed to obtain the reduced form of the Navier-Stokes equations in other coordinate systems is straightforward. Hence, in general, the reduced forms of Eqs. (2) and (3) can be recast as

$$\nabla \cdot (\rho \vec{V} \vec{V}) + \nabla P - \frac{(\nabla \cdot \tau)}{Re} R = 0 \quad (15)$$

and

$$\nabla \cdot (\rho h_0 \vec{V}) - \left\{ \nabla \cdot \left[\frac{C_p}{Re} \left(\frac{\mu_L}{Pr_L} + \frac{\mu_T}{Pr_T} \right) \nabla T \right] \right\}_R - \left[\nabla \cdot \left(\frac{\tau \cdot \vec{V}}{Re} \right) \right]_R = 0 \quad (16)$$

where the subscript R refers to the approximated or reduced form of the noted term.

The reduced form of the Navier-Stokes equations, Eqs. (1), (15) and (16) is the starting point for the discussion of the governing equations to be used for this study. The intent is to demonstrate that this set of equations is not well posed for solution by spatial forward marching when applied to the class of problems considered in this study, i.e., supersonic flow with embedded subsonic boundary layer regions. Although it does not appear that a rigorous analysis has been obtained for the compressible reduced form of the Navier-Stokes equations, model sets of equations have been investigated and the results can be used to give indications of the nature of the compressible reduced form of the Navier-Stokes equations. The Euler equations for compressible flow are one such relevant model system and are of interest here since it is desired to have a stable integration scheme for this system which we can reasonably expect to encounter in those high Reynolds number essentially inviscid regions of the flows considered. It is well known that all characteristics of the Euler equations are real for supersonic flow, and thus it is inferred that these equations are well posed for solution by spatial forward marching (e.g., Ref. 2). Apparently, the supersonic reduced form of the Navier-Stokes equations are also well posed for solution by spatial forward marching because entirely supersonic flow solutions have been obtained using marching techniques (e.g. Ref. 2). In view of the presence of imaginary characteristics associated with subsonic flows, it is inferred that both the compressible Euler equations (Ref. 17) and the incompressible reduced Navier-Stokes equations are unsuitable for solution by spatial forward marching (Ref. 18). The fact that these two sets of equations are ill posed as initial value problems leads one to suspect that the reduced Navier-Stokes equations for mixed supersonic-subsonic flows are also not well posed for solution by spatial forward marching. Examination of the characteristics analysis for the incompressible reduced Navier-Stokes equations shows that the imaginary roots can be affected by the streamwise pressure gradient term (Ref. 6). If this streamwise pressure gradient term is either a priori specified or neglected, the characteristic equations yield only real roots for subsonic flows. Thus, to create a well posed set of governing equations suitable for solution by spatial forward marching, much effort has concentrated on approximation or modification of this term in the reduced form of the Navier-Stokes equations. Efforts to create new sets of equations which may be solved by spatial marching which either approximate

the reduced Navier-Stokes equations or permit stable iterations which, upon convergence, represent numerical solutions of the reduced Navier-Stokes equations are reported in Refs. 4-8. In view of the present interest in flows with strong pressure gradients, equation systems which contain approximations to the pressure gradient, in particular the streamwise pressure gradient, are viewed with concern. Equation systems which require global iteration, i.e. repeated streamwise sweeps through the entire flow, yet treat the pressure gradient terms without approximation upon convergence, are of course much more preferable for this class of problems. The present desire is to make few approximations to the pressure gradient terms yet achieve the computational efficiency of a noniterative forward marching algorithm.

A second set of model equations was investigated by Garvine (Ref. 3). In this case, the reduced form of the Navier-Stokes equations is approximated by the spatially hyperbolic Euler equations in the inviscid region, and the spatially parabolic boundary layer equations in the viscous region. The behavior of the solution of this combined set of equations, both of which are separately well posed for solution by spatial forward marching in their given flow regimes, was shown to be unstable because of the existence of an exponentially diverging term in the solution. The unstable behavior was caused by the interaction process at the boundary between the two sets of equations. A physical interpretation of the unstable interaction process can be given for the case of an adverse pressure gradient from a supersonic region being impressed on a subsonic region (e.g. a shock wave-boundary layer interaction). The adverse pressure gradient causes the subsonic layer to increase in thickness. The growing subsonic layer in turn causes the supersonic flow to be displaced causing a further increase in the magnitude of the adverse pressure gradient. This process is obviously unstable as there is no restraining mechanism present at the boundary between the subsonic and supersonic regions. The cause of this phenomenon, which is sometimes referred to as a departure or branching behavior, has been encountered in numerous studies of supersonic interacting boundary layers. Note that branching is an entirely different phenomenon than the growing modes which cause the subsonic reduced Navier-Stokes equations to be ill posed for solution by spatial forward marching. The subsonic reduced Navier-Stokes equations possess imaginary characteristics and consequently

are ill posed for forward marching, while the two sets of equations analyzed by Garvine are individually well posed for forward marching. Rather, it is the interaction at the boundary between two sets of equations that causes their growing modes.

The approach taken in this investigation is to find further approximations which when utilized within the reduced form of the Navier-Stokes equations will produce a set of governing equations which are well posed for solution by spatial forward marching. It is realized that such further approximations to the Navier-Stokes equations will almost certainly introduce further limitations on the domain of accurate physical representation of the flow. However, it is believed that approximations can be made that will leave the essential physical process of interest intact for a wide range of practical cases. It is further believed, that the increase in computational efficiency which will result from using a noniterative spatial forward marching technique, when compared to current (iterative) techniques for solving the full Navier-Stokes equations, justifies the use of the approximations.

The previous discussion of the character of the reduced form of the Navier-Stokes equations in mixed supersonic-subsonic flow gives little guidance for the choice of further modifications or approximations that will yield a set of well posed governing equations. However, three important points were made in that discussion: (1) numerical experience indicates that the compressible reduced equations are well posed for solution by spatial forward marching if the flow is entirely supersonic, (2) the reduced equations are known to be ill posed for solution by spatial forward marching if the flow is subsonic and (3) the use of different sets of governing equations in the supersonic and subsonic flow regions may still be ill posed for solution by spatial forward marching even though each set of equations is by itself well posed in the region in which it is applied. The problem here arises because of the unstable interaction occurring at the boundary between the regions.

In this investigation, the strategy taken is to divide the flow into supersonic and subsonic flow regions and to utilize different approximations, resulting in different sets of governing equations, in each region. This aspect of the approach is not unlike that utilized by other investigators (Refs. 5-12), however, the approximations used in obtaining the governing

equations in the subsonic region are different than those previously used, and hence the interaction of the two sets of equations at the subsonic-supersonic boundary is also different. In this study, the technique is to utilize the reduced form of the Navier-Stokes equations in the supersonic region(s) of the flow, Eqs. (1), (15) and (16), and what can be considered to be a model set of equations in the subsonic region(s) of the flow. The model set of equations used in the subsonic region(s) is obtained by starting with the reduced form of the Navier-Stokes equations and making appropriate physical approximations in this region to obtain a new set of governing equations such that the coupled system of the inner subsonic flow and the outer supersonic flow are stable when solved as an initial value problem in space.

For the problems of interest in this study, high Reynolds number supersonic flow with embedded subsonic regions in internal flow devices, the boundary layer thickness, δ , will in many cases be small with respect to a characteristic vertical dimension of the device. In this investigation, the less restrictive assumption is made that the thickness of the subsonic portion of the boundary layer is small with respect to the vertical dimension. In this subsonic portion of the boundary layer, the usual boundary layer approximations for high Reynolds number flow are certainly valid. (Note, for instance, that at $M = 2$ a turbulent flat plate boundary layer is supersonic within the viscous sublayer which typically has a nondimensional y^+ value on the order of 10. Thus, except at very low Reynolds numbers, the sonic point is at least one order of magnitude or more smaller than the boundary layer thickness). As a result, an order of magnitude analysis of the terms in the reduced form of the Navier-Stokes equations allows the convection and the diffusion terms to be neglected in the subsonic normal (to the wall) momentum equation. This equation can then be expressed as a balance between the normal pressure gradient and the centrifugal (curvature) forces, $\partial p / \partial n = U^2 / R$, in 2-D streamline coordinates, where R the streamline radius of curvature, U the streamwise velocity and n the normal to the streamline. In general orthogonal coordinates, X_1 , X_2 and X_3 with corresponding metric coefficients h_1 , h_2 and h_3 and velocity components w_1 , w_2 and w_3 this equation is expressed as

$$\frac{\partial P}{\partial x_n} = (-l)^T \frac{w_T}{h_T} \left(w_3 \frac{\partial h_3}{\partial x_l} - w_n \frac{\partial h_n}{\partial x_3} \right) + (-l)^n \frac{w_l}{h_l} \left(w_l \frac{\partial h_l}{\partial x_n} - w_n \frac{\partial h_n}{\partial x_l} \right) \quad (17)$$

where X_n and X_t respectively refer to the appropriate cross-sectional direction normal to and tangential to wall (n and t have values of 2 or 3; direction l is the nominally streamwise direction). It is further possible to integrate the continuity equation from the wall to an arbitrary point in the subsonic portion of the boundary. This yields in general orthogonal coordinates.

$$h_l h_T \rho w_n \Big|_s = - \int_0^{x_s} \left[\frac{\partial}{\partial x_l} (h_2 h_3 \rho w_l) + \frac{\partial}{\partial x_T} (h_l h_n \rho w_T) \right] dx_n + h_l h_T \rho w \Big|_w \quad (18)$$

where again the subscripts n and T refers to the cross flow direction normal and tangential to the wall, s refers to the evaluation at the arbitrary point in the subsonic region and the subscript w refers to the evaluation at the wall. For the class of high Reynolds number flows considered, the boundary layer thickness is assumed to be small and as noted earlier the subsonic portion of the supersonic turbulent boundary layer, X_s , is usually at least an order of magnitude smaller than the boundary layer thickness. Restricting our attention to flows where the subsonic region is sufficiently small allows the integral in Eq. (18) to be neglected and hence this equation can be approximated by

$$h_l h_T \rho w_n \Big|_s = h_l h_T \rho w_n \Big|_w \quad (19)$$

For the case of an impermeable wall Eq. (19) further reduces to

$$w_n \Big|_s = 0 \quad (20)$$

In summary then, Eqs. (17) and (18), the streamwise and tangential components of the vector Eq. (15), and Eq. (16), the energy equation, constitute the

model set of governing equations utilized in the embedded subsonic regions. In two-dimensional and axisymmetric flows the terms normal and tangential directions to the wall are unambiguous and are defined as the X_2 - and X_3 -directions respectively. For the case where the cross plane is nonaxisymmetric (e.g. a rectangular cross section) ambiguity is avoided by referring to the normal and tangential direction relative to the nearest wall in the subsonic region of the flow. Far from the corners little concern arises from use of the nearest wall approach. The corner region is treated by defining a corner bisector in the subsonic regions and thus allowing the definitions of normal and tangential to change when crossing this line.

There are several important features of the subsonic model set of governing equations. First, no approximation was made to the streamwise pressure gradient term (or any other term in the streamwise momentum equation). Hence, the full effect of this term will be felt in the subsonic portions of the flow. In addition, the reduced form of the tangential momentum equation (i.e. the tangential component of Eq. (15)) is unmodified in the subsonic region. This allows the effect of the tangential pressure gradient to be felt in the subsonic regions as, for instance, would physically occur in the case of a glancing shock wave-boundary layer interaction. The assumption needed to modify the normal momentum and continuity equations in the subsonic regions is the relatively unrestrictive condition that the subsonic layer is thin relative to the characteristic transverse dimension of the flow device. For the case of an impermeable wall, this leads to the condition that within the viscous subsonic layer the normal velocity component is negligible, Eq. (20). Since the boundary layer approximation already assumes that the normal velocity is small, this condition can be considered to be a further approximation, to be applied only in the thin subsonic portion of the boundary layer. The importance of the specification of the normal velocity is that a mechanism has now been established to prevent the growing mode caused by the interaction between the subsonic and supersonic layers, i.e., the branching phenomenon. In summary, the new set of governing equations consisting of the reduced form of the Navier-Stokes equations in the supersonic portion of the flow and the model set of equations in the subsonic regions of the flow has, on the basis of numerical experimentation (to be

presented herein) been found to be well posed for solution by spatial forward marching for a wide range of practical problems.

Initial and Boundary Conditions:

To uniquely define the problem of interest, it is necessary to specify both initial and boundary conditions. For a spatial forward marching procedure, the initial conditions refer to the set of conditiions that must be specified at the initial marching station. Boundary conditions must be set on the boundaries of the cross-sectional marching plane. For the calcualtion of internal flows, two types of initial conditions were utilized in this study. The first, which is primarily used for flows into devices which have sharp leading edges, sets the initial conditions as the free stream conditions. Analysis of the characteristics of the supersonic Euler equations shows that there are five characteristics entering the upstream boundary of the computational domain. Hence, five conditions must be set on this boundary. In this study those conditions are chosen as the three velocity components, the pressure and the temperature. Usually, but not necessarily, the conditions are chosen to be uniform everywhere in the initial plane. The second type of initial condition is primarily used for cases where information exists at an initial plane such that a reasonable approximation to a complete set of initial data can be constructed. In its most pure form, this would be an initial plane where experimental data were available such that all the initial conditions were known. Usually a limited amount of information is available where, for instance, free stream conditions, a boundary layer thickness, and a skin friction coefficient might be known. In this case a theoretical boundary layer profile of the pertinent variables (velocity components, temperature, pressure, etc.) can often be derived and matched with the free stream portion of the flow. It is to be emphasized that the initial conditions must in some sense be consistent with the governing equations. In supersonic flow computations inconsistencies, perturbations, etc. can persist far downstream.

As used in this investigation, the boundary conditions utilized on the bondaries of the cross-sectional plane can be divided into three categories: (1) wall conditions, (2) symmetry conditions and (3) external flow conditions. Analysis of the charcteristics of the boundary layer equations shows that four conditions must be specified on walls. For this study, the no-slip

conditions are used for the streamwise and tangential cross plane velocity components, i.e.,

$$w_l = 0 \quad (21)$$

and

$$w_T = 0 \quad (22)$$

where again the subscript l refers to the streamwise direction and the subscript T refers to the cross plane tangential velocity direction. For the cross plane normal velocity component either the normal velocity or the normal mass flux are specified, i.e.,

$$w_n = w_w \quad (23)$$

$$\rho w_n = \rho_n w_n \quad (24)$$

where the subscript w refers to the specified wall value. The fourth condition used, the thermal condition, is either to specify an adiabatic wall or to specify the wall temperature (a cold or hot wall). The conditions can be specified respectively as

$$\vec{n}_w \cdot \nabla T = 0 \quad (25)$$

or

$$T = T_w \quad (26)$$

where in this case \vec{n}_w^+ represents the unit vector normal to the wall. In addition, a fifth condition, not required by the characteristic analysis, is used for convenience to close the set of equations. The need for this fifth condition could be removed by the use of one-sided differencing or by applying one of the governing equations at the wall. In this study, the second method was used and the boundary layer approximation to the normal momentum equation was applied at the wall. This can be expressed as

$$\vec{n}_w \cdot \nabla P = 0 \quad (27)$$

Studies have indicated that there is little difference between using this equation and the full normal momentum equation (e.g. Ref. 19).

The symmetry conditions are meant to be applied on a plane or axis of symmetry. The velocity conditions require that the cross plane velocity velocity conditions require that the cross plane velocity component normal to the axis or plane of symmetry equals zero, i.e.,

$$\vec{n}_s \cdot \vec{V} = 0 \quad (28)$$

where \vec{n}_s is the unit vector normal to the axis or plane of symmetry and that the first derivatives of the remaining two velocity components equal zero. Two other conditions must be set on the axis or plane of symmetry. Usually the symmetry conditions on pressure and temperature are used, viz.

$$\vec{n}_s \cdot \nabla P = 0 \quad (29)$$

and

$$\vec{n}_s \cdot \nabla T = 0 \quad (30)$$

The final category of boundary conditions used in this investigation are those on external surfaces, specifically on the boundary upstream of the cowl surface of a supersonic inlet (Fig. 2). In this case a shock wave is generated by the ramp and passes out of the computational domain upstream of the cowl lip. Upstream of the point where the shock wave passes out of the computational domain, the free stream conditions are appropriate as boundary conditions and downstream of this point the post shock (Rankine-Hugoniot) relationships are valid. Two techniques are commonly used to define shock waves, shock fitting and shock capturing. The shock fitting technique recognizes the failure of Taylor series expansion through the discontinuity so first locates the position of the shock wave, and then enforces the Rankine-Hugoniot conditions across the wave. This can occur either on the boundary or an interior portion of the computational domain. This technique has been used in Ref. 5 to locate the bow shock for external flow cases. For internal flow cases, the shock structure can in many cases become very complex, and attenuated following the 'boundary layer' interactions. Thus, the logic needed to locate the shock waves (especially in three dimensions) can become very complex. In addition, in the case of shock

wave-boundary layer interactions, the shock wave at some point in the interaction process ceases being a shock wave and in this region the shock fitting procedure becomes very unclear. The shock capturing technique used in this study allows the shock waves to be formed as a consequence of the solution of the governing equations. Although the presence of the shock wave violates the Taylor series representation of the solution used to construct the numerical derivatives, it is very convenient. Its use in the present study is only justified *a posteriori* by virtue of the adequacy of the results for the problems considered. Returning to the boundary condition upstream of the cowl, the approach taken here is to find a set of boundary conditions that can be applied on this interior flow 'boundary' that will permit the exterior region to be neglected yet that will allow all disturbances which originate from within the computational domain to pass through this boundary without spurious reflection. The technique used in this investigation is predicted on the concept that in a simple wave region the flow properties remain constant along Mach lines (the presumption here is that the regions fore and aft of the shock wave are simple wave regions). Thus, the first derivatives of the flow variables in the direction of the Mach angle should be small and are here set equal to zero. The technique is termed Mach wave extrapolation and yields the boundary conditions

$$\vec{n}_m \cdot \nabla \vec{V} = 0 \quad (31)$$

$$\vec{n}_m \cdot \nabla P = 0 \quad (32)$$

and

$$\vec{n}_m \cdot \nabla T = 0 \quad (33)$$

where \vec{n}_m is the unit vector in the direction of the local Mach angle. This technique requires computation of the Mach angle, and has been successfully applied to a number of test cases both by the present authors and the authors of Refs. 20 and 21. The boundary conditions allow the flow upstream of the shock wave to remain undisturbed, and permit the shock wave to pass out of the computational domain without reflection. The resulting 'free stream' flow behind the shock very closely approximates the appropriate theoretical post shock values.

III. SOLUTION OF THE GOVERNING EQUATIONS

The governing equations in both the supersonic and the embedded subsonic portions of the flow are simultaneously solved by the consistently split linearized block implicit (LBI) technique described in detail in Refs. 2 and 20. This technique can be logically divided into three parts:

(1) linearization of the governing equations, (2) discretization of the resulting set of linearized equations by finite difference approximation of derivative terms and (3) simultaneous solution of the resultant set of linear coupled algebraic equations. Application of the LBI technique to a set of governing equations (and boundary conditions) that is well posed for forward marching is straightforward. It is presumed that a solution is known at some arbitrary i^{th} streamwise station and it is desired to march that solution to the $i + 1^{\text{st}}$ station, at some distance Δx apart (See Fig. 1). Using notation similar to that of Ref. 20 at a single grid point, the system of governing equations can be written in the following form:

$$\frac{\partial H(\phi)}{\partial x} = D(\phi) + S(\phi) \quad (34)$$

where ϕ is the column vector of dependent variables (w_1, w_2, w_3, ρ, h_0), H and S are column vector algebraic functions of ϕ , and D is a column vector whose elements are the spatial differential operators which generate all spatial derivatives appearing in the governing equation associated with that element.

The solution procedure is based on the following implicit marching direction difference approximations of Eq. (34)

$$\frac{H^{i+1} - H^i}{\Delta x} = D^{i+1} + S^{i+1} \quad (35)$$

where, for example, H^{i+1} denotes $H(\phi^{i+1})$. A local spatial linearization (Taylor series expansion about ϕ^i) of requisite formal accuracy is introduced, and this serves to define a linear differential operator L such that

$$D^{i+1} = D^i + L^n(\phi^{i+1} - \phi^i) + O(\Delta x^2) \quad (36)$$

Similarly,

$$H^{i+1} = H^i + \left(\frac{\partial H}{\partial \phi}\right)^i (\phi^{i+1} - \phi^i) + O(\Delta x^2) \quad (37)$$

$$S^{i+1} = S^i + \left(\frac{\partial S}{\partial \phi}\right)^i (\phi^{i+1} - \phi^i) + O(\Delta x^2) \quad (38)$$

Eqs. (36) through (38) are inserted into Eq. (35) to obtain the following system which is linear in ϕ^{i+1}

$$(A - \Delta x L^i)(\phi^{i+1} - \phi^i) = \Delta x (D^i + S^i) \quad (39)$$

and which is termed the linearized block implicit (LBI) scheme. Here A denotes a square matrix defined by

$$A = \left(\frac{\partial H}{\partial \phi}\right)^i - \Delta x \left(\frac{\partial S}{\partial \phi}\right)^i \quad (40)$$

Eq. (40) is $O(\Delta X)$ accuracy.

It is well known that the finite difference analogue of the governing equation system may have an associated stability restriction (Ref. 23). For simple equations, the stability criterion can often be analytically obtained, for instance using the Fourier technique of von Neumann (Ref. 23). For complex systems of equations (including boundary conditions) it is often impossible to derive a closed form criterion which can be easily interpreted. In this case, the stability bounds (if they exist) may be determined by numerical experimentation. For this investigation, second order central differences have been used throughout except for the streamwise derivatives (which are represented by first order backward differences although other choices are clearly permissible). These differences are used with the previously described linearized block implicit scheme and a numerical analogue of the governing equation system constructed. As far as can be determined by experimental investigation, there is no stability restriction associated with the resulting scheme. The tests used to substantiate these remarks will be discussed later.

To obtain an efficient algorithm, the linearized system, Eq. (39) is split using ADI techniques. To obtain the split scheme, the multidimensional operator, L, is rewritten as the sum of two 'one-dimensional' suboperators

L_i ($i = 2,3$) each of which contains all terms having derivatives with respect to the i^{th} -cross plane coordinate. The split form of Eq. (39) can be derived either as in Ref. 20 by following the procedure described by Douglas and Gunn (Ref. 24) in their generalization and unification of scalar ADI schemes, or using the approximate factorization as in Ref. 26. For the present system of equations, the split algorithm is given by

$$(A - \Delta x L_1^i)(\phi^* - \phi^i) = \Delta x (D^i + S^i) \quad (41)$$

$$(A - \Delta x L_2^i)(\phi^{i+1} - \phi^i) = A(\phi^* - \phi^i) \quad (42)$$

where ϕ^* is the consistent intermediate solution (Ref. 22). If spatial derivatives appearing in L_i and D are replaced by the difference formulae, as indicated previously, then each step in Eqs. (41) and (42) can be solved by a block tridiagonal elimination.

Combining Eqs. (41) and (42) gives

$$(A - \Delta x L_1^i) A^{-1} (A - \Delta x L_2^i)(\phi^{i+1} - \phi^i) = \Delta x (D^i + S^i) \quad (43)$$

which approximates the unsplit scheme, Eq. (39) to $O(\Delta x^2)$. Since the intermediate step is also a consistent approximation to Eq. (39), physical boundary conditions can be used for ϕ^* (Refs. 22, 26).

IV. TEST CASES

The preceding analysis was incorporated into a very general computer program with the acronym PEPSIS. To validate the ability of this computer program to accurately predict flows which are suited for solution by spatial forward marching, a series of test cases were run for which there existed either experimental data, an analytical solution or a numerical solution obtained by another computer program. Calculations were made for both two and three dimensional cases in cartesian, general orthogonal, axisymmetric and nonorthogonal coordinate systems. Both laminar and turbulent test cases were considered. In addition, options within the code were constructed to solve the conventional two dimensional boundary layer equations, and to solve the system proposed by Rudman and Rubin (Ref. 4) and Lubard and Hellwell (Ref. 5) so that results obtained from the present analysis (the reduced form of the Navier-Stokes equations) could be compared with other proposals and conventional boundary layer calculations. The boundary layer option solves the streamwise momentum equation (with specified streamwise pressure gradient) and the continuity and energy equations. The numerical solution procedure for all these options is the same, appropriately reduced to reflect the different sets of governing equations. The only significant numerical difference is that in the boundary layer option the continuity equation is solved by a trapezoidal integration technique to avoid the need to specify a vertical velocity condition at the outer boundary. The boundary conditions used in the boundary layer option were the no slip conditions and appropriate thermal condition at a wall and specified conditions at the outer boundary.

CASE I - Incompressible Laminar Flat Plate Boundary Layer

Initially a low Mach number virtually incompressible zero streamwise pressure gradient laminar flat plate case was run with the boundary layer analysis to determine how that version of the computer code would reproduce the Blasius solution. The case calculated was for a free stream Mach number of 0.1 and a Reynolds number per unit length of 10^5 per meter. The wall temperature was chosen as the adiabatic wall temperature. The computational

domain is as shown in Fig. 3. 100 grid points were nonuniformly distributed in the transverse direction with grid points concentrated in the region close to the wall. The initial boundary layer profile was generated from a Blasius solution at an axial location of $X/L = 2.0$ from the leading edge of the flat plate. (L was chosen to equal 1 meter). The initial boundary layer (point where $u/u_e = 0.999$) was contained within the first 65 grid points corresponding to a thickness of $\delta/L = 0.0267$. The initial displacement and momentum thickness Reynolds numbers were 297.0 and 771.7 respectively. The initial profile was marched downstream 500 steps to a streamwise location of $X/L = 6.99$ at a constant marching step size of $\Delta X/L = 0.01$ (this corresponds to a streamwise marching step size of $\Delta X/\delta = 0.375$ of the initial boundary layer thickness). The calculated streamwise velocity profile at $X/L = 6.99$ (plotted in terms of the Blasius similarity variable $\eta = Y \sqrt{\rho u_e / \mu_0 X}$) is compared with the theoretical Blasius profile in Fig. 4. Agreement with the Blasius profile is excellent. In Fig. 5 the calculated streamwise distribution of skin friction coefficient is compared with the Blasius result. Agreement between the two results is again excellent. The ability of the boundary layer version of the code to accurately predict the Blasius solution is viewed as a prerequisite before more complex cases can be attempted. In addition, since the subsonic layer approximations used in the more general analysis are similar to the boundary layer equations, the numerical scheme must be able to solve this related set of equations.

CASE II - Supersonic Laminar Flat Plate Boundary Layer

Next both the boundary layer option and the more general analysis were used to predict the laminar supersonic flow over a flat plate. This case was confined to a model fluid having a laminar viscosity proportional to the temperature and a unity Prandtl number. For this case, the Dorodnitsyn-Howarth similarity solution of Ref. 27 can be used as an initial condition and as a means of generating a theoretical downstream solution. The case run was for a free stream Mach number of 5.0 the Reynolds number per unit length was 10^5 per meter, the wall temperature was specified at 25% of the free stream temperature and the reference length, L , was 1.0 meter.

One hundred (100) grid points were nonuniformly distributed in the transverse direction with grid points concentrated in the region close to the wall. The initial profile was specified at a streamwise location of $X/L = 2.0$ from the leading edge. The initial displacement and momentum thickness Reynolds numbers were 297.0 and 771.7 respectively. The initial boundary layer profile was contained within the first 68 grid points corresponding to a boundary layer thickness of $\delta/L = 0.0359$. The subsonic portion of the initial boundary layer was contained within the first 25 grid points corresponding to a subsonic thickness of 6.55% of the boundary layer thickness. Both the boundary layer and the more general analysis versions of the computer code were utilized to march the initial solution downstream in 500 equal steps of $\Delta X/L = 0.01$ (corresponding to a Courant number of 0.81) to a streamwise location of $X/L = 6.99$. The boundary conditions for the boundary layer version were the same as for the previous case except that the wall temperature was now specified. The more general analysis utilized the no slip conditions, specified zero normal pressure gradient and specified temperature at the wall and Mach line extrapolation at the outer surface as boundary conditions.

The streamwise velocity profiles (plotted at $X/L = 6.99$ in terms of the Blasius similarity variable $\eta = y \sqrt{\rho u_\infty / \mu_\infty X}$) predicted by both the boundary layer and the more general analysis are compared with the theoretical profile in Fig. 6. As can be seen, the agreement is excellent as the calculations and the theoretical solutions are indistinguishable from one another. In Fig. 7 the calculated streamwise distribution of surface skin friction coefficient is compared with the theoretical values. As can be seen the agreement between the boundary layer and more general analysis and the theoretical distribution is excellent. Similar excellent agreement can also be observed in the plot of the streamwise distribution of momentum thickness Reynolds number, Re_θ (see Fig. 8).

The purpose of the above case was to demonstrate that when the interaction effects of displacement are negligible the more general analysis yields approximately the same results as a boundary layer analysis (in this case the boundary layer profile, a local property - the skin friction coefficient and an integrated property - the momentum thickness Reynolds number were compared). The inference is, of course, that the assumptions utilized to make the governing subsonic equations of the more general analysis well posed for

solution by spatial forward marching did not compromise the physics of the flow. The case chosen was a high Mach number flow with a highly cooled wall where the displacement effects were expected to and evidently did have only a small influence on the boundary layer flow.

CASE III - Supersonic Turbulent Flat Plate Boundary Layer

The next case considered was the supersonic turbulent flow over a flat plate. As with the previous case solutions were obtained with both the boundary layer and the more general analysis. The energy equation was approximated by assuming constant stagnation enthalpy. Boundary conditions were the same as used for the previous case. The method of Maise and McDonald (Ref. 28) was applied to the incompressible Musker profile (Ref. 29) to obtain both an initial compressible flow condition and as a basis for comparison with the calculated downstream results. For this test case, the free stream Mach number was chosen as 3.0, the Reynolds number per unit length was 10^5 per meter and the reference length, L, was 1.0 meter. An initial boundary layer thickness of $\delta/L = 0.1365$, a momentum thickness Reynolds number of 934.6, and a skin friction coefficient of 2.5×10^{-3} were assumed. 50 grid points were nonuniformly distributed in the vertical direction with the initial boundary layer encompassing 17 grid points. The subsonic portion of the initial boundary layer had a thickness of $0.01152L$ and was contained within the first 4 grid points. The corresponding subsonic nondimensional distance $y^+ = \rho_w y u_T / \mu_w$ was 9.5. The initial profile was located at a value of $X/L = 1.0$ and was marched downstream in 350 unequal steps to a downstream location of $X/L = 180$. The initial step size was $\Delta X/L = 0.15$ corresponding to a Courant number of 2.88.

Results from the test case are presented in Figs. 9-12. In Figs. 9 and 10 the skin friction coefficient vs. the momentum thickness Reynolds number results generated by both versions of the computer code are compared with results from the transformed profile of Musker. Except for some relatively minor deviations near the initial station the agreement is good for both cases. It is believed that the minor deviations in this region are due to the numerical method adjusting to the given initial profile (which for convenience assumed zero initial transverse velocity). The transformed

generalized velocity defect predicted by both versions of the code was compared with those given by the analytic Musker profile in Figs. 11 and 12 respectively. As can be seen from these figures the theoretical and calculated agreement is good.

CASE IV - Hypersonic Laminar Corner Flow

The fourth case considered was that of the hypersonic laminar strong interaction flow in a 90° corner formed by two sharp flat plates aligned with the free stream. A schematic of the flow system is shown in Fig. 13 along with the prescribed coordinate system. A viscous layer starting near the leading edge forms the continuum merged layer; the strong interaction regime appears downstream with a discrete boundary layer, inviscid region and shock wave structures. In the corner region the two layers which form on each of the plates merge together and it is this region in particular that is examined here. The computational study was conducted at a free stream Mach number of 11.2 and a Reynolds number of 5.9×10^5 per meter. The reference length, L, was chosen as the height and width of the computational domain, 0.134 meters. This case was experimentally studied by Cresci (Ref. 30). The free stream and wall temperature were 361°K and 305.55°K respectively. To determine the distribution of cross plane and streamwise grid points necessary to adequately resolve the physics of this case, the two dimensional analog of this case was first run, i.e., hypersonic laminar flow over a flat plate. Using criteria determined from running the two dimensional case, it was decided that the cross plane would require a 50 × 50 mesh of grid points. Grid points were packed in the vicinity of the walls and the shock region (see Fig. 14). The boundary layer option is inappropriate for this and subsequent cases and so was not run. The more general analysis was forward marched 120 streamwise steps corresponding to a streamwise location of $X/L = 1.316$. For the first 100 steps (corresponding to a Courant number of 0.286) the step size, ΔX , was kept constant at $\Delta X/L = 0.01$; thereafter the step size was allowed to increase by 5% per step. In the calculation, uniform free stream conditions were used as initial conditions. After marching the free stream conditions for two streamwise steps, the flow encountered the leading edge of the corner and the flow was allowed to

naturally develop. In this approach the leading edge singularity is ignored and smeared over by the computational scheme. The governing equations used for this case were the three momentum equations, the continuity equation and the energy equation. The no-slip conditions, the zero pressure gradient condition and specified temperature were used as the wall boundary conditions. On all other boundary surfaces the symmetry conditions were imposed.

Fig. 15 presents the comparison of the calculated and experimental wall pressure distribution normal to either of the two flat plates (i.e. in the Z direction) at streamwise location $X/L = .990$ corresponding to an interaction parameter, $\chi = 5.1$ ($\chi = C^{1/2} M_\infty^{-3} / R_\infty^{1/2}$, $R_\infty = \rho_\infty u_\infty X / \mu_\infty$ where C is the constant of proportionality between viscosity and temperature and X is the distance from the leading edge). It can be seen that $\chi \propto 1/X^{1/2}$, Ref. 31. Considering the uncertainties in the experimental data, the calculated wall pressure agrees very well with the measurements both in the location of the peak pressure and the general form of the pressure distribution. Fig. 16 compares the Stanton number C_H where $C_H = q_w / [\rho_\infty U_\infty (h - h_w)]$ at streamwise location $X/L = 0.990$ or $\chi = 8.2$. In general the agreement is good, with the analysis showing a slightly thinner peak heating region. Fig. 17 shows the comparison between computed and measured skin friction coefficient at $X/L = 0.990$ or $\chi = 5.17$. The apparent discrepancy between the data and the calculation is large, although the general form of the curves are similar. Since it was not clear why such a large discrepancy occurred, the original source of the data (Ref. 30 and 32) were reviewed carefully to determine possible sources for such disagreement. In Ref. 30 it is reported that the skin friction coefficient was estimated by using the gradient of axial velocity normal to the wall which was calculated from the measurements of the total temperature and Mach number distributions in the corner regions. Furthermore, it was found that the nearest measuring station was approximately 0.1 cm from the wall. Thus, for the purpose of comparison with the data, it was felt to be reasonable to calculate the predicted skin friction coefficient in a like manner by using the numerically calculated velocity gradient normal to the wall with the first grid point 0.1 cm off the wall. As is shown in Fig. 17 (dotted line) this calculation

produced a skin friction coefficient distribution that is in much better agreement with the experimental data. Fig. 18 shows the streamwise development of the stagnation pressure isobars. The development of the merged region, separation of the shock wave from the viscous region and the complex corner flow structure are easily identified as the flow proceeds downstream.

CASE V - Three-Dimensional Glancing Shock Wave - Boundary Layer Interaction

A typical flow phenomenon occurring in internal supersonic flow is the interaction of a sidewall boundary layer with a cowl generated glancing shock wave. This flow configuration gives rise to a strong interaction region in the corner between the sidewall and the cowl resulting in the formation of a corner vortex as the flow proceeds downstream. A well documented extensive experimental investigation of the phenomenon has been performed by Oskam, Vas and Bogdonoff and is reported in Ref. 33 and Ref. 34. Fig. 19 schematically depicts the flow. A supersonic turbulent boundary layer is produced on the walls of the test section. A shock generator in the form of a sharp edged plate is mounted vertically between the tunnel floor and ceiling and turned to some desired angle, ϕ , to the incoming flow. The glancing shock formed by the generator then interacts with the boundary layer formed along the floor of the test section. For the case under consideration in this study the plate was inclined at $\phi = 10^\circ$ to the free stream which had a Mach number of 2.94. The pre-interaction boundary layer thickness was 1.40cm and the Reynolds number based on that thickness was 9.68×10^5 . For this case experimental data were obtained at three stations (see Fig. 20). The mean flow data taken were static pressure (cone-cylinder probe), stagnation pressure (cobra probe), total temperature (theremocouple probe) and yaw angle (cobra probe). The yaw angle, α , in the context of the coordinate system of Fig. 20 is defined as

$$\alpha = \tan^{-1} \left(\frac{v}{u} \right) \quad (44)$$

where u is the streamwise velocity and v is the velocity component perpendicular to the wind tunnel side wall.

The cross-sectional area of the test section is 8 x 8 inches, and hence the reference length, L , was chosen as 8 inches (20.32 cm). The computational domain chosen for this calculation consists of the region starting at $X = 2.98$ cm, i.e., $X/L = 0.147$ upstream of the leading edge of the shock generator and proceeding to a distance of $X = 25.14$ cm, i.e., $X/L = 1.237$ downstream of the leading edge. Because of the vertical symmetry, the computation only had to be made in the lower half of the test section. The spanwise domain was bounded by the shock generator on one surface, and a free stream boundary located far enough away such that the shock wave will not exit through this surface for the streamwise extent of this computation. The coordinate system used for this calculation was generated by using a Schwarz-Christoffel transformation technique of Anderson (Ref. 35) to generate a set of conformal coordinates. The initial conditions were calculated by assuming a mixture of a boundary layer profile on the floor of the test section and free stream conditions elsewhere. The initial boundary layer velocity profile was calculated by the method of Maise and McDonald (Ref. 28) with a transverse velocity set to zero. The pre-interaction boundary layer thickness of 1.40 cm ($\delta/L = 0.0689$), a skin friction coefficient of 1.2×10^{-3} , a momentum thickness Reynolds number of 3×10^{-4} , and a wall temperature of 297° were used to calculate the profile. The initial enthalpy and temperature profiles were calculated by use of the modified Crocco profile (Ref. 36). Boundary conditions on the shock generator surface, and the floor of the test section are the no-slip conditions for the three velocity components, specified temperature for the thermal condition (279°K for the test section floor and 236°K for the shock generation surface), and imposition of the normal pressure gradient equals zero condition. The two above surface temperatures are nominally average values of these parameters during a run. Due to the nature of test facility, the free stream stagnation temperature decreases on the order of 55°K during a run. This causes the surface temperature to also vary; however, since the shock generator has a low heat capacity, its temperature decreases more rapidly than the test section floor temperature, and thus the above temperatures are the mean temperatures during the run. This time-dependent nature of the experiment will undoubtedly lead to some

(undetermined) error in assessing the values of the experimental data. The boundary conditions on the bounding surface upstream of the leading edge of the shock generator as well as the two other boundary surfaces (the plane of symmetry and the surface opposite the shock generator) utilize symmetry boundary conditions. The mixing length model is based on minimum distance to the nearest wall, in this case the distance from a surface is taken to be the minimum of the distance to either the shock generator surface or the test section floor. The laminar and turbulent Prandtl numbers used for this calculation were 0.74 and 0.90, respectively. The initial solution was marched downstream 400 stations at a computational step size that varied from a minimum of $\Delta X/L = 0.002$ in the vicinity of the tip of the shock generator to a maximum of $\Delta X/L = 0.005$ further downstream. At the initial plane, this minimum step corresponds to a physical distance of approximately $\Delta X/L = 0.02$ or a Courant number of 8.70. The cross plane utilized a 40×40 grid point structure with grid point packing about both the shock generator surface and the test section floor. As was the case for the previous calculation, the shock wave was generated as part of the solution rather than as part of the initial profile. The equations solved in this case were the three orthogonal momentum equations, the continuity equation and the energy equation.

Results in the form of calculated and measured pitot pressure, static pressure, total temperature and yaw angle are presented in Figs. 21-29. Pitot pressure measurements were obtained at the four measuring stations shown in Fig. 20, static pressure and total temperature at two stations and yaw angle at three stations. Agreement between the calculations and the data is excellent both from a qualitative and quantitative perspective. (Data at a value of $YG = .25$ in is within the wind tunnel floor boundary layer. All other data is outside the boundary layer.) The agreement between the calculated and experimental static pressure (Figs. 21 and 27) indicates proper placement of the shock wave. Results at the streamwise station $X = 7.60$ in vertical distances from the shock generator of 2.75 and above (i.e. values of YG (Fig. 20)) there is some minor deviation between the calculation and experiment. This is probably due to some

smearing of the shock wave as it was in this region that the fewest number of transverse grid points were used. The pitot pressure profiles (Figs. 23-26) again show overall good agreement between the calculation and data. The pitot pressure can be viewed as a composite variable which measures the level of the static pressure as well as the boundary layer streamwise velocity profile. The near wall data values of pitot pressure especially in the corner region show some deviation from the calculated values. Comparisons between data and calculated values of the yaw angle are shown in Figs. 27-29. The agreement is excellent both qualitatively and quantitatively throughout. Some minor deviations can be seen within the boundary layers. However, when one considers that it is usually more difficult to accurately calculate the cross flow velocity components than the streamwise velocity component, the amount of deviation must be considered minimal. The yaw angle distribution is one means of determining both the position and strength of the corner vortex which is located in the corner region and grows as the flow proceeds downstream. The ability to accurately calculate the yaw angle, therefore, implies an ability to accurately calculate the strength and location of the vortex. Referring back to the statement about the local maximum in the total temperature, it can be seen from examining the yaw angle distribution that the local maximum in total temperature occurs in the vicinity of the edge of the vortex associated with the shock wave.

CASE VI - Supersonic/Turbulent Flow in a Variable Area Ratio Duct

The next test case considered was the two-dimensional turbulent flow through a channel of varying cross-section. The geometry and computational mesh used for this calculation is shown in Fig. 30. For this case, a nonorthogonal coordinate system was utilized. The streamwise coordinate is obtained by using a $Y/\delta(X)$ transformation, where $\delta(X)$ is the equation of the height of the top surface taken normal to the lower, flat surface. The equations solved were the transformed Cartesian streamwise and transverse momentum equation and the transformed continuity equation. The stagnation enthalpy was assumed constant. Boundary conditions on both surfaces are the

no-slip conditions and zero normal pressure gradient. The flow conditions for this case were a free stream Mach number of 1.9 and a Reynolds number per unit length of 4.64×10^7 per meter. The reference length, L, is taken as the minimum distance between the upper and lower surfaces, i.e., 0.01018 meters. Ninety-nine (99) grid points were utilized in the transverse direction with packing in the vicinity of the two walls. The marching step size was taken at a constant value equal to $\Delta X/L = 0.01$ (corresponding to a Courant number of 1.37). The initial profiles on both surfaces were again generated by using the method of Maise and McDonald (Ref. 28). The boundary layer thickness on the lower and upper surfaces were $\delta_1/L = 0.06074$ and $\delta_2/L = 0.12149$, respectively. The corresponding skin friction coefficients were 3.94×10^{-3} and 3.32×10^{-3} . Corresponding momentum thickness Reynolds numbers were 400 and 750, respectively. These values were the same as were used in the calculation of Ref. 38. In Ref. 38 the same prediction was performed by numerically solving the full Navier-Stokes rather than with a reduced form as is done here.

Figure 31 shows the comparison of the upper surface static pressure distribution calculated by both the spatial forward marching analysis and the Navier-Stokes code. Initially, the agreement between the two predictions is good, but the forward marching procedure predicts a higher peak pressure in the compression region and a corresponding greater expansion further downstream. The differences of the two methods in this region could be due to the neglecting of the streamwise diffusion in the forward marching analysis (and hence the neglecting of upstream influence). The difference could also be due to the higher level of accuracy obtained by the forward marching procedure due to the use of a finer streamwise grid structure than was used in the Navier-Stokes analysis. The forward marching run was terminated as the shock wave approached the lower wall due to the formation of a suddenly expanding subsonic region near the lower wall. The streamwise location that this phenomenon occurred was approximately the same location that the Navier-Stokes analysis predicted the existence of a Mach stem, and hence a corresponding suddenly expanding subsonic region. Although the forward marching procedure cannot calculate through such a region, it is

significant that at least in this case, the analysis predicted the initial formation of such a region.

VII - Supersonic Turbulent Shock Wave-Boundary Layer Interaction

A well-documented experimental investigation of a shock wave-boundary layer interaction flow has been made by Rose (Ref. 36). A schematic of the experimental apparatus is shown in Fig. 32. A conical shock wave is generated by a 9° half angle cone situated in the center of an axisymmetric test section of radius, $L = 2.64$ cm. The shock wave interacts with a turbulent boundary layer on the wall of the test section. The free stream Mach number was 3.88 and the Reynolds number based on the pre-interaction boundary layer thickness of 0.51 cm was 8.7×10^4 . Experimental data were obtained in the turbulent boundary layer on the wall of the test section in the vicinity of the interaction region. The mean flow data consists of measured pitot and total temperature profiles and surface static pressure distribution. The cone half angle was chosen to produce a shock strength near to that required to produce streamwise separation.

The computational domain for this calculation consists of the transverse region between the cone surface and the test section wall starting at the streamwise position $X/L = 0.364$ upstream of the cone tip and extending downstream $X/L = 5.053$. Because the cone is placed in the center of the axisymmetric test section the resulting flow is axisymmetric, and hence it is only necessary to solve the usual axially symmetric set of governing equations. A conformal coordinate system was generated by means of the previously discussed Schwarz-Christoffel transformation technique of Anderson (Ref. 35). The initial conditions consist of a turbulent boundary layer on the test section wall generated by the method of Maise and McDonald (Ref. 28). The boundary layer thickness was 0.51 cm, ($\delta/L = 0.1923$), the skin friction coefficient was 1.72×10^{-3} , the momentum thickness Reynolds was 2000, and the wall temperature was 277.8°K . The initial enthalpy and temperature profile is calculated using the modified Crocco-Busmann profile (Ref. 37). Finally, the pressure on the initial plane is assumed constant at the test section free stream value. The equations solved were orthogonal axisymmetric streamwise and transverse momentum, continuity and energy equations. Boundary conditions on the cone surface and the test section wall are identical, i.e. no-slip for the velocity components, a specified wall

temperature of 277.8°K and zero normal pressure gradient. On the axis of symmetry upstream of the cone tip, symmetry conditions are imposed. The laminar and turbulent Prandtl numbers were set to 0.71 and 1.0, respectively. The initial solution was marched downstream 800 stations at a constant computational step size of $\Delta X/L = 0.01$ corresponding to a Courant number of 0.42. At the initial station this corresponds to a physical step size that is 1% of the distance from the tip of the cone to the test section wall. For this calculation, 99 transverse grid points were utilized with packing about the cone and test section wall. It is to be noted that the shock wave generated by the cone is not input as an initial condition. Rather, the shock wave is generated as a result of the coordinate system, the governing equations and the applied boundary conditions.

Results in the form of calculated and measured pitot pressure are presented in Fig. 33. The experimental data were obtained at equally spaced streamwise stations in the vicinity of the interaction. Basically, the first three profiles are in the pre-interaction region and the remaining are in the interaction and post interaction regions. The incident shock wave can be seen in the pitot pressure profile plots (Fig. 33), at the second and third data stations. At the sixth and subsequent data stations, the shock wave reflects off the boundary layer and proceeds back towards the cone. As can be seen from Fig. 33, the calculated and measured values of pitot pressure are in substantial agreement. Qualitatively, they agree at all data stations. Qualitatively the agreement in the pre-interaction and throughout most of the interaction region is excellent. The calculation does predict a slightly thicker (on the order of 10%) emerging boundary layer thus resulting in some disagreement between the calculated and experimental pitot pressures in the outer portions of the boundary layer at the downstream stations. This can perhaps be attributed to the use of a constant boundary layer thickness in the turbulence model of Eq. (9). To date, no attempt has been made to use a varying boundary layer thickness in the turbulence model. Initially, the wind tunnel boundary layer had four grid points within the subsonic portion of the layer (corresponding to 0.004% of the distance between the wall and the axis of symmetry). During the iteration process, the adverse pressure gradient causes the flow to decelerate. At one point the subsonic portion of the boundary layer was contained within 12 grid points corresponding to 2.1% of the distance between the cone and the wind tunnel wall.

Numerical simulation of the Rose experiment were also performed with the computer code constructed to perform on option the calculation according to the method of Rudman and Rubin (Ref. 4) and Lubard and Helliwell (Ref. 5). It will be recalled that Rudman and Rubin neglected the streamwise pressure gradient in their procedure while the Lubard and Helliwell technique used explicit spatial lagging for the calculation of the streamwise pressure gradient term. The Rudman-Rubin approach was not proposed for use in this type of flow (it was proposed for hypersonic flow over highly cooled walls where the streamwise pressure gradient is negligible with respect to the other terms of the momentum and energy equations). Here it is used only to give perspective to the role that streamwise pressure gradient term plays in the flow of interest. For both techniques the linearization of the governing equations, their finite difference approximation and solution of the resultant set of linear algebraic equations was achieved by the same method as described in the previous section, i.e., the same method as was used to solve the governing equations of the present analysis. Although this numerical method of solving the governing equations was not used by either Rudman and Rubin or Lubard and Helliwell, the governing equation and finite difference representation of derivatives, grid point distribution, boundary conditions and initial conditions were the same. Hence, the only factor of consideration is the governing equations themselves.

Results for the simulation of the Rudman and Rubin techniques are presented in Fig. 34. At this first streamwise data station the calculated boundary layer profile agrees well with the experimental data as they should since at this point, i.e., in the preinteraction region, the streamwise pressure gradient is small. However, at the third streamwise station the calculated shock wave location noticeably lags the data, and as the flow proceeds downstream the calculated flow bears little resemblance to this data. It should be re-emphasized here that the Rudman and Rubin technique was not developed for this problem and that the results indicate only that this type of approach is not satisfactory for predicting typical flow phenomena that occur in internal flow devices.

Using the method of Lubard and Helliwell no stable calculation could be obtained with any marching step size used. The calculations displayed the well known symptoms of branching, i.e., a large increase in pressure was predicted which in turn causes a strong streamwise recirculation zone

to form. Initially this calculation was run with a streamwise marching step of 0.01% of the reference length, L (the same as was used for the general analysis and the Rudman and Rubin calculation). Subsequent calculations using a marching step as large as 10% of the reference length were attempted, but these calculations were also unstable. The step size of 10% of the reference length corresponds to approximately twice the stable marching step size predicted by Lubard and Hellwell in Ref. 9. This is not surprising as the authors infer that their criterion is only approximate. No step sizes larger than 10% were used as it was felt that streamwise step sizes of this magnitude are surely too large to adequately resolve the interaction process. The failure of this method to give a stable solution supports the previously stated objection that methods that have a minimum step size criterion may not be acceptable for flow situations of interest where large streamwise pressure gradients exist. It is to be expected, although it has not been demonstrated here, that the other methods which have a similar minimum step size criterion; would also not give a stable solution for this case.

VI - Axisymmetric Inlet

The last two test calculations performed under this effort were for the Boeing axisymmetric mixed compression type inlet. Details of this inlet and the experimental test conditions are available in Ref. 39. A schematic of the inlet is provided in Fig. 35. The test conditions were for a free stream Mach number of 3.5 with a Reynolds number (based on the lip diameter) of 2.8×10^{-6} . The reference length L, was chosen as half of the lip diameter of 49.723 cm. Calculations were performed at both 0° and 3° angle of attack. Surface contours of the centerbody and cowl are listed in Table 1. At the design Mach number of 3.5, the centerbody is in the fully retracted position providing a capture mass-flow ratio of unity. The axisymmetric centerbody's half angle is initially inclined at 10° to the horizontal. The Schwarz-Christoffel transformation technique of Anderson (Ref. 35) was used to generate a conformal coordinate system for this inlet (see Fig. 36). The computational domain consisted of the region between the centerbody and the cowl. The upstream limit of the computational domain was chosen to be slightly upstream of the leading edge of the centerbody; the downstream

extent terminated downstream of the geometric throat. For the 0° angle of attack case the flow is axisymmetric and hence only the axisymmetric equations had to be solved. In this case, the equations solved were streamwise and transverse momentum, continuity and the energy equations. Ninety-nine (99) grid points were used in the transverse direction with grid packing in the vicinity of the centerbody and the cowl surface. For the 3° angle of attack case, the flow is three-dimensional. However, a plane of symmetry exists and hence the computation only has to be made in the half plane. In this case, streamwise, radial and circumferential momentum, continuity and energy equations had to be solved. Fifty radial grid points were used for the 3° case with grid packing in the vicinity of the centerbody and the cowl surfaces. Nineteen equally spaced grid points were used in the circumferential direction (corresponding to 10° increments). The boundary conditions on both the centerbody and the cowl surface were the no-slip conditions for the velocity components, zero normal pressure gradient and the adiabatic wall condition. The effects of bleed (which was utilized in the experiment) were not considered for these two cases. On the free surface corresponding to the upstream extension of the cowl surface, Mach line extrapolation was utilized. Since the calculation procedure was initiated upstream of the leading edge of the centerbody, a boundary condition had to be set on this surface (corresponding to the upstream extension of the centerbody surface). In this case, symmetry conditions were used for streamwise velocity (circumferential velocity for the 3° angle of attack case), pressure and temperature. The normal velocity component on the upstream extension remained unchanged. Finally, for the 3° angle of attack case symmetry conditions were used on the plane of symmetry. The initial condition for both cases were the uniform free stream conditions. Thus, the shock wave is produced by the calculation procedure and is not input as a part of the initial conditions.

For the 0° angle of attack case the initial conditions were marched 470 streamwise steps at a constant step size of $\Delta X/L = 0.02$. Corresponding to a Courant number of 3.00. This corresponds to an initial step size equal to 2% of the distance from the centerbody to the upper surface (see Fig. 35). The computation terminated slightly upstream of the geometric throat (a large recirculation zone formed on the cowl surface). The displaced scale Mach number profiles are shown in Figs. 37 and 38. Figure 37 shows the plots in

physical space while Fig. 38 shows the plots in computational space. Although the propagation of the shock waves is somewhat difficult to discern in Fig. 37, the shock waves propagation is very distinct in the computational space plots of Fig. 38. The centerbody shock passes out in front of the cowl. A shock wave forms off the cowl, impinging on the centerbody, reflecting and impinging on the cowl surface where a recirculation zone forms. Comparison of the centerbody and cowl static pressure distributions are presented in Figs. 39 and 40. Considering that the effects of bleed are not considered, the agreement with data is good. In Fig. 38, it can be seen that the region where the calculation terminated due to a large recirculation zone was also (evidently with good reason) a region where the flow was subjected to wall bleed.

The 3° angle of attack case was run mainly as a demonstration case of an off-design condition. The centerbody location was specified to be that of the 0° angle of attack location. Under this condition, it is to be expected that the shock wave will hit inside the cowl on the windward side and fall further outside the cowl on the leeward side. However, the strength of the shock will be stronger on the windward side. This case was run with a variable marching step size. The step size was chosen such that initially a step size of $\Delta X/L = 0.02$ was used (corresponding to a Courant number of 1.45). After encountering the centerbody the step size was gradually increased to a step size of $\Delta X/L = 0.4$ and then gradually decreased to a step size of $\Delta X/L = 0.01$ slightly upstream of the cowl. Downstream of the cowl entrance region the step size was gradually increased again to a maximum of $\Delta X/L = 0.04$. The purpose of varying the step size is to increase resolution in regions of large streamwise flow gradients and to decrease resolution of a larger step can be taken. This calculation was marched downstream 270 steps before the calculation terminated. Termination was due to the generation of a recirculation zone on the leeward side of the centerbody.

Results of the calculating of the off-design 3° angle of attack case are presented in Fig. 41-48. No comparison is made with data since data was not obtained for the 3° case in the off-design condition. In Figs. 41-43, the streamwise pressure distributions on the centerbody and the cowl surfaces are shown on the leeward, waterline and windward rays. On the leeward side of the cowl, the shock passes in front of the cowl entrance. The turned flow then encounters the cowl entrance and forms a shock wave. This can be seen

by the spike-like rise followed by a decrease in pressure (as the cowl at this point becomes concave) followed by an increasing rise in pressure as the cowl surface becomes convex again. Similar features can be seen on the waterline and windward rays. In this case the shock formed by the centerbody impinges on the cowl surface. A similar spike-like behavior followed by expansion and compression zones can be observed. The corresponding displaced scale Mach number plots are shown in Figs. 44-46. By looking up into the inlet, the shock structure can be discerned. Figure 47 shows typical secondary flow velocity vectors. The streamwise location is approximately at a value of $X/L = 2.45$. The windward side is on the left; the leeward side is on the right. The position of the shock wave is clearly discernable as a discontinuity in flow direction. It can be seen that the shockwave is closer to the windward surface than to the leeward surface. Mach number contours at the same station are shown in Fig. 48. The approximate position of the shock wave is shown by the concentration of the Mach number contours.

All of the above test cases were run on the NASA-LRC IBM 370-3033 computer. The CPU run times are 5.43×10^{-3} sec/grid point for the two-dimensional runs 1.43×10^{-2} sec/grid point for the three-dimensional runs. The total run time for a given case scales linearly with respect to the number of grid points, thus for instance the Rose case which used 99 transverse grid points and marched 800 streamwise stations had a run time of 430 seconds. The difference in run times between two- and three-dimensions is due to the three-dimensional calculation having an additional momentum equation to solve plus the additional terms in all equations because of the presence of the third dimension. There is also additional overhead costs since the three-dimensional cases uses mass storage to transfer information in and out of core while the two-dimensional cases always have all the necessary information in core. The PEPSIS computer code was developed as a very general research tool and hence no attempt has been made to optimize its computational efficiency for a specific class of problems. The run times would decrease significantly if the number of terms in the governing equations could be reduced as for instance would occur for simpler geometric configurations. The present version has a general orthogonal capability as well as a limited nonorthogonal capability (see section on the User's Manual).

V. DISCUSSION AND CONCLUSIONS

The primary objective of this investigation was to develop and validate an efficient numerical procedure for the calculation of two- and three-dimensional supersonic flows (with embedded subsonic regions) in internal flow devices. It is felt that this objective has been achieved, and a new set of governing equations has been developed which are well-posed for solution by an efficient spatial forward marching procedure. This procedure has been validated by application to a series of test cases characteristic of the phenomena that occur in internal flow devices and the results in general give very good agreement with the available experimental data. Numerous additional test cases have been successfully run by the present authors and by other investigators (Refs. 20 and 21) and branching or other unstable behavior has not been observed even when the marching step size has been several orders of magnitude below the minimum of the stability criterion that restrict schemes which have a minimum step size. Thus, the restrictive requirement of a minimum marching step size has not been observed for this set of governing equations. It should be emphasized that no approximation was made to the streamwise pressure gradient in the present approach. This is viewed as being extremely important for internal supersonic flows where so many of the phenomena of interest have associated with the large streamwise pressure gradients. Finally, the efficiency of the spatial forward marching procedure is such that a million grid point calculations can be performed in approximately four hours of IBM 370-3033 CPU run time (this is equivalent to approximately one hour of CRAY I run time). This procedure could be used on a routine basis for design type calculations for internal flow devices such as supersonic inlets.

IV. USER'S MANUAL

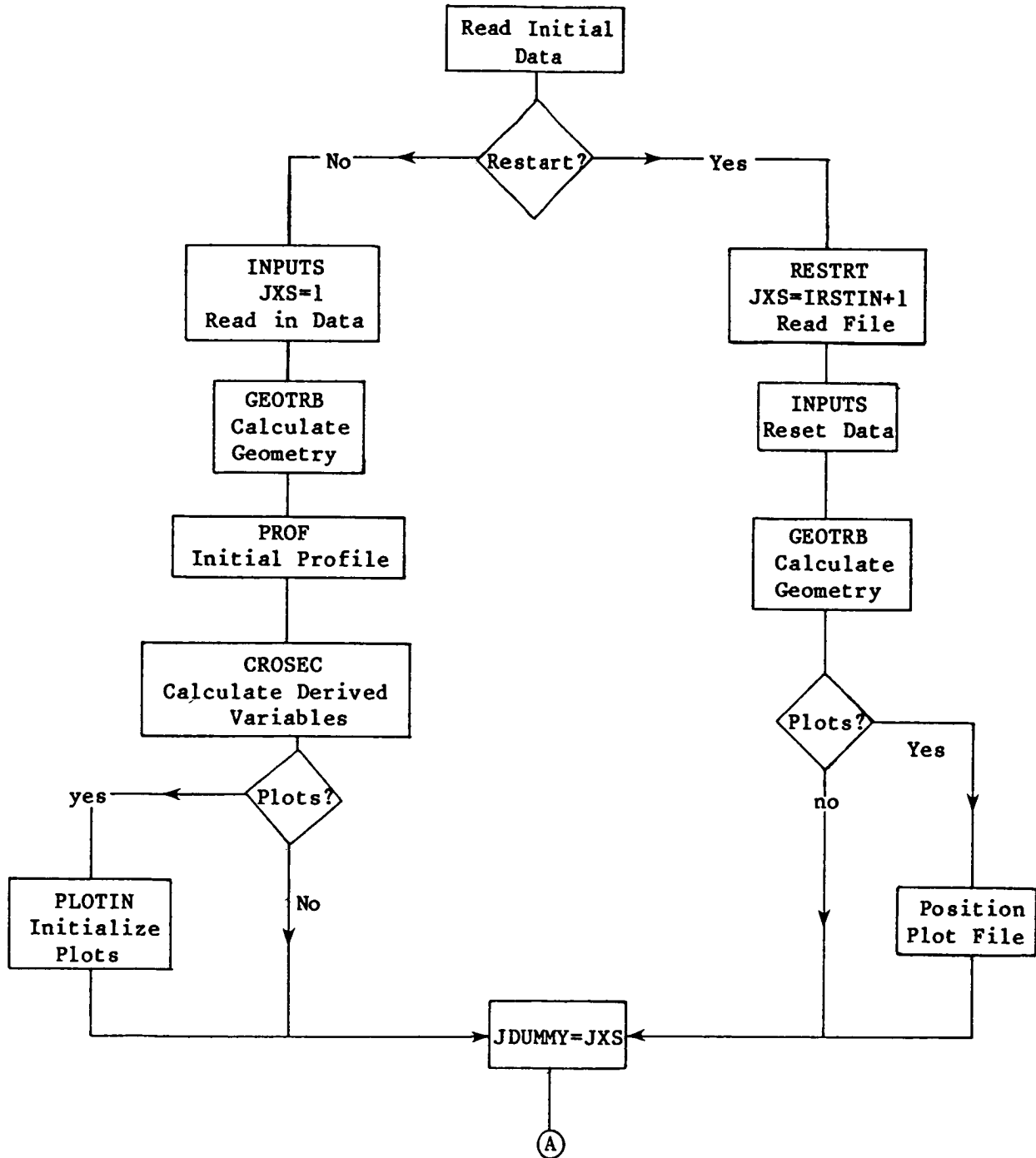
The PEPSIS users' manual is meant to serve as a guide in helping the user make successful runs with the PEPSIS computer program. The degree of success obtained by the user will depend on the skill of the user and his ability to correctly apply the code to his particular problem. The code will solve the governing equations, subject to the user supplied boundary conditions, however, meaningful results will only be obtained if the boundary conditions are appropriate to the problem. In addition the user must specify viscosity models, initial conditions, a coordinate system and the location of grid points to adequately resolve the flow. The user with a good knowledge of the physics involved in his problem and how the code models the physics should, with a moderate amount of experience, be able to successfully apply the code to a wide variety of supersonic flow problems.

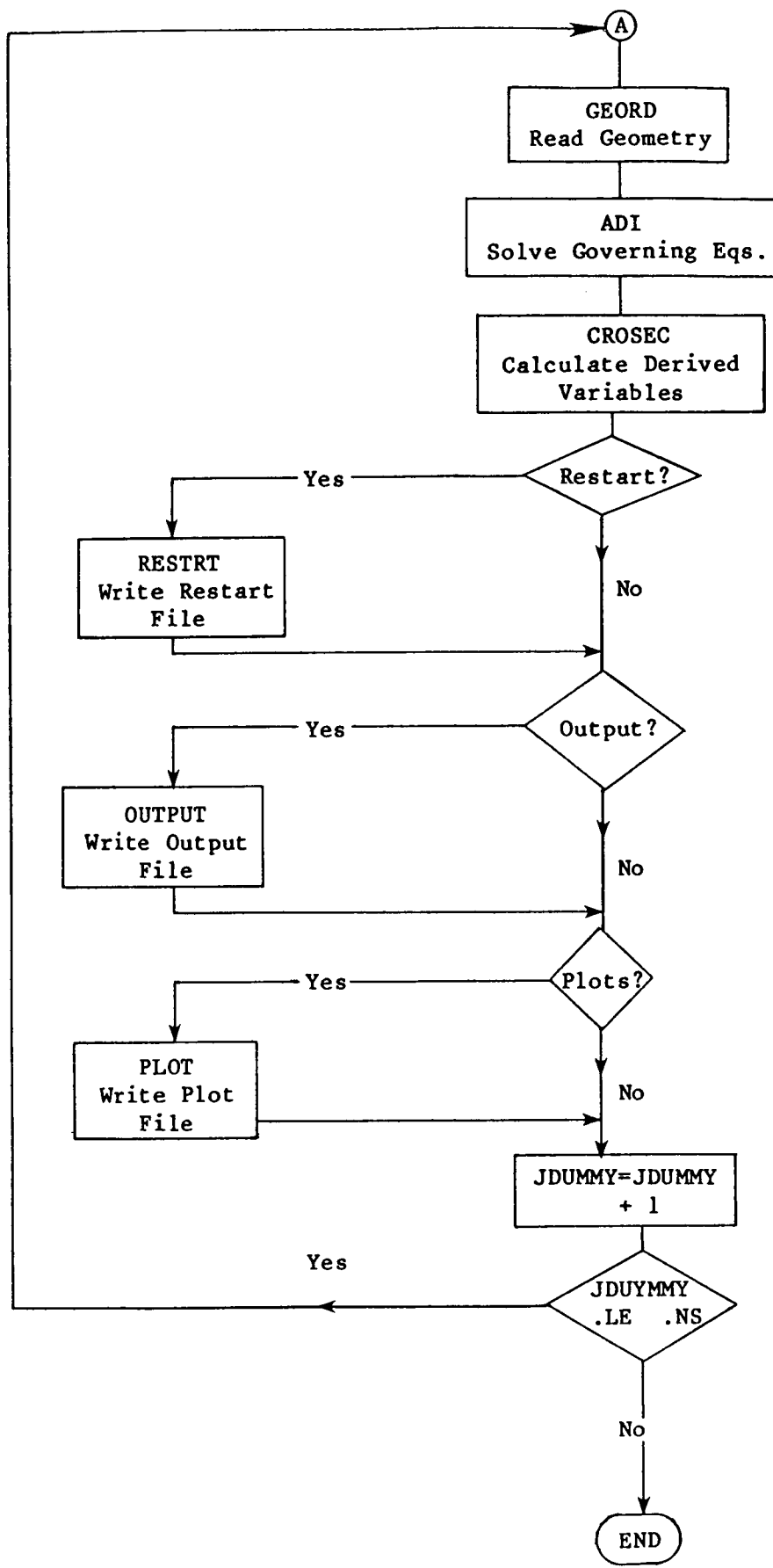
The users' manual is divided into eight parts consisting of: (1) a flow diagram, (2) a brief description of each subroutine and its use, (3) a list of the Fortran variables and a description of their meaning, (4) a description of the logical file units utilized by the PEPSIS computer code, (5) a detailed description of the input required by the PEPSIS computer code, (6) a description of the common error conditions that may be encountered during the execution of a PEPSIS run and the corrective action to be taken, (7) sample input for two and three-dimensional cases and (8) sample output for the corresponding cases.

Flow Diagram

The purpose of the flow diagram is to help the user understand the basic flow of information within the PEPSIS computer code. Because of the size of the code (approximately 13,000 cards), a detailed flow diagram would be prohibitively large and probably be of little value to the user. Therefore, the flow diagram is intended only to give a general overview of the structure of the code. The interested user is urged to consult the program listing for details.

Flow Diagram for the PEPSIS Computer Code





PEPSIS Subroutines

<u>Subroutine</u>	<u>Purpose</u>
ADDRES	Calculate addresses for finite difference representation of metric and fluid dynamic variables.
ADI	Master control subroutine for ADI procedure.
ADICP	Control subroutine for coupled equations.
ADIUN	Control subroutine for uncoupled equations.
AMARCH	Linearizes streamwise convective terms.
AMATRX	Linearizes all streamwise terms.
ARTVIS	Artificial dissipation subroutine.
AVRG	Calculates averaged quantities in cross plane.
BC	Boundary condition subroutine.
BLKDATA	Stores default values of key variables.
BLT	Calculates boundary layer thickness.
BULEEV	Calculates Buleev turbulent mixing length.
CONVCT	Linearizes cross plane convective terms.
CORBND	Calculates geometry transformation information on boundaries.
CORTRN	Calculates geometry transformation information for interior points.
CROSEC	Control subroutine for calculation of derived variables.
CURVT	Linearizes curvature terms.
DATAS	Logical file control subroutine.
DELTX	Calculates transformation information for ICORD = 2 option.
DELTXZ	Calculates transformation information for ICORD = 3 option.

<u>Subroutine</u>	<u>Purpose</u>
DIFF	Linearizes diffusion terms.
DISFCN	Calculates dissipation function.
DIV	Calculates divergence of velocity.
DOP2	Control subroutine for linearization of Y-direction and source terms.
DOP3	Control subroutine for linearization of Z-direction terms.
EOS	Equation of state subroutine linearizes and updates pressure and temperature.
FGFUN	Calculates geometry groupings.
GAUSS	Solves uncoupled tri-diagonal set of equations.
GENCBC	Control subroutine for coupled boundary conditions.
GENUBC	Control subroutine for uncoupled boundary conditions.
GEORD	Controls reading of metric information from logical file unit LDRUM.
GEOTRB	Generates metric information on logical file unit LDRUM.
INDIC	Determines if flow is subsonic or supersonic at grid points.
INPUTS	Input subroutine. Input data enters and is processed.
INTEBC	Performs a two-dimensional linear interpolation for wall transpiration rates.
LAMP	Calculates laminar profile.
LAW	Calculates nondimensional velocity, U^+ as a function of nondimensional distance, Y^+ .
LENGTH	Calculates turbulent mixing length.
LOADUP	Brings into core dependent and derived variables at appropriate points.

<u>Subroutine</u>	<u>Purpose</u>
MAIN	Main control program.
MATPRT	Prints elements block tridiagonal matrix.
MGAUSS	Control subroutine for solving block tridiagonal systems of equations.
MGERR	Calculates error associated with solving block tridiagonal system of equations.
NMLIST	Subroutine for printing namelist input information.
OUTPUT	Control subroutine for printing out results on a cross-sectional (Y-Z) plane.
PLOT	Writes plot information on logical file unit JPLOT.
PLOTIN	Writes first record of general information on logical file unit JPLOT.
PROF	Generates initial profiles.
QUICK	Matrix elimination subroutine.
READZ	Prepares variables for printing.
RESTRT	Reads and writes restart information.
ROTATE	Rotates data from columns to rows and vice versa.
SETBVL	Updates boundary information a line at a time.
SHEAR	Control subroutine for the calculation of wall shear velocity.
SPREAD	Spreads two-dimensional data to three dimensions.
SUB	Contain special subsonic logic.
SWITCH	Calculates streamwise location for switch of boundary condition.
TANHYP	Grid stretch subroutine.
TNDER	Calculates normal derivative of temperature at a wall.

<u>Subroutine</u>	<u>Purpose</u>
TRANS	Transition model subroutine.
TURB	Turbulence model subroutine.
TURBP	Calculates turbulent profile based on theory of Maise-McDonald.
VISCOS	Constant and laminar viscosity subroutine.
WALLFN	Calculates wall shear velocity.
WRMATR	Writes block tridiagonal dump information on logical file device NUNERR.
YCALC	Calculates Y and Z locations.
ZERO	Zeros out linearization arrays.

Logical File Units Utilized by PEPSIS Computer Code

The PEPSIS COMPUTER code utilizes up to twelve (12) logical file units during the execution of a run stream. In many cases not all twelve units are used, and hence in these cases there is no need to define all twelve units. All references to a logical file unit in the PEPSIS computer code is accomplished through the use of a FORTRAN name rather than through a specific unit number. Thus, if the user desires to change a logical file unit number, this can be done through the input file. A list of the logical file units utilized by the PEPSIS computer code, their FORTRAN name, default value unit number, and a brief description of the use of the unit is presented below. All units are sequential.

<u>FORTRAN Name</u>	<u>Default Unit Number</u>	<u>Description</u>
MIN	5	Input data unit.
MOUT	6	Printed output unit.
MASS1	8	First unit which stores dependent and derived variables either by rows or columns. Not needed for two-dimensional cases, i.e., when TWOD = .TRUE.
MASS2	9	Second unit which stores dependent and derived variables either by rows or by columns. Not needed for two-dimensional cases, i.e., when TWOD = .TRUE.
MSDD	15	Unit which stores dependent and derived variables by rows only. Not needed for two-dimensional cases, i.e., when TWOD = .TRUE.
JDRUM	11	Unit which contains output of ADD computer code. Only needed when IGEOM = 10 or 11.
LDRUM	12	Intermediate unit used in generations of final metric information file. Only needed when IGEOM = 10 or 11.
KDRUM	13	Unit which stores final metric information. Needed in all cases.

<u>FORTRAN Name</u>	<u>Default Unit Number</u>	<u>Description</u>
NUNEER	14	Unit which stores information concerning the block tridiagonal matrix inversion. Needed when MGDMR ≠ 0.
JPLOT	16	Unit which stores plotting information. Needed when IPLOT ≠ 0.
JRSTIN	10	Input restart unit. This unit contains appropriate common block information and the value of the dependent and derived variables at each cross-sectional grid point at the restart streamwise station. Needed only when IRSTIN ≠ 0.
JRSTOT	10	Output restart unit. This unit contains appropriate common block information, and the values of the dependent and derived variables at each cross-sectional grid point at the restart streamwise station. Needed only when IRSTOT = 0. Default is JRSTIN = JRSTOT; however, it is desired to have separate input restart and output restart files set JRSTOT = 17.

PEPSIS Input

Except for an initial title card and plot file input data the entire PEPSIS input is entered by means of the NAMELIST format. There are two primary advantages to the use of the NAMELIST format: (1) if the default values (defined in the block data subroutine) are acceptable, the user need not input that variable, and (2) the order (within a given NAMELIST) in which the variables are entered is irrelevant. There are six NAMELIST input files in the PEPSIS code, \$REST and \$LIST1 through \$LIST5. The first file is read in the main program and enters restart information. The remaining NAMELIST files are read in subroutine INPUTS. Basically, the NAMELISTS \$LIST1 through \$LIST5 can be divided by function. \$LIST1 enters information about the governing equations and appropriate boundary conditions, \$LIST2 enters reference and free stream conditions, \$LIST3 enters geometric information, \$LIST4 enters viscosity model and initial profile information and \$LIST5 enters file output information. A description of all the PEPSIS input information will be given below.

Plot File Input

Card 1

<u>Columns</u>	<u>Format</u>	<u>Variable</u>	<u>Function</u>
1-24	6A4	TITLE(I)	Title Card

Card 2

<u>Columns</u>	<u>Format</u>	<u>Variable</u>	<u>Function</u>
1-2	1I2	ISYM	Reciprocal of Symmetry
3-12	1F10.0	SYSTEM	SYSTEM = 1 - Quasi-Cartesian Coordinates SYSTEM = 2 - Quasi-Cylindrical Coordinates

Namelist Input Description

Namelist or variable name	Description
	Restart Options
IRSTIN	<p>Marching station number when data is to be read for restart case.</p> <p>IRSTIN = 0: Dead start case.</p> <p>IRSTIN ≠ 0: Restart case started at station IRSTIN. Default value is 0.</p>
IRSTOT	<p>Interval for saving restart information.</p> <p>IRSTOT = 0: No restart information is saved.</p> <p>IRSTOT ≠ 0: Information is saved at each IRSTOTth station. Default value is 0.</p>
JRSTIN	<p>Logical file name of input restart file. Default value is 10.</p>
JRSTOT	<p>Logical file name of ouput restart file. JRSTOT and JRSTIN do not have to be same file. Default value is 10.</p>
NFILE	<p>File number on unit JRSTIN desired for restart. Default value is 0.</p>
NSAVED	<p>Number of restart stations saved on JRSTOT.</p> <p>On a restart by setting JRSTOT = JRSTIN and NFILE + NSAVED, one file can be used for both reading and writing without destroying the information previously saved. Default is -1.</p>
ICOMP	<p>Flag for computer options:</p> <p>ICOMP = 1: Univac computer option.</p> <p>ICOMP = 2: CDC computer option.</p> <p>ICOMP = 3: IBM computer - virtual memory option.</p> <p>ICOMP = 4: Disk writing computer option Default value is 4.</p>

Namelist Input Description

<u>LIST1</u>	<u>Description</u> <u>Equations and Boundary Conditions</u>
IHSTAG	IHSTAG = 0: Energy equation formulated in terms of static enthalpy. IHSTAG = 1: Energy equation formulated in terms of stagnation enthalpy. IHSTAG = 2: Stagnation enthalpy constant. Default value is 1.
IBOUND(IBC)	Computational domain boundary characteristics (wall or non-wall). IBOUND(IBC) = 1: Solid wall boundary at surface IBC (see list of FORTRAN variables for definition). IBOUND(IBC) = 2: Non-wall boundary at surface IBC. Default values are 1, 1, 2, 1.
IEQBC(IBC, IEQ)	Boundary condition of the governing equation IEQ at solid wall boundary IBC. Default values are: 12*2, 4*16, 4*11, 8*2.
JEQBC(IBC, IEQ)	Boundary condition of the governing equation IEQ at non-wall boundary IBC. Default values are: 4*11, 2*2, 4*11, 2*2, 16*11. Boundary condition options used either IEQBC or JEQBC are as follows: φ: Any dependent variable P: Pressure T: Temperature n= Normal to boundary

Namelist Input Description

<u>Equations and Boundary Conditions</u>		Description	<u>LIST1</u>
<u>Index</u>		<u>Function Type Description</u>	
1		$\Delta\phi = 0$ (No change of ϕ at boundary)	
2		$\phi = 0$	
3		V or W known	
4		ρV or ρW known	
5		$\Delta P = 0$	
6		P = PRESS(IBC)	
7		$\Delta T = 0$	
8		T = TWALL(IBC)	
<u>Derivative Type</u>			
		<u>Description</u>	
11		$\frac{\partial \phi}{\partial n} = 0$ (gradient of ϕ normal to boundary)	
12		Mach line extrapolation using one-sided difference	
13		Slip boundary condition for velocity using wall function	
14		$\frac{\partial P}{\partial n} = 0$ (gradient of pressure normal to boundary)	
15		$\frac{\partial P}{\partial n}$ = curvature (pressure gradient normal to boundary with curvature effects)	

Namelist Input Description

<u>LIST1</u>	<u>Index</u>	<u>Derivative Type Description</u>
	16	Momentum equation in direction normal to boundary
	17	$\frac{\partial T}{\partial n} = 0$ (adiabatic condition for wall or symmetry condition for non-wall)
	18	$\frac{\partial T}{\partial n} = \text{DTDN(IBC)}$
	19	Wall function boundary condition for temperature
	20	$\frac{\partial \phi}{\partial n} = 0$ (same as 11, but applied at one grid point off the wall)
	21	Mach line extrapolation using central difference scheme at one point off the boundary
	41	$\frac{\partial^2 \phi}{\partial n^2} = 0$
	42	$\frac{\partial^2 p}{\partial n^2} = 0$
	43	$\frac{\partial^2 T}{\partial n^2} = 0$
	44	$\frac{\partial U_c}{\partial n_c} = 0$
	45	$\frac{\partial V_c}{\partial n_c} = 0$
	46	$n_c \cdot \nabla p = 0$
	47	$n_c \cdot \nabla T = 0$

LIST1Description

TWALL(IBC)	Specified temperature at boundary IBC. Default values are 4*1.0.
PRESS(IBC)	Specified pressure at boundary IBC. Default values are 4*0.0.
DTDN(IBC)	Specified temperature gradient at boundary IBC at boundary condition. Default values are 4*0.0.
ASW(IBC) BSW(IBC) CSW(IBC) DSW(IBC)	Coefficient of a cubic polynomial fit for IBCth surface to determine the axial location where boundary characteristics at boundary IBC should be changed from wall to non-wall or vice versa, i.e., IBOUND(IBC) automatically changed. Default values are: ASW = 4*1.0E + 10 BSW = 4*0.0 CSW = 4*0.0 DSW = 4*0.0

LIST2Freestream and Reference Conditions

IUNITS	Sentinel for units. IUNITS = 1: English units IUNITS = 2: Metric units Default value is 2.
LREF	Reference length (ft or m) No default.
REPL	Reynolds number per unit length. No default.
MINF	Free stream Mach number. No default.
PINF	Free stream static pressure (lbf/ft^2 or nt/m^2) No default.

LIST2Reference and Reference Conditions

PZERO	Free stream stagnation pressure (lbf/ft^2 or nt/m^2) No default.
PR	Laminar Prandtl number. Default value if 0.74.
PRT	Turbulent Prandtl number. Default value if 1.0.
XOB(IBC)	Location on IBCth surface where the boundary type switches from non-wall to wall. Default values are $4*1.0E + 06$.
ICORD	Flag for coordinate transformation. ICORD = 1: Conformal coordinates ICORD = 2: Nonorthogonal coordinates $X \rightarrow X$ $Y \rightarrow Y$ $Z \rightarrow \zeta(X, Z)$ ICORD = 3: Nonorthogonal coordinates $X \rightarrow X$ $Y \rightarrow \eta(X, Y, Z)$ $Z \rightarrow Z$ Default value is 1.
NE(IADI)	Number of grid points in the Y(IADI = 1) and Z(IADI) = 2) directions. No default values.
NS	Number of last streamwise stations which solution is to marched to. No default value.

LIST2

XENTR, DELX,
IAP(10), AP(10),
DXMIN(10), DXMAX(10)

Freestream and Reference Conditions

XENTR is the initial streamwise location. DELX is the initial stepsize in the streamwise (marching direction, i.e., $X(2) = XENTR + DELX$). At streamwise station I the streamwise position is given by $X(I) = X(I-1) + AP(X(I-1) - X(I-2))$ where if AP is greater than 1.0, the streamwise step size will increase by $(AP-1.0)$ percent each step. If AP is less than 1.0, the streamwise step size will decrease by $(1.0-AP)$ percent each step. DXMIN and DXMAX are lower and upper overriding limits on the step size. AP, DXMIN and DXMAX are dimensional so that streamwise step size variation can be changed by the IAP parameter, IAP denoting the streamwise location where these variables change. Values of XENTR and DELX should normally only be set on the initial run as these variables are automatically calculated for restarts.

XENTR, DELX,
IAP(10), AP(10),
DXMIN(10), DXMAX(10)
(CONTINUED)

XENTR = 0.0
DELX = No default value
IAP = 1,9*1000000
AP = 10*1.0
DXMIN = 10*0.0
DXMAX = 10*1.0E + 06

IGEOM

Flag for coordinate options
IGEOM = 1: Cartesian coordinates
IGEOM = 2: Cylindrical coordinates
IGEOM = 3: Polar coordinates
IGEOM =10: General orthogonal coordinates
(Cartesian in cross plane)
IGEOM =11: General orthogonal coordinates
(axisymmetric)
Default value is 1.

LIST3

Geometric Options

LIST4

Initial Profile, Turbulence Information

LIST4Initial Profile, Turbulence Information

CFP(BCP)

Skin friction coefficient on surface IBCP needed to generate the initial turbulent boundary layer profile.

No default values.

IPROF

Flag for initial profile options.

IPROF = 1: Freestream profiles

IPROF = 2: Initial profiles supplied by user

IPROF = 3: Boundary layer profiles based on necessary input

IPROF = 4: Same as IPROF = 3, but angular components are obtained for general orthogonal coordinates

Default value is 1.

IMIXL

Flag for mixing length options.

IMIXL = 1: McDonald-Camarrata mixing length model based on prescribed boundary layer thickness (DELTAB). With wall shear value used to calculate nondimensional distance

IMIXL = 2: Buleev mixing length model

IMIXL = 3: McDonald-Camarrata mixing length model based on dynamically obtained boundary layer thickness with fixed wall shear

IMIXL = 4: Same as IMIXL = 1, but local shear is used to calculate nondimensional distance

IMIXL = 5: Same as IMIXL = 3, but local shear is used

Default value is 1.

BETA

Angle of attack in degrees.

Default value is 0.0.

YAW

Yaw angle in degrees.

Default value is 0.0.

LIST4Initial Profile, Turbulence Information

IVISC

Flag for viscosity options.

IVISC = 1: Constant viscosity

IVISC = 2: Laminar viscosity obtained from
Sutherland's relationIVISC = 3: Turbulent viscosity is obtained
from mixing length model
Sutherland's law for laminar viscosity;IVISC = 4: Turbulent viscosity obtained from
TKE - mixing length model
Sutherland's law for laminar viscosity;
Default value is 1.

DELTAB(IBC)

Specified boundary layer thickness on surface IBC
for mixing length model of turbulence.
No default values.

ITRANS

Flag which tells whether transition turbulence
model logic is used.

ITRANS = 0: No transitional model is used

ITRANS ≠ 0: Transitional model is used
Default value is 0.

IBLT

Flag which tells whether boundary layer thickness
is input or calculated dynamically.

IBLT = 0: Boundary layer thickness is input

IBLT ≠ 0: Boundary layer thickness is dynamically
calculated.

Default values is 0.

TKEINF

Freestream turbulent kinetic energy.
is 0.0.

Default value is 0.0.

IVARPR(I)

Index of variables to be printed. Needed only for
three-dimensional flow.

IVARPR(I) = 0: No print

IVARPR(I) = 1: Print every IPRINT steps

IVARPR(I) = 2: Print every JPRINT steps

Default values are 5*1, 2*0, 3+1, 7+0.

LIST4Initial Profile, Turbulence Information

I = 1: UVEL
I = 2: VUEL
I = 3: WVEL
I = 4: Density
I = 5: Enthalpy
I = 6: Turbulent kinetic energy
I = 7: Turbulent dissipation
I = 8: Pressure
I = 9: Temperature
I = 10: Mach Number
I = 11: Mach Number Indicator
I = 12: Stagnation temperature
I = 13: Stagnation pressure
I = 14: Pressure coefficient
I = 15: Laminar viscosity
I = 16: Mixing length
I = 17: Turbulent viscosity
I = 18: Effective viscosity

IPLOT

Marching station interval for storage of plotting information.

IPLOT = 0: No plotting

IPLOT ≠ 0: Store plotting information every IPLOT station; IPLOT cannot be changed during a run.

Default value is 0.

IPRINT

Primary marching station interval for printing.

Default value is 1.

JPRINT

Secondary marching station interval for printing.

Default value is 1.

Error Conditions in the PEPSIS Computer Code

Failure of the PEPSIS computer code to successfully execute a runstream can occur because of either inconsistent or incorrect input data or because of an attempt to apply the PEPSIS code to a case where the physics violate the assumptions inherent in the code. This section will address only the former mode of failure. Avoidance of the latter failure mode is dependent primarily on the users understanding of the basic physics of the case he is going to run, and the degree to which the PEPSIS code can be expected to model the physics.

One method of discussing the inconsistent or incorrect input data mode of failure is by examining the possible failures in the various subroutines. Since the individual subroutines are responsible for separate tasks during the execution of a run, (e.g. overall control of the program geometry generation, etc.), this technique will in essence outline the possible failure modes as the tasks are performed. Discussion will occur in the same order as the run is executed.

SUBROUTINE RESTRT

There are two modes by which SUBROUTINE RESTRT can fail. Both involve improper use of the restart file. A message, RESTART INFORMATION REQUESTED AT (IRSTIN marching number) BUT STORED INFORMATION AT SEQUENCE (NFILE) IS AT STATION (Station number). This message occurs because the marching station number read off the NFILEth restart file does not match the input value of IRSTIN. The corrective action is to make NFILE and IRSTIN consistent with each other. Another possible mode of failure occurs when NFILE exceeds the number of files on the restart device, JRSTIN, in which case an END OF INFORMATION (or analogous statement) will appear in the day file. The corrective action is to recheck the input value of NFILE. If JRSTIN ≠ JRSTOT, the value of NFILE is the number of the restart on device JRSTIN.

SUBROUTINE INPUTS

There are two failure modes in SUBROUTINE INPUTS. In the first case, the message NS = (input value of NS) GREATER THAN NSMAX = (dimension of X vector) will be printed if the number of marching stations exceeds the

dimensioned value of X, the streamwise locations. The corrective action is to lower the value of NS. The second failure mode occurs when the Buleev turbulence model is specified for a two-dimensional case. Since this model is not applicable to two-dimensional cases, the message CANNOT USE BULEEV TURBULENCE MODEL IN TWO-DIMENSIONAL FLOW is printed. The corrective action is to specify an alternate turbulence model.

SUBROUTINE GEOTRB

At present SUBROUTINE GEOTRB is coded to calculate metric information for values of IGEOM = 1, 2, 3, 10 and 11. Values of IGEOM 4-9 are left for various coordinates that may be coded in the future. Input value of IGEOM = 4-9 will result in the message INVALID OPTION IN GEOTRB. The corrective action is to either change the value of IGEOM or to code in a new option. For IGEOM options 10 and 11 (conformal-Cartesian cross-section and conformal-axisymmetric cross-section) the metric information is externally generated by the ADD computer code. In this case, logical file units JDRUM and KDRUM must be defined. JDRUM contains the ADD code data which is then interpolated onto the PEPSIS mesh system. If the PEPSIS values of the streamwise coordinate is less than the first value of the ADD code streamwise coordinate no streamwise interpolation is possible and the message FAILURE IN GEOTRB - SQ12 = (PEPSIS position) SQ1 = (first ADD code position) SQ2 = (second ADD code position). The corrective action is to increase the value of XENTR (the first PEPSIS position) to a value greater than SQ1. On the other hand, if the value of a PEPSIS streamwise coordinate exceeds the last streamwise position generated by the ADD code an END OF INFORMATION message will appear in the day file. The corrective action is to either rerun the ADD code such that the maximum PEPSIS streamwise coordinate does not exceed the maximum ADD code streamwise coordinate or to reduce the maximum PEPSIS streamwise coordinate to an acceptable value.

SUBROUTINE INTEBC

SUBROUTINE INTEBC performs a two-dimensional linear interpolation of the transpiration schedules on both X-Y planes at X-Z planes. If the number of streamwise stations on a surface at which data is input exceeds 15 (the dimensioned size of the data arrays) a message FAILURE IN INTEBC VALUE OF

NPTSX (surface number IBC) = (value of NPTSX(IBC) EXCEEDS DIMENSION LIMITS OF 15 is printed. The corrective action is either to updimension NPTSX and associated variables or to decrease the value of NPTSX. Likewise, in the Y or Z direction data can be input at up to 15 locations. If the value of NPTSYZ exceeds 15, the message FAILURE IN INTEBC VALUE OF NPTSYZ (streamwise location, surface number) = (value of NPTSYZ) EXCEEDS DIMENSION LIMITS OF 15 is printed. The corrective action is either to updimension NPTSYZ and associated variables or to decrease the value of NPTSYZ.

SUBROUTINE QUICK

If the choice of boundary conditions is incorrectly made, it is possible that a singular matrix will result. This will manifest itself in SUBROUTINE QUICK in an attempt to divide by zero. The corrective action is to re-evaluate the choice of input boundary conditions to determine the source of the singularity. An example of an improper choice of a boundary condition set would be to choose as boundary conditions the three no-slip conditions for the three momenta equations, the normal pressure condition for the continuity equation and the normal momentum equation for the enthalpy equation. In this case, the enthalpy does not appear in any of the boundary conditions, and hence a singular matrix would result.

SUBROUTINE CROSEC

Often, if a case is not going to successfully run, the code will cease operation in SUBROUTINE CROSEC. This will occur because of the existence of a negative temperature in which case the Mach number calculation will fail in SQRT. There can be many reasons for this failure mode. Usually, however, it can be related to inadequate numerical resolution of the physical processes that are occurring. For instance, a lack of transverse grid points might lead to large oscillations in the pressure or too large a streamwise step in the region where a wall inclination is rapidly changing might result in a temperature becoming negative. Sometimes it is difficult to know a priori what grid resolution is necessary for a given problem. Usually, experimentation with two-dimensional cases can provide some guidelines for three-dimensional cases. This in addition with the users' overall experience with the code and his understanding of the physical processes will usually provide the means of resolving the above problem.

PEPSIS FORTRAN VARIABLES

FORTRAN SYMBOL	COMMON BLOCK	DESCRIPTION
ACON	LAWW	CONSTANT IN ARGUMENT OF EXPONENTIAL FUNCTION FOR TRANSITIONAL MODEL
AG(NN,9,2)	OPER	DIFFERENCE WEIGHTS IN PHYSICAL COORDINATES
AGEO	GEOM	COEFFICIENTS OF POLYNOMIAL FIT FOR BOUNDARY SHAPE
AG1D(9)	EGCOM	TEMPORARY STORAGE ARRAY OF METRIC INFORMATION
AG1P	EGCOM	TEMPORARY STORAGE ARRAY OF METRIC INFORMATION
AG2D(9)	EGCOM	TEMPORARY STORAGE ARRAY OF METRIC INFORMATION
AHP(5)	EGCOM	TEMPORARY STORAGE ARRAY OF METRIC INFORMATION
AH1D(5,9)	EGCOM	TEMPORARY STORAGE ARRAY OF METRIC INFORMATION
AIE(NN,7)	PFILE	INITIAL PROFILE ARRAY
AM(NCPLD,3*NCPLD+1)CCOM		UTILITY MATRIX USED IN BLOCK MATRIX INVERSION
AMACRT	SUPER	MACH NUMBER CRITERION USED IN LOCATING SONIC LINE
AN(NEQS,NN)	LIN	STORAGE FOR LINEARIZATION COEFFICIENTS OF X - DERIVATIVES
AP(10)	GEOM	AMPLIFICATION RATE OF MARCHING STEP SIZE
APLUS	LAWW	CONSTANT IN ARGUMENT OF EXPONENTIAL FUNCTION FOR VAN DRIEST DAMPING FORMULA
ASW(4)	BOUND	COEFFICIENTS OF POLYNOMIAL FIT FOR SWITCHING THE BOUNDARY SURFACE TYPE
AVISC(2,NEQS)	VISC	COEFFICIENT USED IN ARTIFICIAL DAMPING
BETA	REF	ANGLE OF ATTACK
BGEO	GEOM	COEFFICIENTS OF POLYNOMIAL FIT FOR BOUNDARY SHAPE
BLOCK1(IADD3)		STORAGE FOR ADD CODE METRIC INFORMATION EQUIVALENCED TO C(1,1,1)
BLOCK2(IADD3)		STORAGE FOR ADD CODE METRIC INFORMATION EQUIVALENCED TO C(1,1,NN/2+1)

FORTRAN SYMBOL	COMMON BLOCK	DESCRIPTION
BLTH(NN,4)	LAWW	DYNAMICALLY DETERMINED BOUNDARY LAYER THICKNESS
BSW(4)	BOUND	COEFFICIENTS OF POLYNOMIAL FIT FOR SWITCHING THE BOUNDARY SURFACE TYPE
BWD	LIN	CRANK-NICHOLSON FACTOR
BWDI	LIN	INVERSE OF BWD
C(NN,NCPLD,NN)	CCOM	BLOCK DIAGONAL MATRIX ELEMENTS
CDUM(NDIM)		TEMPORARY STORAGE ARRAY TO ROTATE DATA FROM COLUMNS TO ROWS AND VICE VERSA - EQUIVALENCED TO C(1,1,1) NDIM = MZVAR * MLEVEL * NN
CEP(4)	PFILE	SKIN FRICTION COEFFICIENT
CGEO	GEOM	COEFFICIENTS OF POLYNOMIAL FIT FOR BOUNDARY SHAPE
CMUINE	VISC	CONSTANT IN TURBULENT VISCOSITY MODEL
CONGEO(11*NN)	GEOM	COORDINATE TRANSFORMATION INFORMATION
CONVDR	UNITS	CONVERSION FACTOR IN GOING FROM DEGREES TO RADIANS
CONVRD	UNITS	CONVERSION FACTOR IN GOING FROM RADIANS TO DEGREES
COOR(NN,4)	GEOM	PHYSICAL COORDINATE INFORMATION WITH RESPECT TO ABSOLUTE ORIGIN AT N+1ST STREAMWISE LOCATION
COORN(NN,4)	GEOM	PHYSICAL COORDINATE INFORMATION WITH RESPECT TO ABSOLUTE ORIGIN AT NTH STREAMWISE STATION
CPINF	FREE	FREE STREAM SPECIFIC HEAT
CPREF	REF	REFERENCE PRESSURE COEFFICIENT
CPREFI	REF	INVERSE OF REFERENCE PRESSURE COEFFICIENT
CRITU	OPER	CRITICAL VELOCITY USED FOR FLARE APPROXIMATION
CSOLN(NCPLD,NN)	CCOM	SOLUTION TO BLOCK TRI-DIAGONAL MATRIX INVERSION
CSW(4)	BOUND	COEFFICIENTS OF POLYNOMIAL FIT FOR SWITCHING THE BOUNDARY SURFACE TYPE

FORTRAN SYMBOL	COMMON BLOCK	DESCRIPTION
CIWO	REF	NUMERICAL CONSTANT IN GOVERNING EQUATION
CXI(NDIEM)	ADDR	STORAGE FOR FIRST DERIVATIVE DIFFERENCE WEIGHTS
CXXI(NDIFM)	ADDR	STORAGE FOR SECOND DERIVATIVE DIFFERENCE WEIGHTS
C1(NN)	CCOM	SUBDIAGONAL MATRIX ELEMENTS
C1SUTH	VISC	COEFFICIENT IN SUTHERLAND'S LAW OF LAMINAR VISCOSITY
C2(NN)	CCOM	DIAGONAL MATRIX ELEMENTS
C2SUTH	VISC	COEFFICIENT IN SUTHERLAND'S LAW OF LAMINAR VISCOSITY
C3(NN)	CCOM	SUPERDIAGONAL MATRIX ELEMENTS
C4(NN)	CCOM	VECTOR ELEMENTS
D	VAR	INDEX FOR DIVERGENCE
DELMAX(NEQS)	EQN	MAXIMUM VALUES OF THE DELTAS
DELTAB(4)	LAWW	SPECIEIED BOUNDARY LAYER THICKNESS FOR MIXING LENGTH MODEL OF TURBULENCE
DELTAP(4)	PFILE	BOUNDARY LAYER THICKNESS
DELX	GEOM	STEP SIZE IN MARCHING DIRECTION
DGEO	GEOM	COEFFICIENTS OF POLYNOMIAL FIT FOR BOUNDARY SHAPE
DIFOP(6)	OPER	DIFFERENCE WEIGHTS IN COMPUTATIONAL COORDINATES
DL	VAR	STORAGE LEVEL OF DIVERGENCE IN GENERAL PURPOSE STORAGE
DM1(NCPLD,NCPLD)	CCOM	GENERAL PURPOSE STORAGE ARRAYS FOR BLOCK TRI-DIAGONAL MATRIX INVERSION
DM2(NCPLD)	CCOM	GENERAL PURPOSE STORAGE ARRAYS FOR BLOCK TRI-DIAGONAL MATRIX INVERSION
DM3(NCPLD,NCPLD)	CCOM	GENERAL PURPOSE STORAGE ARRAYS FOR BLOCK

FORTRAN SYMBOL	COMMON BLOCK	DESCRIPTION
		TRI-DIAGONAL MATRIX INVERSION
DS	VAR	INDEX FOR DISSIPATION FUNCTION
DSL	VAR	STORAGE LEVEL OF DISSIPATION FUNCTION IN GENERAL PURPOSE STORAGE
DSW(4)	BOUND	COEFFICIENTS OF POLYNOMIAL FIT FOR SWITCHING THE BOUNDARY SURFACE TYPE
DTDN(4)	BOUND	SPECIFIED TEMPERATURE GRADIENT NORMAL TO BOUNDARY
DTDNW(NN,4)	BOUND	STORAGE ARRAY FOR TEMPERATURE GRADIENT NORMAL TO BOUNDARY
DX	OPER	STEP SIZE IN X-DIRECTION
DXI	OPER	INVERSE OF DX
DXMAX(10)	GEOM	MAXIMUM MARCHING STEP SIZE
DXMIN(10)	GEOM	MINIMUM MARCHING STEP SIZE
D1(NEQS,NDIEM,NN)	LIN	STORAGE FOR LINEARIZATION COEFFICIENTS OF Y - DERIVATIVES
D1L(NEQS,NDIEM)	LIN	STORAGE OF LINEARIZATION COEFFICIENT FOR TEMPERATURE AND PRESSURE COMPUTATION
D2(NEQS,NDIEM,NN)	LIN	STORAGE FOR LINEARIZATION COEFFICIENTS OF Z - DERIVATIVES
E(NN,NCPLD,NN)		ARRAY USED IN MGAUSS ERROR CHECK - EQUIVALENCED TO C(1,1,1)
EPS	VAR	INDEX FOR DISSIPATION OF TURBULENCE KINETIC ENERGY
EPSMWE	LAWW	CONVERGENCE CRITERION FOR WALL FUNCTION FORMULATION
F(14,NN)	ZPLOT	TEMPORARY STORAGE FOR PLOT INFORMATION

FORTRAN SYMBOL	COMMON BLOCK	DESCRIPTION
FACLM(4)	LAWW	MULTIPLICATION FACTOR TO BOUNDARY LAYER THICKNESS
FG(8,3,NN)	METRIC	STORAGE FOR METRIC COEFFICIENTS AND DERIVATIVES
GAM(3)	GEOM	COORDINATE TRANSFORMATION COEFFICIENT FOR BOUNDARY CONDITIONS
GAMMA	REE	RATIO OF SPECIFIC HEATS
GC	UNITS	GRAVITY CONSTANT
H	VAR	INDEX FOR ENTHALPY
HFORM	REE	HEAT OF FORMATION
HINF	FREE	FREE STREAM ENTHALPY
HREF	REF	REFERENCE ENTHALPY
HREFI	REF	INVERSE OF REFERENCE ENTHALPY
IA	CCOM	INDEX REFERRING TO SUBDIAGONAL MATRIX ELEMENTS
IADDO(NDIEM)	ADDR	ADDRESSES IN THE OPPOSITE DIRECTION
IADDP(NDIEM)	ADDR	ADDRESSES IN THE PRIMARY DIRECTION
IADDS1(NN)	ADDRE	ADDRESS FOR POINT LOGIC OF FLUID VARIABLES
IADDS2(NDIEM,NN)	ADDRE	ADDRESS FOR Y DERIVATIVE OF FLUID VARIABLES
IADDS3(NDIEM,NN)	ADDRE	ADDRESS FOR Z DERIVATIVE OF FLUID VARIABLES
IADDS4(NDIEM**2,NN)	ADDRE	ADDRESS FOR MIXED DERIVATIVE OF FLUID VARIABLES
IADDS5(NDIEM**2,NN)	ADDRE	ADDRESS FOR MIXED DERIVATIVE OF FLUID VARIABLES
IADD1	ADD	NO. OF GEOMETRIC VARIABLES USED IN ADD CODE
IADD2	ADD	NO. OF TRANSVERSE GRIDPOINT USED IN ADD CODE
IADD3	ADD	RECORD SIZE USED IN ADD CODE
IADI	SWEET	ADI SWEEP DIRECTION
IADIM1	SWEET	IADI - 1
IAP(10)	GEOM	MARCHING STEP INDEX AT WHICH AP,DXMIN,DXMAX

FORTRAN SYMBOL	COMMON BLOCK	DESCRIPTION
		ARE REINITIALIZED
IB	CCOM	INDEX REFERRING TO DIAGONAL MATRIX ELEMENTS
IBC	BOUND	INDEX FOR BOUNDARY SURFACE IDENTIFICATION
IBCP	PFILE	BASIC SURFACE FOR INITIAL PROFILE GENERATION
IBLT	LAWW	FLAG WHICH TELLS WHETHER BOUNDARY LAYER THICKNESS IS INPUT OR CALCULATED DYNAMICALLY
IBOUND(4)	BOUND	BOUNDARY SURFACE TYPE INDICATOR
IC	CCOM	INDEX REFERRING TO SUPERDIAGONAL MATRIX ELEMENTS
ICDC(NN+1,2)	CDC	RECORD INDEX FOR READMS AND WITEMS MASS STORAGE DEVICES-CDC COMPUTER ONLY
ICOMP	REST	FLAG FOR COMPUTER OPTIONS
ICONS(3,NEQS)	OPER	FLAG FOR CONVECTIVE FORMULATION BASED ON MACH NUMBER AND EQUATION
ICORD	GEOM	FLAG FOR COORDINATE TRANSFORMATION OPTIONS
ICPLD(NEQS,2)	EQN	COUPLED EQUATION SENTINEL
ID	CCOM	INDEX REFERRING TO VECTOR MATRIX ELEMENTS
IDIF(40)	OPER	INDEX FOR TYPE OF DIFFERENCING OF BOUNDARY CONDITIONS
IDMPY	DMP	DUMP LINE NO. IN Y DIRECTION
IDMPZ	DMP	DUMP LINE NO. IN Z DIRECTION
IDUM2(NN)	ADDRG	INDICATOR OF THE POINT IN DIFFERENCE MOLECULE WHERE Y DERIVATIVE IS TAKEN
IDUM3(NN)	ADDRG	INDICATOR OF THE POINT IN DIFFERENCE MOLECULE WHERE Z DERIVATIVE IS TAKEN
IEQ	EQN	EQUATION NUMBER INDEX
IEQRC(4,NEQS)	BOUND	SPECIFIED BOUNDARY CONDITION FOR WALL

FORTRAN SYMBOL	COMMON BLOCK	DESCRIPTION
IEQNUM(NEQS)	EQN	IDENTIFICATION NUMBER OF EQUATIONS TO BE SOLVED
IFLARE	OPER	SENTINEL WHICH TELLS IF FLARE OPTION IS USED
IGDMP	DMP	FLAG FOR DUMP OPTIONS
IGEOM	GEOM	FLAG FOR COORDINATE SYSTEM OPTIONS
IH	GRID	UPPER BOUNDARY POINT ON THE LINE WHERE IMPLICIT SOLUTION IS OBTAINED
IHSITAG	EQN	FLAG FOR ENERGY EQUATION OPTIONS
IJ	DIFCOM	COLUMN OR ROW NUMBER ON WHICH CALCULATION IS BEING MADE
IL	GRID	LOWER BOUNDARY POINT ON THE LINE WHERE IMPLICIT SOLUTION IS OBTAINED
IMIXL	LAWW	FLAG FOR MIXING LENGTH OPTIONS
IND	VAR	FLAG WHICH TELLS IF MESH POINT BELONGS TO SUPERSONIC OR SUBSONIC REGION
INDC(NN)	DIFCOM	MACH NUMBER INDICATOR
INDL	VAR	STORAGE OF MACH NUMBER INDICATOR IN GENERAL PURPOSE STORAGE
INH12	ADD	SENTINEL USED TO DETERMINE FORMULATION USED IN CALCULATION OF TRANSVERSE DERIVATIVE OF H1
INH21	ADD	SENTINEL USED TO DETERMINE FORMULATION USED IN CALCULATION OF STREAMWISE DERIVATIVE OF H2
INH31	ADD	SENTINEL USED TO DETERMINE FORMULATION USED IN CALCULATION OF STREAMWISE DERIVATIVE OF H3
INH32	ADD	SENTINEL USED TO DETERMINE FORMULATION USED IN CALCULATION OF TRANSVERSE DERIVATIVE OF H3
IOPTWF	LAWW	SENTINEL WHICH DETERMINES WALL FUNCTION FORMULATION

FORTRAN SYMBOL	COMMON BLOCK	DESCRIPTION
IOPTYZ(3,NEQS,2)	OPER	FLAG FOR DIFFERENCING FORMULATION BASED ON MACH NUMBER, EQUATION, AND ADI DIRECTION
IPLOT	CIO	MARCHING STATION INTERVAL FOR STORAGE OF PLOTTING INFORMATION
IPRINT	CIO	PRIMARY MARCHING STATION INTERVAL FOR PRINTING
IPROF	PRFILE	FLAG FOR INITIAL PROFILE OPTIONS
IPRTE	GASL	FLAG WHICH DETERMINES EQ. OF STATE FORMULATION
IRSTIN	REST	STREAMWISE STATION NUMBER FOR RESTART
IRSTOT	REST	STREAMWISE INTERVAL FOR SAVING RESTART INFORMATION
ISONIC	SUPER	FLAG FOR SONIC LINE INTERPOLATION LOGIC
ISS(NN,4)	SUPER	GRID POINT LOCATION OF SONIC LINE
ISSHET	SUPER	INDEX USED TO DETERMINE IF SONIC LINE IS LAST SUBSONIC POINT OR FIRST SUPERSONIC POINT
ISTART	METRIC	INITIAL CONDITION INDEX
ISW	UNIVAC	SENTINEL FOR WORD ADDRESSABLE OR SECTOR-ORIENTED MASS STORAGE DEVICE - UNIVAC ONLY
ISYM	ZPLOT	SYMMETRY OPTION FOR PLOTS
ITRANS	LAWW	FLAG WHICH TELLS WHETHER TRANSITION TURBULENCE MODEL LOGIC IS USED
IUNITS	UNITS	FLAG USED TO DETERMINE SET OF DIMENSION UNITS USED
IVARNO(NEQS)	EQN	IDENTIFICATION NUMBER OF DEPENDENT VARIABLES
IVARPR(25)	PRNT	INDEX OF VARIABLES TO BE PRINTED
IVISC	VISC	FLAG FOR VISCOSITY OPTIONS
IWAFL	VISC	SENTINEL WHICH DETERMINES IF WALL FUNCTION LOGIC IS NEEDED IN THE CALCULATION OF WALL

FORTRAN SYMBOL	COMMON BLOCK	DESCRIPTION
		VISCOSITY
IWR	CIO	SENTINEL FOR NAMELIST REST PRINT
IYGD(NDIEM)	ADDR	GEOMETRY ADDRESSES
IZCT(3)	ZEX1	RELATIVE UNIT NO. FOR VIRTUAL MEMORY STORAGE
I1IG(8,3)	FGCOM	INDEX NEEDED IN THE CALCULATION OF METRIC INFORMATION
I2IG(8,3)	FGCOM	INDEX NEEDE IN THE CALCULATION OF METRIC INFORMATION
JA(3)	ADDRE	SHIFT LOGIC INDEX
JADDO(NDIEM)	ADDR	ADDRESSES IN THE OPPOSITE DIRECTION
JADDP(NDIEM)	ADDR	ADDRESSES IN THE PRIMARY DIRECTION
JBOUND(NN,4)	BOUND	BOUNDARY TYPE INDICATOR AT EACH POINT ON BOUNDARY
JDMAX	EQN	Y GRID POINT LOCATION OF MAXIMUM DELTA
JDRUM	CIO,	ADD CODE DEVICE
JDUM	DIFCOM	INDEX DENOTING RELATIVE POINT ABOUT WHICH DERIVATIVE IS LOCATED
JEQBC(4,NEQS)	BOUND	SPECIFIED BOUNDARY CONDITION FOR NON-WALL
JEQN(NEQS,2)	EQN	EXTERNAL EQUATION NUMBER
JGSTOR	LIN	VALUE OF JG NEEDED BY SUBROUTINE EOS
JPLOT	CIO	DEVICE FOR PLOTTING
JPRINT	CIO	SECONDARY MARCHING STATION INTERVAL FOR PRINTING
JPROF(4)	PFILE	SENTINEL FOR BOUNDARY VALUES DURING INITIAL PROFILE GENERATION
JRSTIN	REST	LOGICAL FILE FROM WHICH RESTART INFORMATION IS READ
JRSTOT	REST	LOGICAL FILE ON WHICH RESTART INFORMATION

FORTRAN SYMBOL	COMMON BLOCK	DESCRIPTION
		IS WRITTEN
JVAR(NEQS,2)	EQN	VARIABLE NUMBER ASSOCIATED WITH EACH EQUATION DURING AN ADI SWEEP
JWR(5)	CIO	SENTINEL FOR NAMELIST PRINT OPTION
JX	OPER	RELATIVE MARCHING STATION COUNTER
JXDUM	OPER	ABSOLUTE MARCHING STATION COUNTER
JXDUMP	DMP	MARCHING STATION WHEN DUMP OUTPUT IS REQUESTED
KA(5)	ADDRG	INDICES NECESSARY TO CALCULATE GEOMETRIC GROUPINGS
KDMAX	EQN	Z GRID POINT LOCATION OF MAXIMUM DELTA
KDRUM	CIO	DEVICE FOR TEMPORARY STORAGE - USED IN GEOMETRY GENERATION
LADD(3)	BOUND	ADDRESSES FOR BOUNDARY CONDITIONS
LDRUM	CIO	DEVICE FOR FINAL METRIC INFORMATION
LEQ1	EQN	LOWEST INDEX OF EQUATIONS SOLVED EITHER BY COUPLED OR UNCOUPLED ADI SWEEP
LEQ2	EQN	HIGHEST INDEX OF EQUATIONS SOLVED EITHER BY COUPLED OR UNCOUPLED ADI SWEEP
LEV(3)	ADDR	GEOMETRY LEVEL
LEVEL	ADDRG	GEOMETRY LEVEL
LGA1(NN)	ADDRG	ADDRESS FOR POINT LOGIC OF GEOMETRIC VARIABLES
LGA2(NDIEM,NN)	ADDRG	ADDRESS FOR Y - DERIVATIVE OF GEOMETRIC VARIABLES
LGA3(NDIEM,NN)	ADDRG	ADDRESS FOR Z - DERIVATIVE LOGIC OF GEOMETRIC VARIABLES
LGA4(NDIEM**2,NN)	ADDRG	ADDRESS FOR CROSS DERIVATIVE(Y-Z) LOGIC OF GEOMETRIC VARIABLES

FORTRAN SYMBOL	COMMON BLOCK	DESCRIPTION
LGAS(NDIEMAX2,NN)	ADDRG	ADDRESS FOR CROSS DERIVATIVE(Z-Y) LOGIC OF GEOMETRIC VARIABLES
LREF	REF	REFERENCE LENGTH
LREFI	REF	INVERSE OF REFERENCE LENGTH
LSHFT	GEOM	SHIFT INDEX FOR COORDINATE TRANSFORMATION
LVG(8)	BOUND	BOUNDARY POINT INDICATOR FOR BOUNDARY CONDITION
MASS1	CIO	GENERAL PURPOSE MASS STORAGE DEVICE
MASS2	CIO	GENERAL PURPOSE MASS STORAGE DEVICE
MCPLD	EQN	NUMBER OF COUPLED EQUATIONS TO BE SOLVED
MEFF	VAR	INDEX FOR EFFECTIVE VISCOSITY
MEFEL	VAR	STORAGE LEVEL OF EFFECTIVE VISCOSITY IN GENERAL PURPOSE STORAGE
MEQK	EQN	LEQ1 - 1
MEQS	EQN	TOTAL NUMBER OF EQUATIONS TO BE SOLVED
MEQS1	EQN	INDEX OF FIRST EQUATION TO BE SOLVED
MEQS2	EQN	INDEX OF LAST EQUATION TO BE SOLVED
MGDMP	DMP	FLAG FOR DUMP OPTIONS
MGD1	GRID	IL + 1
MGD2	GRID	IH - 1
MIN	CIO	INPUT DEVICE
MINE	FREE	FREE STREAM MACH NUMBER
ML	VAR	INDEX FOR MIXING LENGTH
MLEVEL	PARAM	MAXIMUM NO. OF STORAGE LEVELS
MLL	VAR	STORAGE LEVEL OF MIXING LENGTH IN GENERAL PURPOSE STORAGE
MN	VAR	INDEX FOR MACH NUMBER

FORTRAN SYMBOL	COMMON BLOCK	DESCRIPTION
MNL	VAR	STORAGE LEVEL OF MACH NO IN GENERAL PURPOSE STORAGE
MOUT	CIO	OUTPUT DEVICE
MREF	REF	REFERENCE MACH NUMBER
MREFI	REF	INVERSE OF REFERENCE MACH NUMBER
MSDD	CIO	TEMPORARY MASS STORAGE DEVICE
MSD1	CIOD	GENERAL PURPOSE MASS STORAGE DEVICE
MSD2	CIOD	GENERAL PURPOSE MASS STORAGE DEVICE
MSGVAR(25)	PRNT	TITLE OF VARIABLES TO BE PRINTED
MU	VAR	INDEX FOR LAMINAR VISCOSITY
MUINE	FREE	FREE STREAM LAMINAR VISCOSITY
MUL	VAR	STORAGE LEVEL OF LAMINAR VISCOSITY IN GENERAL PURPOSE STORAGE
MUREF	REF	REFERENCE VISCOSITY
MUREFI	REF	INVERSE OF REFERENCE VISCOSITY
MUT	VAR	INDEX FOR TURBULENT VISCOSITY
MUTL	VAR	STORAGE LEVEL OF TURBULENT VISCOSITY IN GENERAL PURPOSE STORAGE
MWINE	FREE	FREE STREAM MOLECULAR WEIGHT
MWREF	REF	REFERENCE MOLECULAR WEIGHT
MWREFI	REF	INVERSE OF REFERENCE MOLECULAR WEIGHT
MZVAR	PARAM	MAXIMUM NUMBER OF STORAGE VARIABLES
NABC	CCOM	NABC = ID
NANG	METRIC	ANGLE OF COORDINATE LINES RELATIVE TO HORIZONTAL
NCPLD	PARAM	MAXIMIUN NUMBER OF COUPLED EQUATIONS
NCPLD2	CCOM	NCPLD**2

FORTRAN SYMBOL	COMMON BLOCK	DESCRIPTION
NCTR	DIFCOM	CENTER OF DIFFERENCE MOLECULE
NCUP	EQN	NUMBER OF COUPLED EQUATIONS
NDIEM	PARAM	MAXIMUM NUMBER OF GRID POINTS IN A DIFFERENCE MOLECULE
NDIEM1	DIFCOM	2*NDIEM
NDIEM1	DIFCOM	NDIEM - 1
NDIEP1	DIFCOM	NDIEM + 1
NE(2)	GEOM	NUMBER OF GRID POINTS IN Y AND Z DIRECTIONS
NEQN(NEQS,2)	EQN	NUMBER OF COUPLED EQUATIONS TO BE SOLVED IN EACH ADI SWEEP
NEQS	PARAM	MAXIMUM NUMBER OF EQUATIONS IN CODE
NEY	GRID	NUMBER OF GRID POINTS IN Y DIRECTION
NEYM1	GRID	NEY - 1
NEZ	GRID	NUMBER OF GRID POINTS IN Z DIRECTION
NEZM1	GRID	NEZ - 1
NE2S	CIO	SENTINEL FOR SPREADING OF 2-D PROFILE TO 3-D
NFILE	REST	SEQUENCE NUMBER OF RESTART INFORMATION
NGEOMV	METRIC	NUMBER OF METRIC COEFFICIENTS AND DERIVATIVES
NH1	METRIC	INDEX FOR METRIC COEFFICIENT IN X-DIRECTION
NH12	METRIC	INDEX FOR DERIVATIVE OF X METRIC IN Y DIRECTION
NH2	METRIC	INDEX FOR METRIC COEFFICIENT IN Y-DIRECTION
NH21	METRIC	INDEX FOR DERIVATIVE OF Y METRIC IN X DIRECTION
NH3	METRIC	INDEX FOR METRIC COEFFICIENT IN Z-DIRECTION
NH31	METRIC	INDEX FOR DERIVATIVE OF Z METRIC IN X DIRECTION
NH32	METRIC	INDEX FOR DERIVATIVE OF Z METRIC IN Y DIRECTION
NIIT	CIO	NO. OF FALSE MARCHING STEPS USED TO GENERATE

FORTRAN SYMBOL	COMMON BLOCK	DESCRIPTION
		THE INITIAL PROFILE
NJD	DIECOM	GRID POINT LOCATION FOR START OF SECOND SWEEP
NMAXWE	LAWW	MAXIMUM NUMBER OF ITERATIONS ALLOWABLE IN CALCULATION OF WALL SHEAR VELOCITY
NN	PARAM	MAXIMUM NUMBER OF GRID POINTS IN Y OR Z DIRECTION
NPADI	EQN	NUMBER OF COUPLED AND UNCOUPLED EQUATIONS TO BE SOLVED DURING EACH ADI SWEEP
NPTSX(4)	INTBC	NUMBER OF STREAMWISE LOCATIONS WHERE TRANSPiration DATA IS INPUT
NPTSYZ(15,4)	INTBC	NUMBER OF CROSS-PLANE LOCATIONS WHERE TRANSPiration IS INPUT
NPUNCH	CIO	PUNCH DEVICE
NRGT(2)	DIECOM	NCTR POINTS FROM RIGHT OR TOP BOUNDARY
NS	GEOM	LAST MARCHING STATION
NSAVED	REST	SEQUENCE NUMBER OF RESTART STATIONS SAVED
NSMAX	PARAM	2 GREATER THAN NS
NUNERR	CIO	DEVICE FOR MGAUSS ERROR CHECK
NVSOLV	EQN	NUMBER OF DEPENDENT VARIABLES
NWORD2(50)	STRAGE	SIZE OF EACH COMMON BLOCK
OMBWD	LIN	1.0 - BWD
OMEGWF	LAWW	UNDER-RELAXATION FACTOR FOR WALL FUNCTION FORMULATION
P	VAR	INDEX FOR STATIC PRESSURE
PCON1	REF	(GAMMA-1.0)/GAMMA
PCON2	REF	0.5 * PCON1
PINF	FREE	FREE STREAM STATIC PRESSURE

FORTRAN SYMBOL	COMMON BLOCK	DESCRIPTION
PL	VAR	STORAGE LEVEL OF STATIC PRESSURE IN GENERAL PURPOSE STORAGE
PLTFLD(NN,NN,8)	ZPLOT	GENERAL PURPOSE STORAGE FOR PLOT INFORMATION
PR	REF	PRANDTL NUMBER
PREF	REF	REFERENCE PRESSURE
PREFI	REF	INVERSE OF REFERENCE PRESSURE
PREPS	VISC	PRANDTL NO. IN TURBULENT ENERGY DISSIPATION EQUATION
PRESS(4)	BOUND	SPECIFIED PRESSURE AT BOUNDARY
PRT	REF	TURBULENT PRANDTL NO.
PRTKE	VISC	PRANDTL NO. IN TURBOLENT KINECTIC ENERGY EQUATION
PZERO	FREE	STAGNATION PRESSURE
Q1D(8,NN)	METRIC	INTERMEDIATE STORAGE ARRAY FOR METRIC INFORMATION
Q2D(8,NN)	METRIC	INTERMEDIATE STORAGE ARRAY FOR METRIC INFORMATION
R	VAR	INDEX FOR DENSITY
RATLD	LAWW	EMPIRICAL NUMERICAL CONSTANT IN MIXING LENGTH COMPUTATION
RE	REF	REYNOLDS NUMBER
REI	REF	INVERSE OF REYNOLDS NUMBER
REI2	REF	2.0 * REI
REPL	FREE	REYNOLDS NUMBER PER UNIT LENGTH
RGAS	REF	GAS CONSTANT
RHO(NDIEM)	ADDR	STORAGE OF DENSITY FOR FIRST DERIVATIVES
RHOINE	FREE	FREE STREAM DENSITY

FORTRAN SYMBOL	COMMON BLOCK	DESCRIPTION
RHOREF	REF	REFERENCE DENSITY
RHOWL(NN,4)	BOUND	STORAGE FOR DENSITY ON THE BOUNDARY
RHREEI	REF	INVERSE OF REFERENCE DENSITY
RUNIV	UNITS	UNIVERSAL GAS CONSTANT
SAVE(NEQS,NN)	EQN	STORAGE FOR CHANGES DURING FIRST ADI SWEEP
SN(NN)	LIN	STORAGE FOR N TH LEVEL TERMS
SQ1	ADD	ADD CODE STREAMWISE LOCATION
SQ2	ADD	ADD CODE STREAMWISE LOCATION
SYSTEM	ZPLOT	SENTINEL FOR COORDINATE SYSTEM - PLOTS ONLY
T	VAR	INDEX FOR STATIC TEMPERATURE
TEMPS(NN,4)	BOUND	STORAGE ARRAY FOR TEMPERATURE ON BOUNDARY
TEMPSN(NN,4)	BOUND	STORAGE ARRAY FOR TEMPERATURE AT NTH STREAMWISE STATION - BOUNDARIES ONLY
TINE	FREE	FREE STREAM STATIC TEMPERATURE
TTITLE(6)	ZPLOT	TITLE FOR PLOT FILE
TKE	VAR	INDEX FOR TURBULENT KINETIC ENERGY
TKEINE	LAWW	FREE STREAM TURBULENT KINETIC ENERGY
TL	VAR	STORAGE LEVEL OF STATIC TEMPERATURE IN GENERAL PURPOSE STORAGE
TREF	REF	REFERENCE TEMPERATURE
TREFI	REF	INVERSE OF REFERENCE TEMPERATURE
TT1(2)	GEOM	MESH DISTRIBUTION FACTOR
TT2(2)	GEOM	MESH DISTRIBUTION FACTOR
TWALL(4)	BOUND	SPECIFIED TEMPERATURE AT BOUNDARY
TWOD	GEOM	FLAG FOR TWO DIMENSIONAL LOGIC
TZERO	FREE	STAGNATION TEMPERATURE

FORTRAN SYMBOL	COMMON BLOCK	DESCRIPTION
T2(2)	GEOM	MESH DISTRIBUTION FACTOR
U	VAR	INDEX FOR VELOCITY IN X-DIRECTION
UDUE(4)	LAWW	BOUNDARY LAYER THICKNESS SAMPLING CRITERIA
UDUM(NDIEM)	ADDR	STORAGE OF VELOCITY FOR FIRST DERIVATIVES
UINF	FREE	FREE STREAM VELOCITY
UREF	REF	REFERENCE VELOCITY
UREFI	REF	INVERSE OF REFERENCE VELOCITY
USCALE	ADD	METRIC SCALE FACTOR
USTAR(NN,4)	LAWW	FRICITION VELOCITY ON SOLID WALL BOUNDARY
UTIL(NDIEM)	ADDR	STORAGE OF DEPENDENT VARIABLE FOR FIRST DERIVATIVES
V	VAR	INDEX FOR VELOCITY IN Y-DIRECTION
VELSQ(NN,NN)		STORAGE FOR $U_{**2} + V_{**2} + W_{**2}$ - EQUIVALENCED TO PLTELD(1,1,4)
VKB	LAWW	SECOND CONSTANT IN LOGARITHMIC LAW OF THE WALL
VKC	LAWW	VON KARMAN CONSTANT
VNO(15,15,4)	INTBC	INPUT TRANSPERSION RATES
W	VAR	INDEX FOR VELOCITY IN Z-DIRECTION
X(502)	GEOM	STREAMWISE LOCATION
XENTR	GEOM	STARTING STREAMWISE LOCATION
XG1(NN,2)	OPER	FIRST DERIVATIVES OF COMPUTATIONAL COORDINATES WITH RESPECT TO PHYSICAL COORDINATES
XG2(NN,2)	OPER	SECOND DERIVATIVES OF COMPUTATIONAL COORDINATES WITH RESPECT TO PHYSICAL COORDINATES
XOB(4)	BOUND	INITIAL LOCATION OF SOLID OBSTACLE IN X DIRECTION
XVNO(15,15,4)	INTBC	STREAMWISE LOCATIONS WHERE TRANSPERSION DATA IS INPUT

FORTRAN SYMBOL	COMMON BLOCK	DESCRIPTION
X0(2)	GEOM	MESH DISTRIBUTION FACTOR
Y(NN,NN,2)		PHYSICAL DISTANCES FROM BOUNDARIES - EQUIVALENCED TO PLTFLD(1,1,2)
YAW	REE	YAW ANGLE
YPLUSL(NN,NN)		STORAGE FOR RHO * UIAU / VISLAM - EQUIVALENCED TO PLTFLD(1,1,1)
YS(2,2)	GEOM	NONDIMENSIONAL EXTENTS OF COMPUTATIONAL DOMAIN
YSAVE(NN,2)	GEOM	COMPUTATIONAL COORDINATES
YZPROF(NN)	PRFILE	TEMPORARY STORAGE ARRAY FOR PHYSICAL COORDINATES
YZVNO(15,15,4)	INTBC	CROSS-PLANE LOCATIONS WHERE TRANSPERSION DATA IS INPUT
ZNTRN(NDIM,3)	ZEX1	ARRAY FOR VIRTUAL MEMORY STORAGE NDIM = NN * NN * MZVAR * MLEVEL
ZZ(M,L,K)	VARZZ	GENERAL PURPOSE STORAGE FOR DEPENDENT AND DERIVED VARIABLES - M = MZVAR, L = MLEVEL, K = NDIEM * NN

Sample Input and Sample Output

Sample input and output for two- and three-dimensional cases are presented in Tables II - V, respectively. The two-dimensional input is that used in running the previously discussed Rose case (Ref. 36) while the three-dimensional input is that used in the running of the Bogdonoff case (Ref. 34). The Rose case input data is for an initial run (IRSTIN=0) with a restart to be written every 200 marching steps (IRSTOT). The case is to be run on our IBM virtual memory marching (ICOMP=3). The streamwise and transverse momentum as well as continuity and stagnation enthalpy (IHSTAG) version of the energy equation are to be solved. On the first boundary, the boundary type as well as the boundary condition are to change at streamwise distance 0.5618 (ASW(1)=0.5618). Wall temperatures on the 1 and 2 surfaces are 3.651111439 times the reference temperature (TWALL(1)=2*3.651111439). The reference length is 0.8666667 ft. (IUNITS=1) the Reynold's number per ft. is 5.22×10^6 , the free stream Mach number 3.88 and the free stream pressure is 5.9.8170527 lbt/ft². Grid point packing about the 1 surface is to be moderate TT1=-0.80 while the packing around the 2 surface is to be considerably tighter TT2=0.95 99 grid points are utilized in the transverse direction (NE(1)=99) and an axisymmetric coordinate system generated by the ADD code (IGEOM=11) is to be utilized. The initial run is to be marched 200 steps (NS=200) starting at a streamwise location of 0.2 (XENTR=0.2). An initial profile is to be supplied off the 2 surface. The boundary layer thickness is 0.130 and the skin friction coefficient is 1.72×10^{-3} . A turbulent mixing length model is used (IMIXL=1). Printout is given every 10 steps (IPRINT=10) and plot information is written every 2 steps (IPLOT=2). The output for the two-dimensional Rose case consists of NAMELIST information and geometric information and maximum change information and flowfield information at each tenth streamwise station. The NAMELIST information is provided as a means for the user to check the input data. The geometric information consists of the nondimensional computational distance (YSAVE), the nondimensional physical distance Y from the lower surface, the three metrics and their derivatives and the X and Y physical location based on an (ADD code) absolute frame of reference. The maximum change information consists of the variable number (IVAR) the grid point position of the maximum change (JMAX and KMAX) and the value of the maximum change of the variable

from one marching station to the next. The next two pages consist of the flowfield information at a given streamwise location. All variables (except the pressure) are in a nondimensional form with respect to the reference conditions which are displayed in NAMELIST LIST2. The pressure terms are nondimensionalized with respect to the free stream pressure. The first page of flowfield output consists of the transverse grid point number, the computational position, the streamwise velocity component, the transverse direction velocity component, the density, the static or stagnation (IHSTAG=0 or IHSTAG=1 or 2) enthalpy, the turbulence kinetic energy, the static pressure, the static temperature, the effective viscosity and the Mach number. The second page of flowfield output again consists of the grid point number at the computational position followed by the subsonic (INDC=1) - supersonic (INDC=3) indicator, the stagnation temperature and pressure, the pressure coefficient, the laminar viscosity, the mixing length, the dissipation function and finally the cell Reynolds number. Following the flowfield information is the subsonic-supersonic grid point position indicator (ISS) with respect to the lower and upper surface and the boundary indicator (IBOUND). The ISS values tell the grid point where the flow transitions from subsonic to supersonic flow while the variable IBOUND tells the type of surface (JBOUND=1 corresponding to a wall and JBOUND=2 corresponding to a nonwall). Finally, plot file information is displayed.

The sample input for a three-dimensional restart case is presented in Table IV. Since this is a restart case the initial input values are retained as defaults and only variables that are going to be changed need appear. For this particular case, the results at step 350 (IRSTIN=350) are going to be marched 50 more steps to station 400 (NS=400). From this input stream it is possible to see how the streamwise step size was varied. The initial step size (which would have to be obtained from the initial input run stream) was decreased by 20% per step over the first 20 stations and allowed to reach a minimum step size of 0.002. At station 21 the step size was increased by 5% per step. From station 41 to 101 the step size remained constant. At station 101 the step size was again reduced by 20% per step with a minimum value of 0.0002. After station 251, the step size increased by 15% per step until it achieved a maximum step size of 0.005. A portion of the output for this case is presented in Table V. The initial three-dimensional output is the same as the two-dimensional output and is not presented here. The format

of the flowfield output is of a different form. Unlike the two-dimensional flowfield output, the three-dimensional output is controlled by the variable IVARPR. All of the variables that were printed in the two-dimensional output can be obtained in three dimensions. For three dimensions, however, the output is in the form of a cross-sectional plane of output. The integer variables IY and IZ represent the transverse and spanwise grid point locations respectively while Z and Y are the corresponding computational positions. Table IV is a portion of the output for the Bogdonoff case i.e., the cross plane distribution of the streamwise velocity (UVEL) and pressure (PRES). Other variables can (and were) printed out but for reasons of economy of space are not presented here.

REFERENCES

1. Davis, R.T. and Rubin, S.G.: Non-Navier-Stokes Viscous Flow Computations, *Computers and Fluids* 8, 101, 1980.
2. McDonald, H. and Briley, W.R.: Three-Dimensional Supersonic Flow of a Viscous or Inviscid Gas, *J. Comp. Physics*, 1975.
3. Garvine, R.W.: Upstream Influence in Viscous Interaction Problems, *The Physics of Fluids*, Vol. 11, Number 7, July 1968.
4. Rudman, S. and Rubin, S.G.: Hypersonic Viscous Flow over Slender Bodies with Sharp Leading Edges, *AIAA Journal*, Vol. 6, No. 10, October 1968.
5. Lubard, S.C. and Hellwell, W.S.: Calculation of the Flow on a Cone at High Angle of Attack, *AIAA Journal*, Vol. 12, No. 7, July 1974.
6. Rakich, J.V., Vigneron, Y.C. and Agarwal, R.: Computation of Supersonic Viscous Flows Over Ogive-Cylinders at Angle of Attack, *AIAA Paper 79-0131*, 1979.
7. Schiff, L.B. and Steger, J.L.: Numerical Simulation of Steady Supersonic Flow, *AIAA Paper 79-0130*, 1979.
8. Lin, A. and Rubin, S.G.: Three-Dimensional Supersonic Viscous Flow Over a Cone at Incidence, *AIAA Paper 81-0192*, 1981.
9. Hellwell, W.S. and Lubard, S.C.: An Implicit Method for Three-Dimensional Viscous Flow with Application to Cones at Angle of Attack, *Computers and Fluids*, Vol. 3, 1975.
10. Lubard, S.C. and Rakich, J.V.: Calculation of the Flow on a Blunted Cone at a High Angle of Attack, *AIAA Paper 75-147*, 1975.
11. Hellwell, W.S., Dickinson, R.P. and Lubard, S.C.: Viscous Flows Over Arbitrary Geometries, at High Angle of Attack, *AIAA Journal*, Vol. 19, No. 2, February 1981.
12. Li, C.P.: Implicit Solution for the Shock-Layer Flow Around General Bodies, *AIAA Journal*, Vol. 20, No. 2, February 1982.
13. Favre, A.: Statistical Equations of Turbulent Gases, *Problems of Hydrodynamics and Continuum Mechanics*, Soc. Indust. and Appl. Math, 1969, pp. 231-266.
14. Beer, J.M. and Chiger, N.A.: *Combustion Aerodynamics*, John Wiley and Sons, Inc., New York 1972.

15. McDonald, H. and Camarata, F.J.: An Extended Mixing Length Approach for Computing the Turbulent Boundary Layer Development, Proceedings Sanford Conference on Computation of Turbulent Boundary Layers, Vol. I, Stanford University, 1969, pp. 83-98.
16. van Driest, E.R.: On Turbulent Flow Near a Wall, Journal of Aeronautical Sciences, November 1956.
17. Von Mises, R.: Mathematical Theory of Compressible Fluid Flow, Academic Press, New York, 1958.
18. Garibedian, P.R.: Partial Differential Equations, John Wiley & Sons, New York, 1964.
19. Cebeci, T. Ed: Numerical Physical Aspects of Aerodynamic Flows, Springer-Verlag, New York, 1982.
20. Anderson, B.H. and Benson, T.J.: Numerical Solution to the Glancing Sidewall Oblique Shock Wave/Turbulent Boundary Layer in Three-Dimension, AIAA Paper 83-0136, 1983.
21. Benson, T.J. and Anderson, B.H.: Validation of a Three-Dimensional Viscous Analysis of Axisymmetric Supersonic Inlet Flow Fields, AIAA Paper 83-0135, 1983.
22. Briley, W.R. and McDonald, H.: Solution of the Multidimensional Compressible Navier-Stokes Equations by a Generalized Implicit Method, J. of Comp. Physics, Vol. 24, No. 4, Aug. 1977, p. 372.
23. Richtmyer, R.D. and Morton, K.W.: Difference Methods for Initial-Value Problems, Interscience Publishers, New York, 1967.
24. Douglas, J. and Gunn, J.E.: A General Formulation of Alternating Direction Methods, Numerische Math., Vol. 6, 1964, p. 2128.
25. Beam, R.M. and Warming, R.F.: An Implicit Factured Scheme for the Compressible Navier-Stokes Equations, AIAA Journal, Vol. 16, April 1978, p. 393.
26. Briley, W.R. and McDonald, H.: On the Structure and Use of Linearized Block ADI and Related Schemes, J. Comp. Physics, Vol. 34, 1980, p. 54.
27. Stewartson, K.: The Theory of Laminar Boundary Layers in Compressible Fluids, Oxford, 1964, pp. 33-41.
28. Maise, G. and McDonald, H.: Mixing Length and Kinematic Eddy Viscosity in a Compressible Boundary Layer, AIAA Journal, Vol. 6, No. 1, Jan. 1968.
29. Musker, A.J.: Explicit Expression for the Smooth Wall Velocity Distribution in a Turbulent Boundary Layer, AIAA Journal, Vol. 17, No. 6, June 1976.

30. Cresci, R.J.: Hypersonic Flow Along Two Intersecting Planes, Pibal Report No. 895, March 1966.
31. Dorrance, W.H.: Viscous Hypersonic Flow, McGraw-Hill, 1962, p. 147.
32. Cresci, R.J., S.G., Rubin, Nardo, C.T. and Lin, T.C.: Hypersonic Interaction Along a Rectangular Corner, AIAA Journal, Vol. 7, No. 12, Dec. 1969.
33. Oskam, B., Vas, I.E., and Bogdonoff, S.M.: Oblique Shock Wave/Turbulent Boundary Layer Interactions in Three-Dimensions at Mach 3, AFFDL-TR-76-48, Part I and II, 1976.
34. Oskam, B., Vas, I.E., and Bogdonoff, S.M.: An Experimental Study of Three-Dimensional Flow Fields in an Axial Corner at Mach 3, AIAA Paper 77-689, 1977.
35. Anderson, O.L.: User's Manual for a Finite-Difference Calculation of Turbulent Swirling Compressible Flow in Axisymmetric Ducts with Struts and Slot Cooled Walls, USAAMRDL-TR-74-50, Vol. I, 1974.
36. Rose, W.C.: The Behavior of a Compressible Turbulent Boundary Layer in a Shock-Wave-Induced Adverse Pressure Gradient, NASA TN D-7092, March 1973.
37. White, F.M.: Viscous Fluid Flow, McGraw-Hill, 1974, p. 627.
38. Liu, N.-S., Shamroth, S.J. and McDonald, H.: Numerical Solution of the Navier-Stokes Equations for Compressible Turbulent Two/Three Dimensional Flows in the Terminal Shock Region of an Inlet/Diffuser, AIAA Paper 83-1892, 1983.
39. Syberg, J. and Kuncsek, J.L.: Experimental Evaluation of a Mach 3.9 Axisymmetric Inlet, NASA CR-2563, 1975.

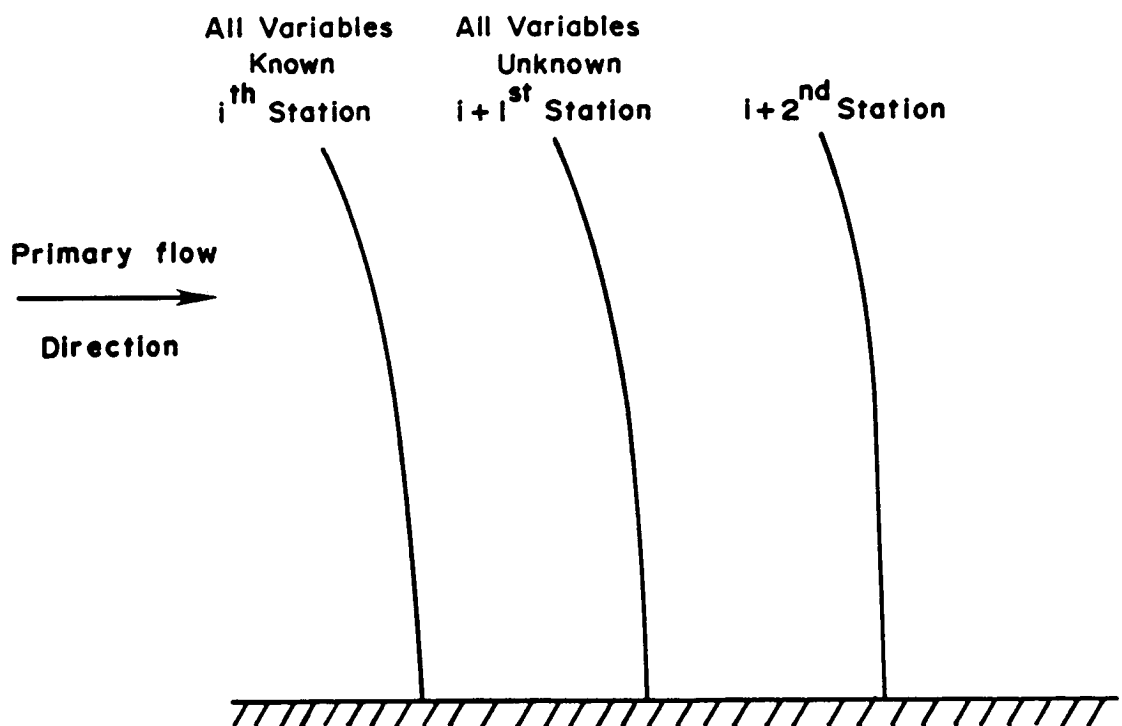
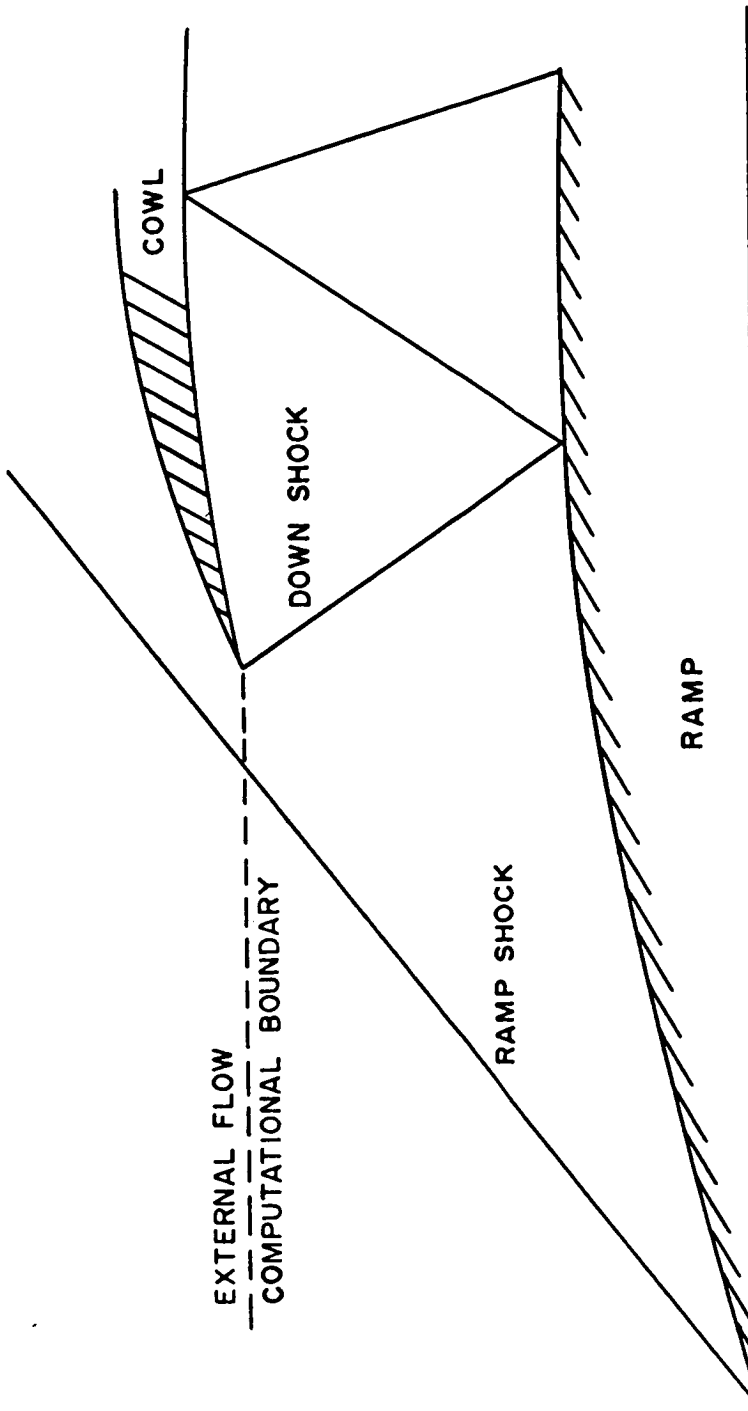


FIGURE I— FORWARD MARCHING PROCEDURE — NOTATION



C - 2

FIGURE 2— TYPICAL HIGH SPEED INLET

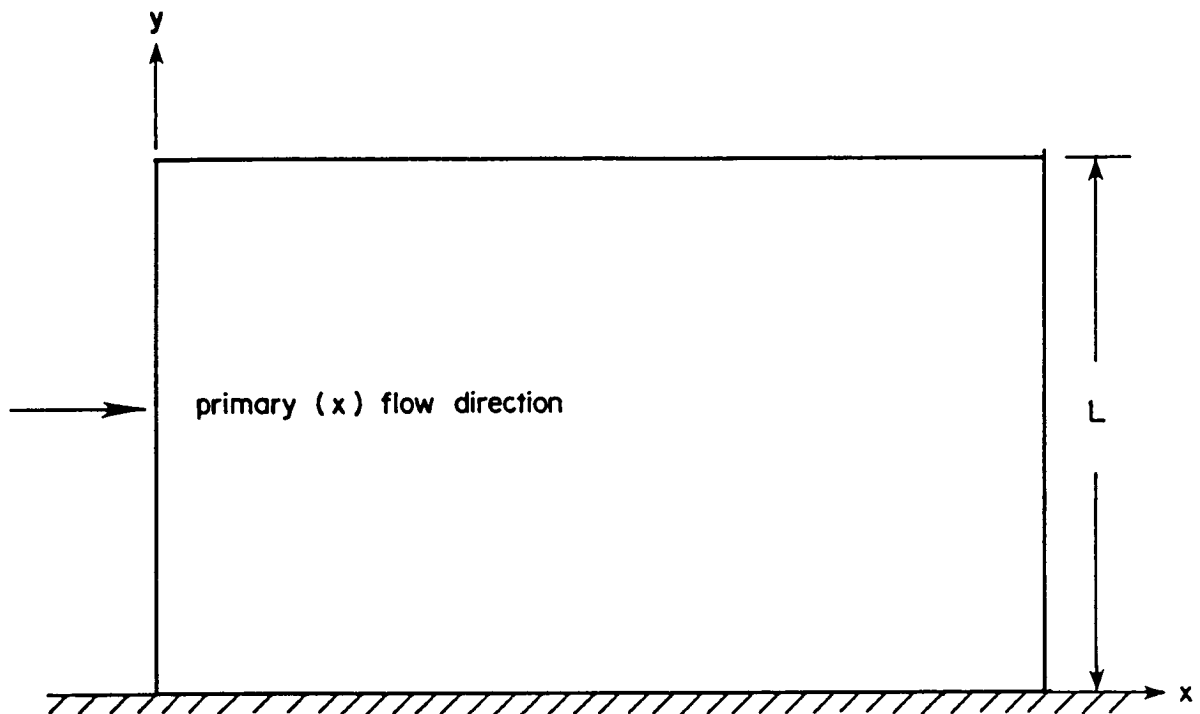


FIGURE 3— TYPICAL COMPUTATIONAL DOMAIN FOR
TWO DIMENSIONAL LAMINAR AND
TURBULENT FLOW CALCULATION

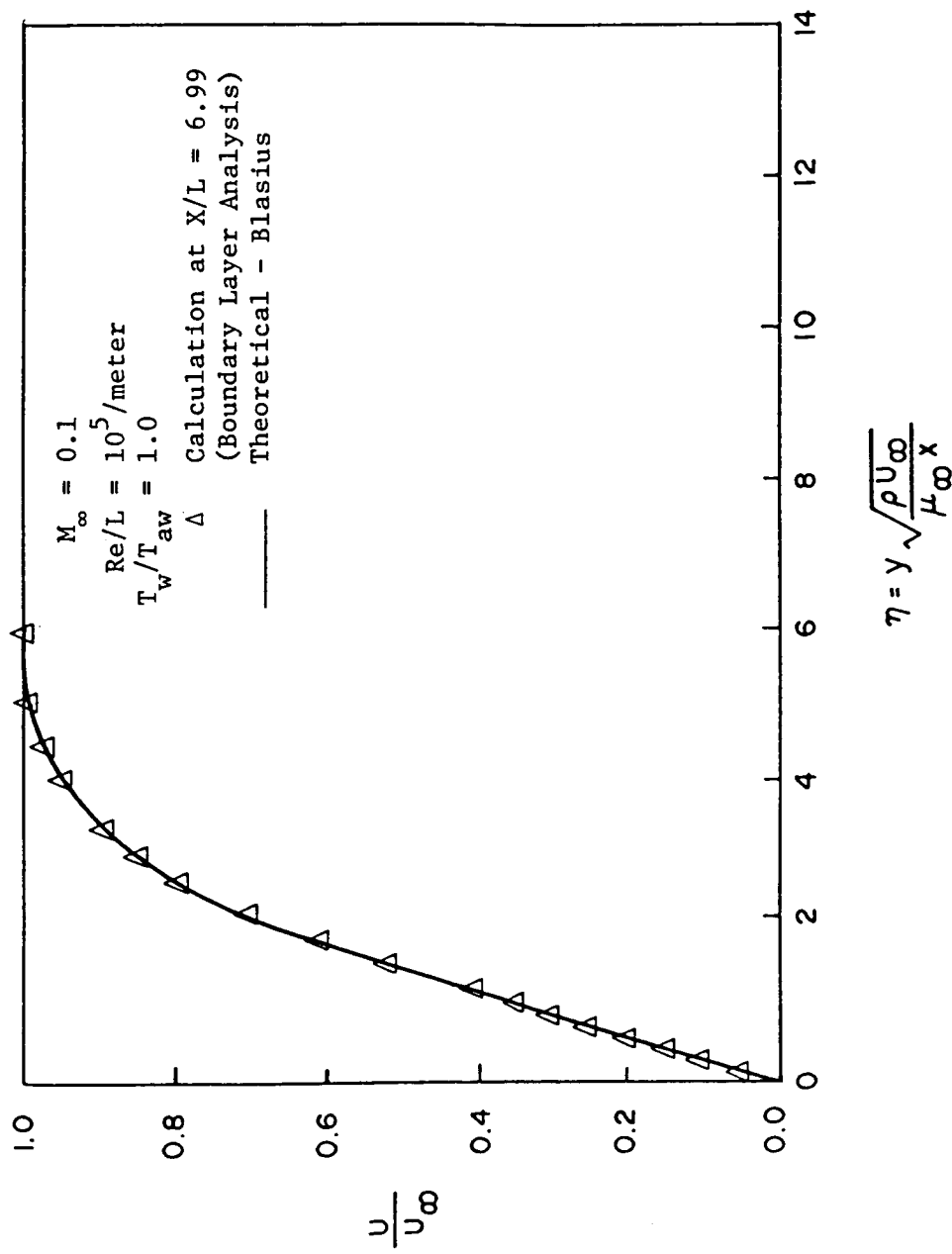


Figure 4. Laminar Flat Plate - Streamwise Velocity Distribution.

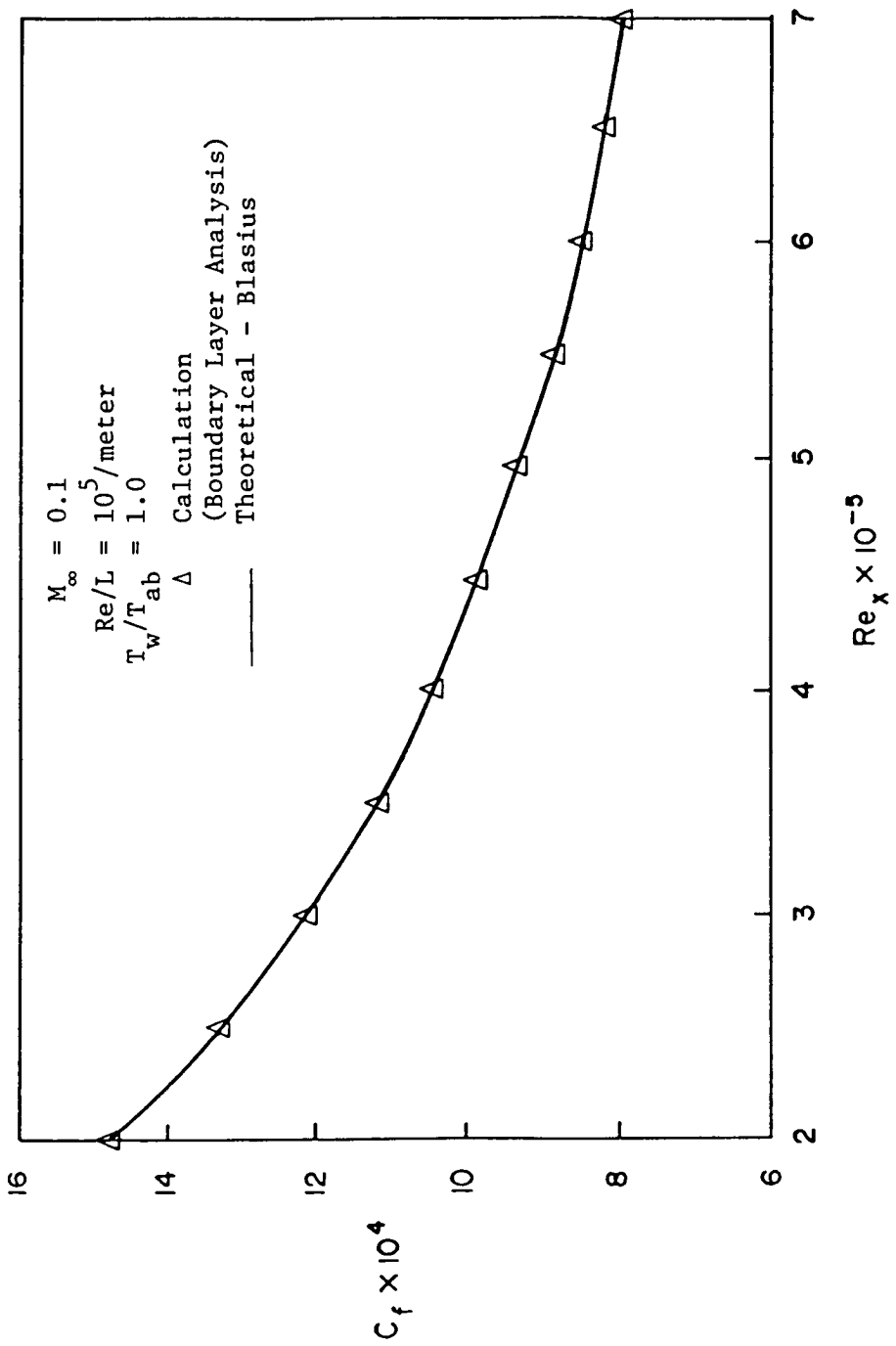


Figure 5. Laminar Flat Plate - Skin Friction Distribution.

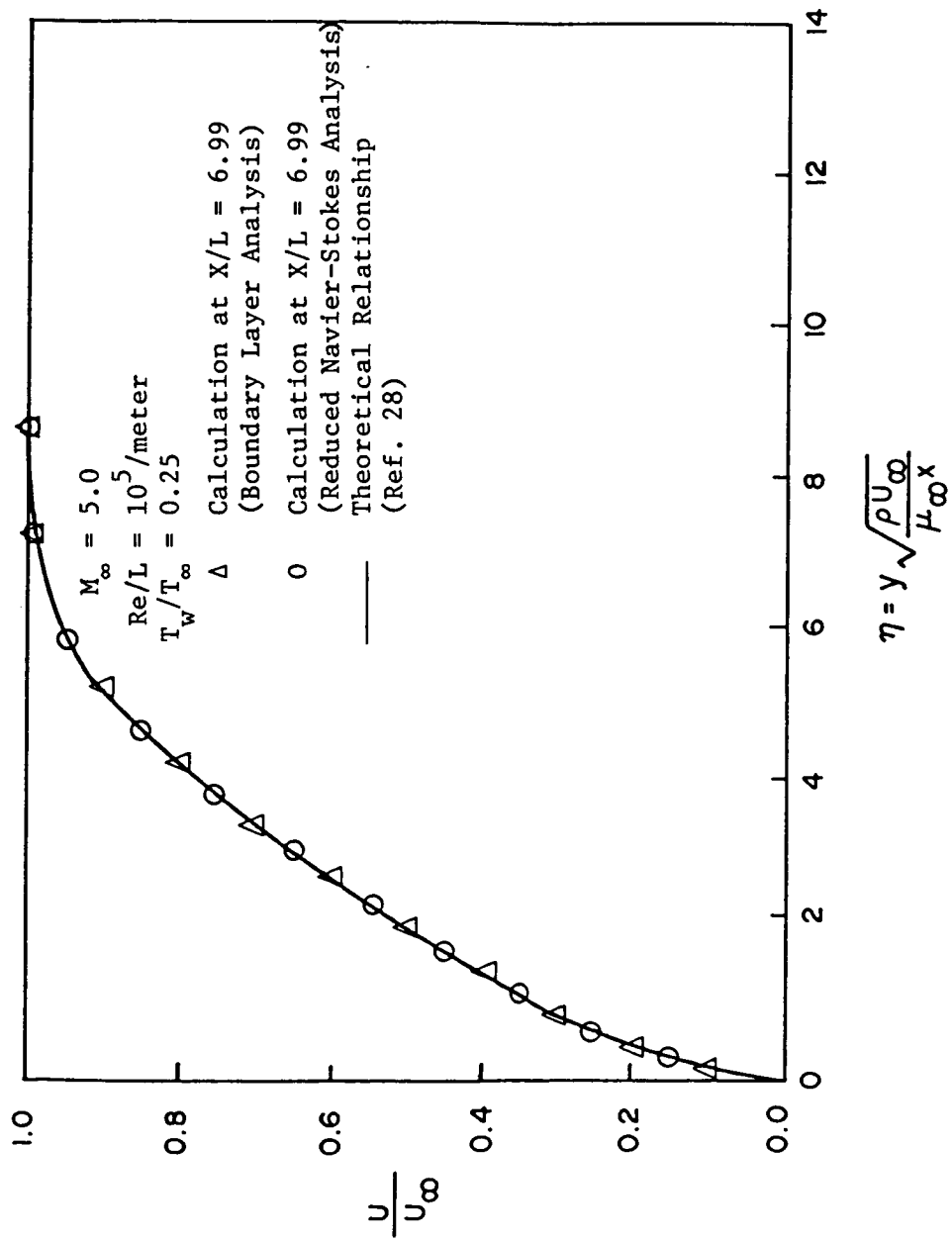


Figure 6. Supersonic Laminar Flat Plate - Streamwise Velocity Distribution.

100

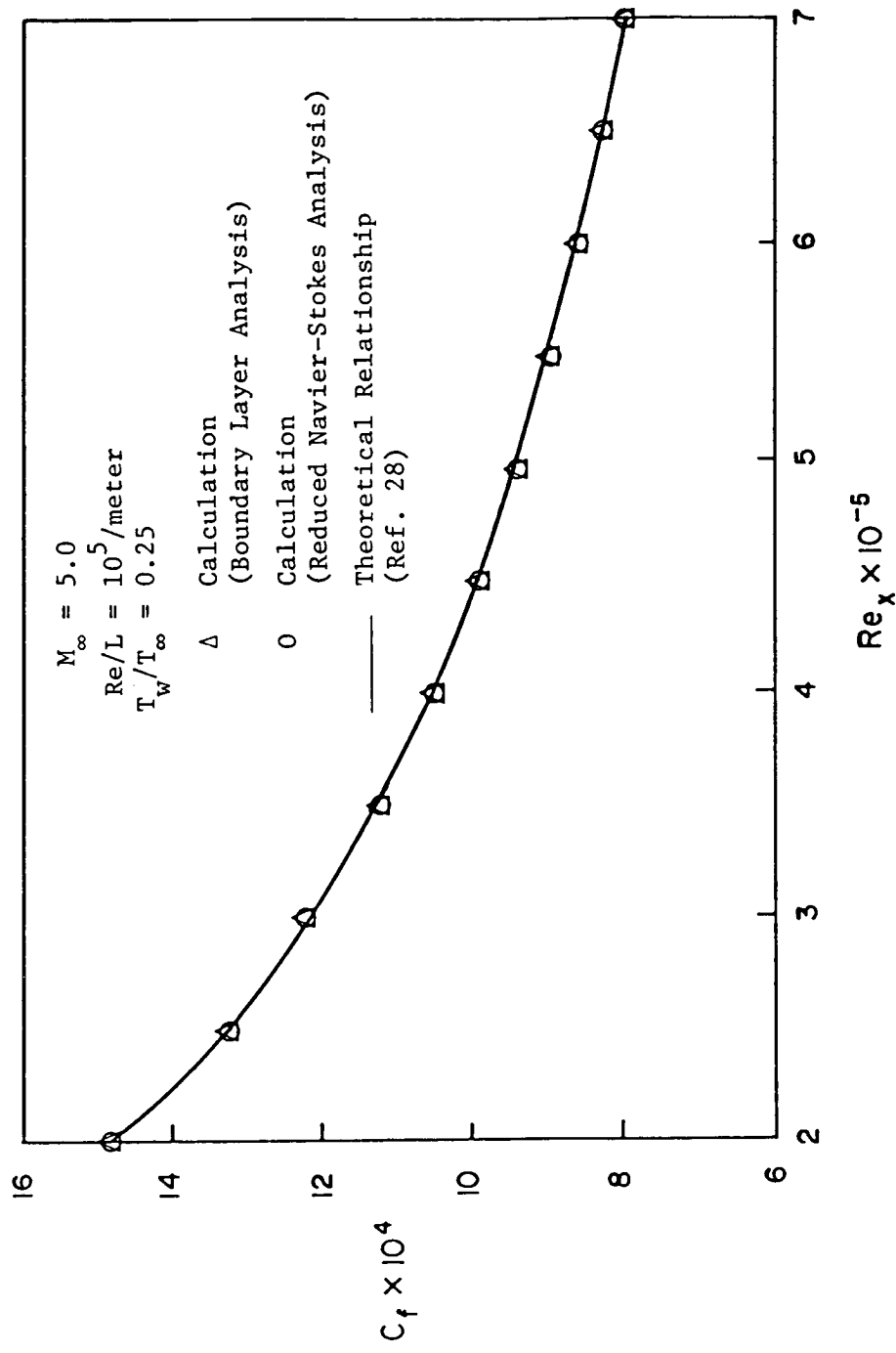


Figure 7. Supersonic Laminar Flat Plate - Skin Friction Distribution.

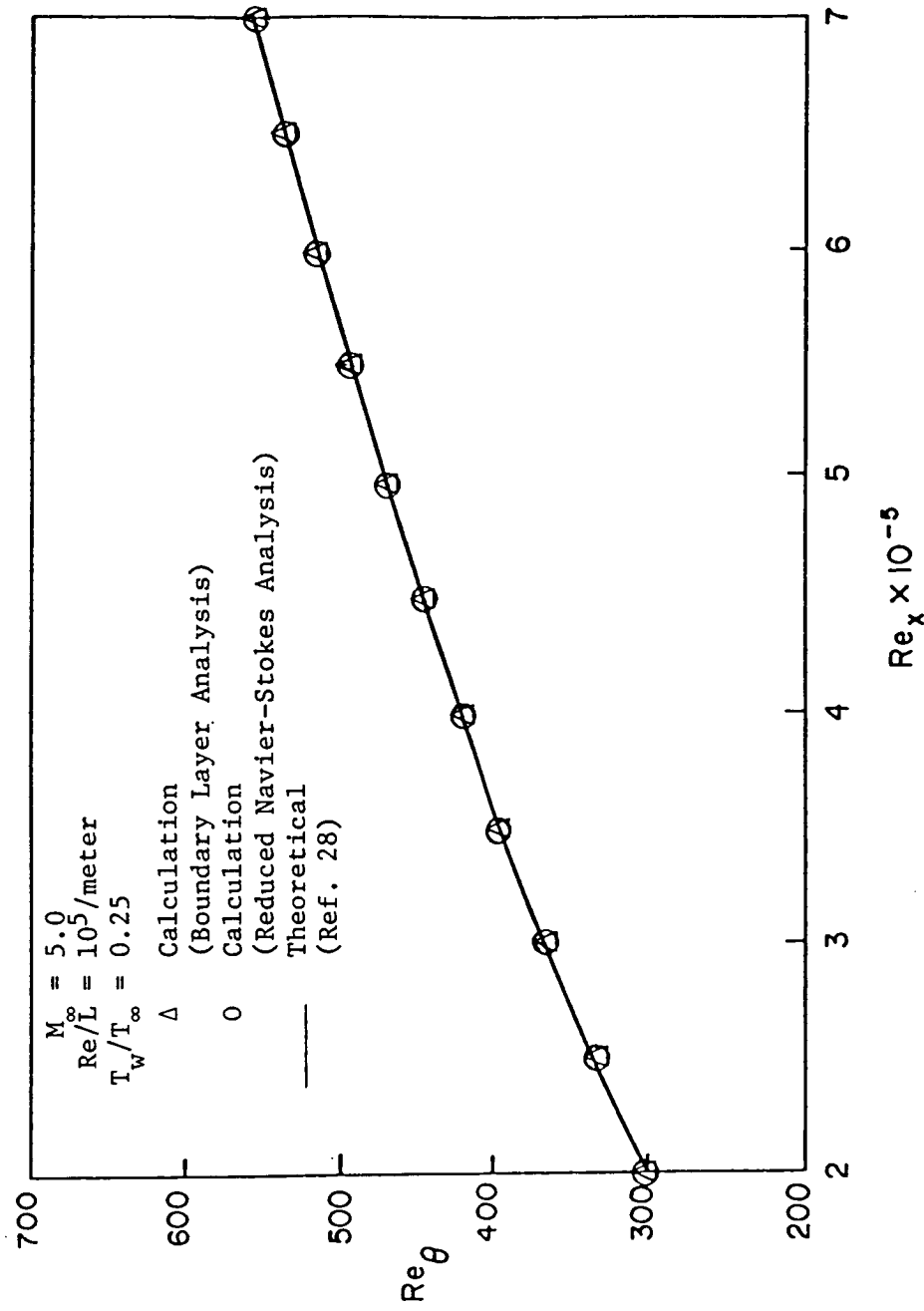


Figure 8. Supersonic Laminar Flat Plate - Momentum Thickness Reynolds Number.

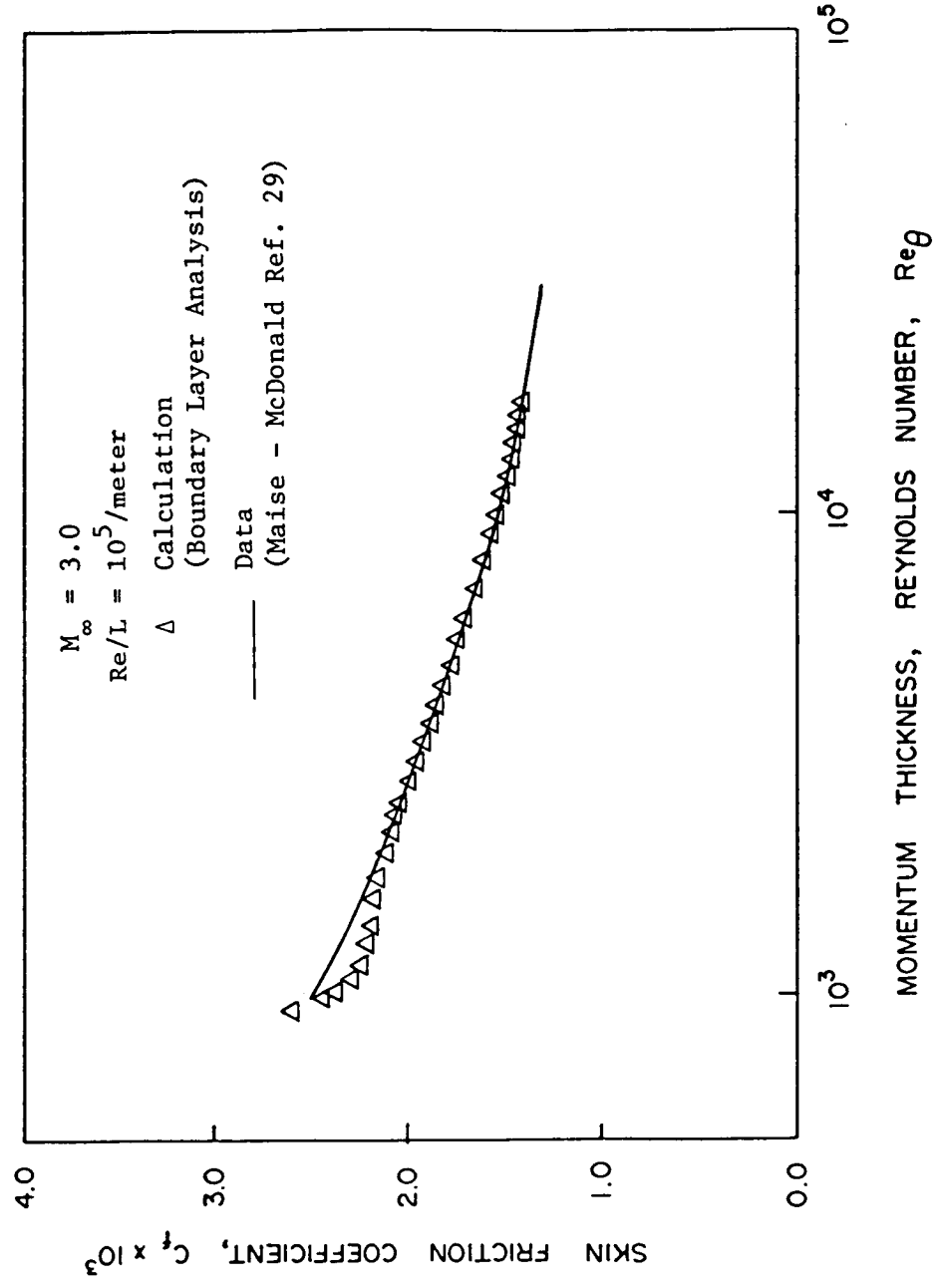


Figure 9. Supersonic Turbulent Flat Plate - Boundary Layer C_f vs Re_θ .

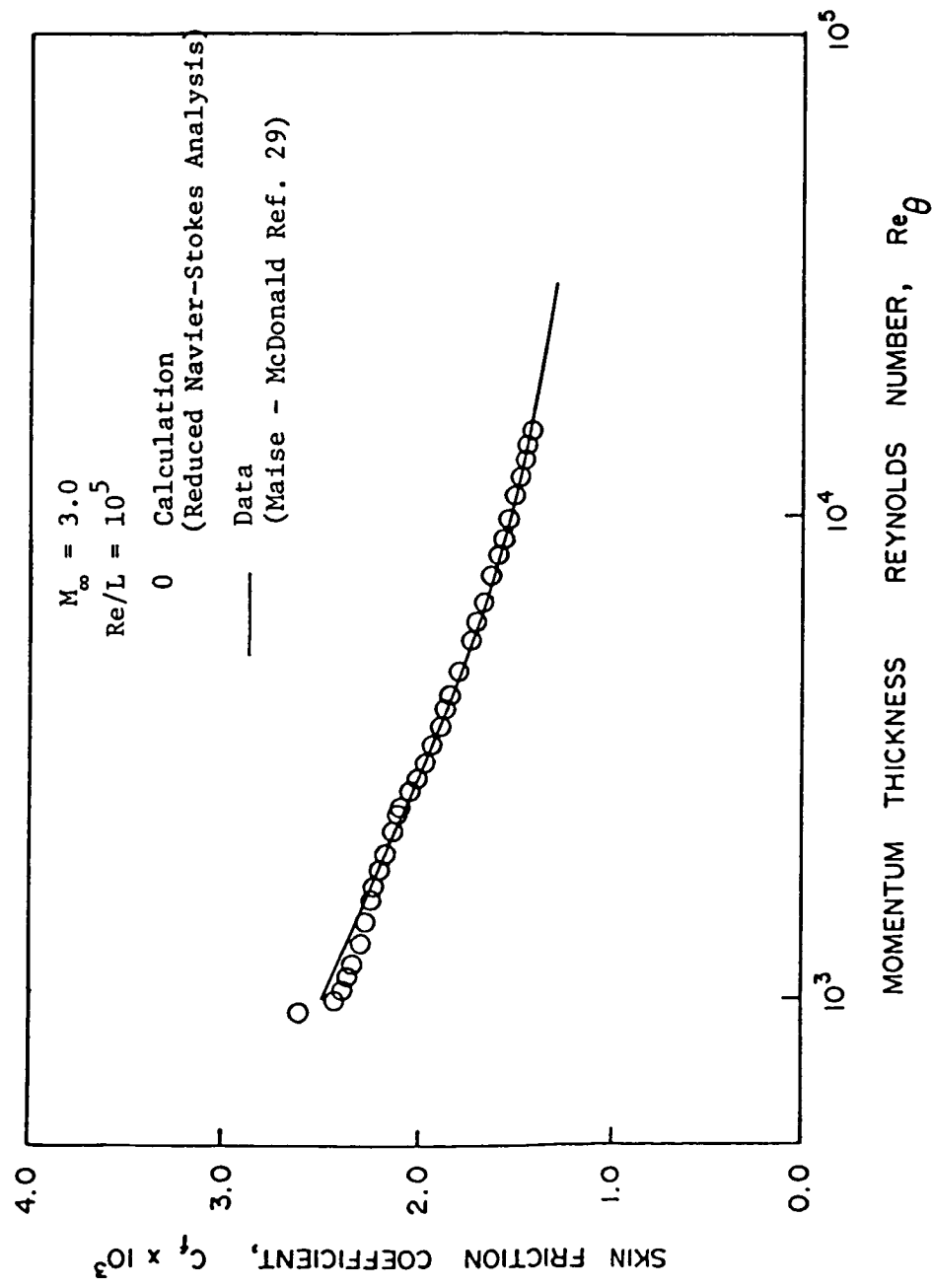


Figure 10. Supersonic Turbulent Flat Plate - Reduced Navier-Stokes C_f vs Re_θ .

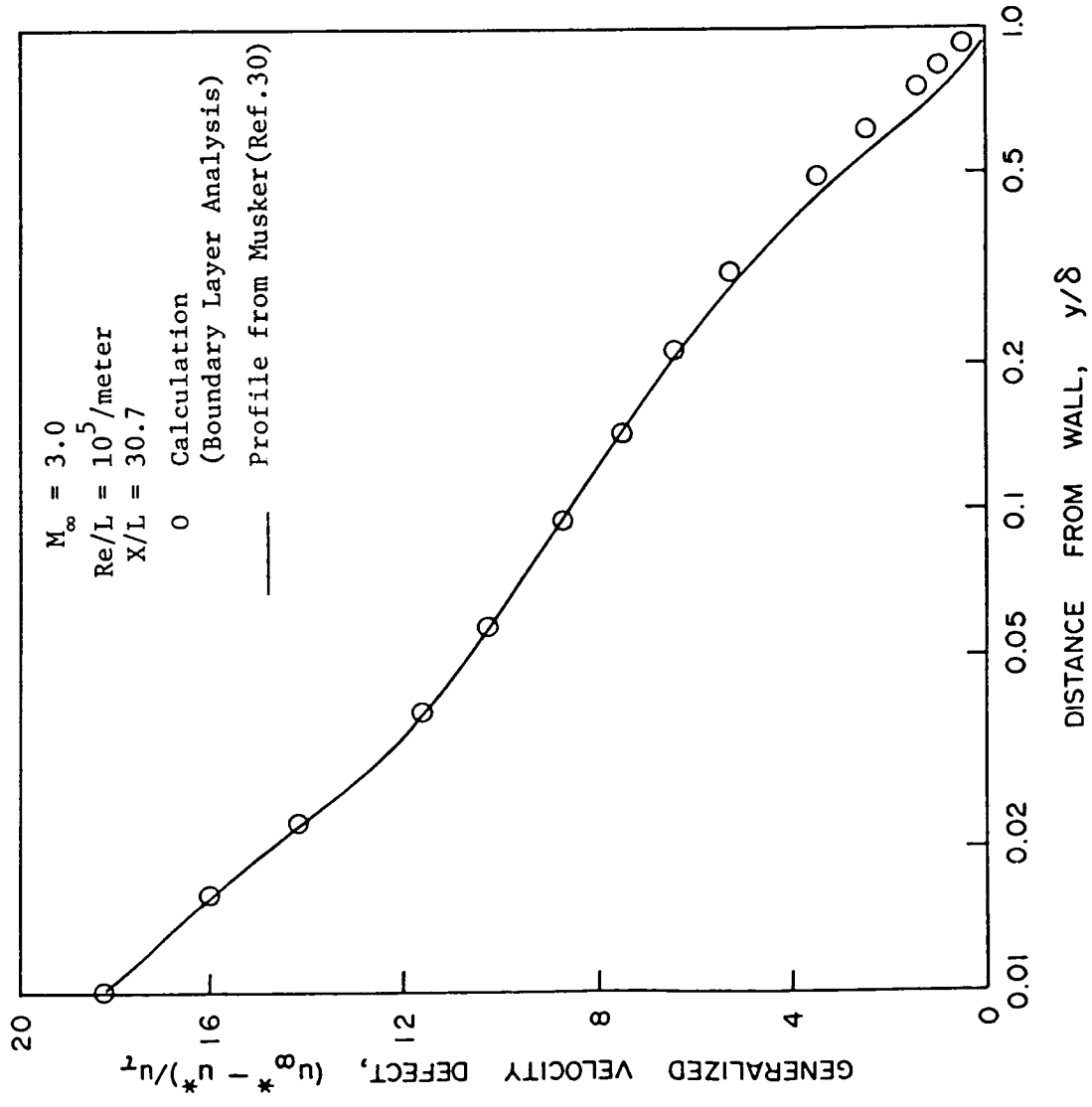


Figure 11. Supersonic Turbulent Flat Plate - Boundary Layer Velocity Defect Profile.

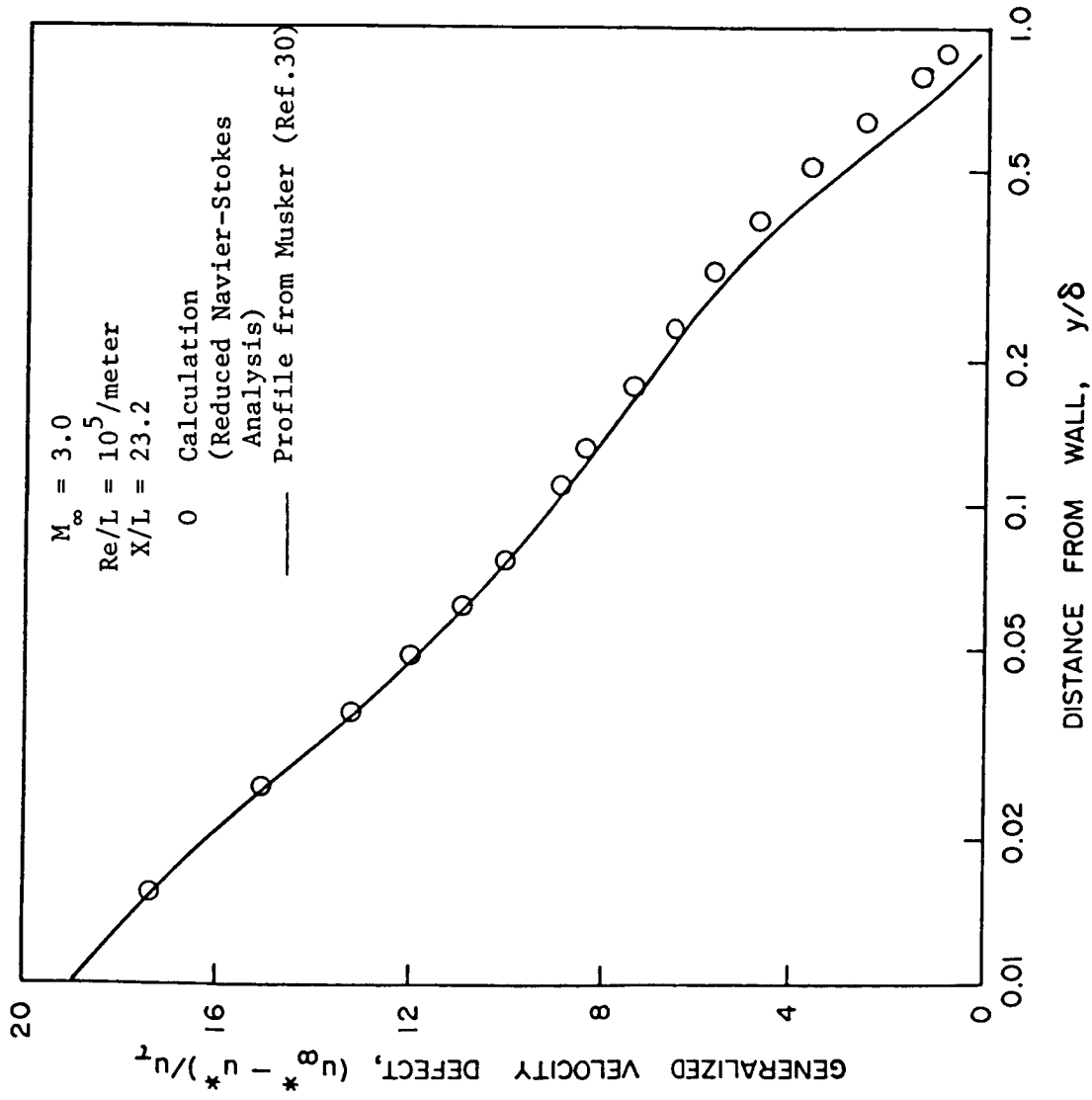


Figure 12. Supersonic Turbulent Flat Plate – Reduced Navier-Stokes Velocity Defect Profile.

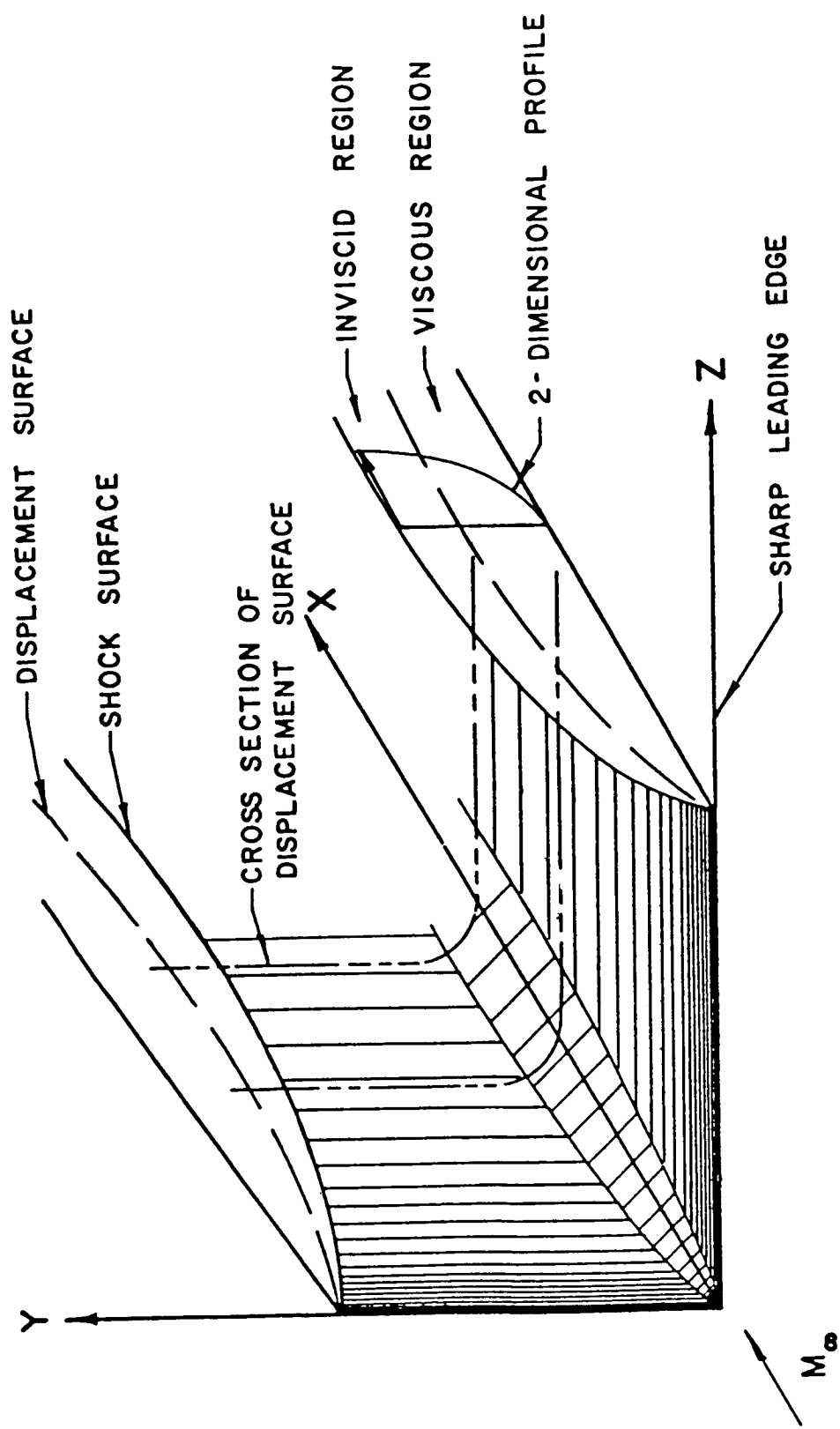


Figure 13. Hypersonic Corner Flow Schematic Representation of Corner Flow System.

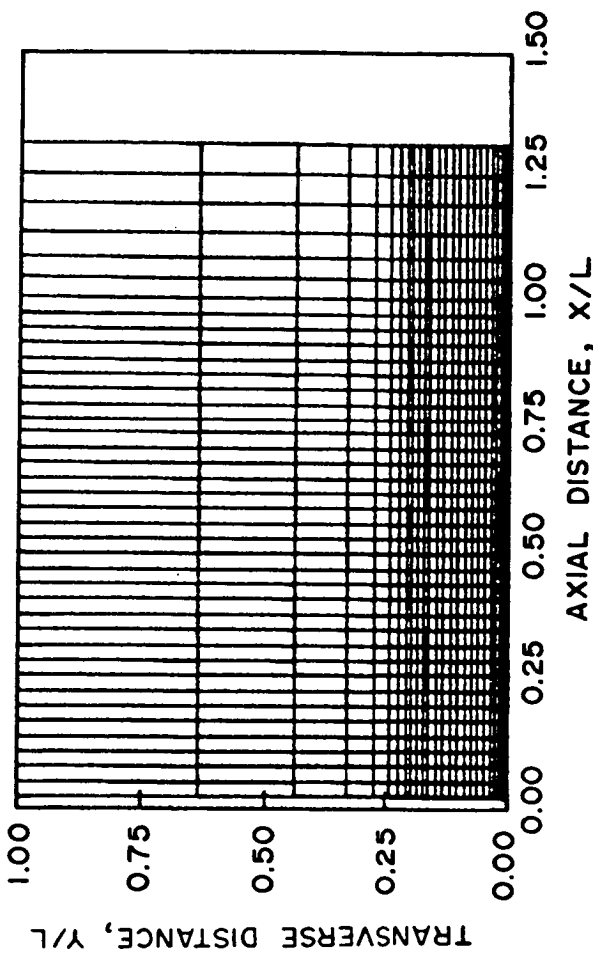


Figure 14. Hypersonic Corner Flow - Computational Mesh in the Streamwise Plane.

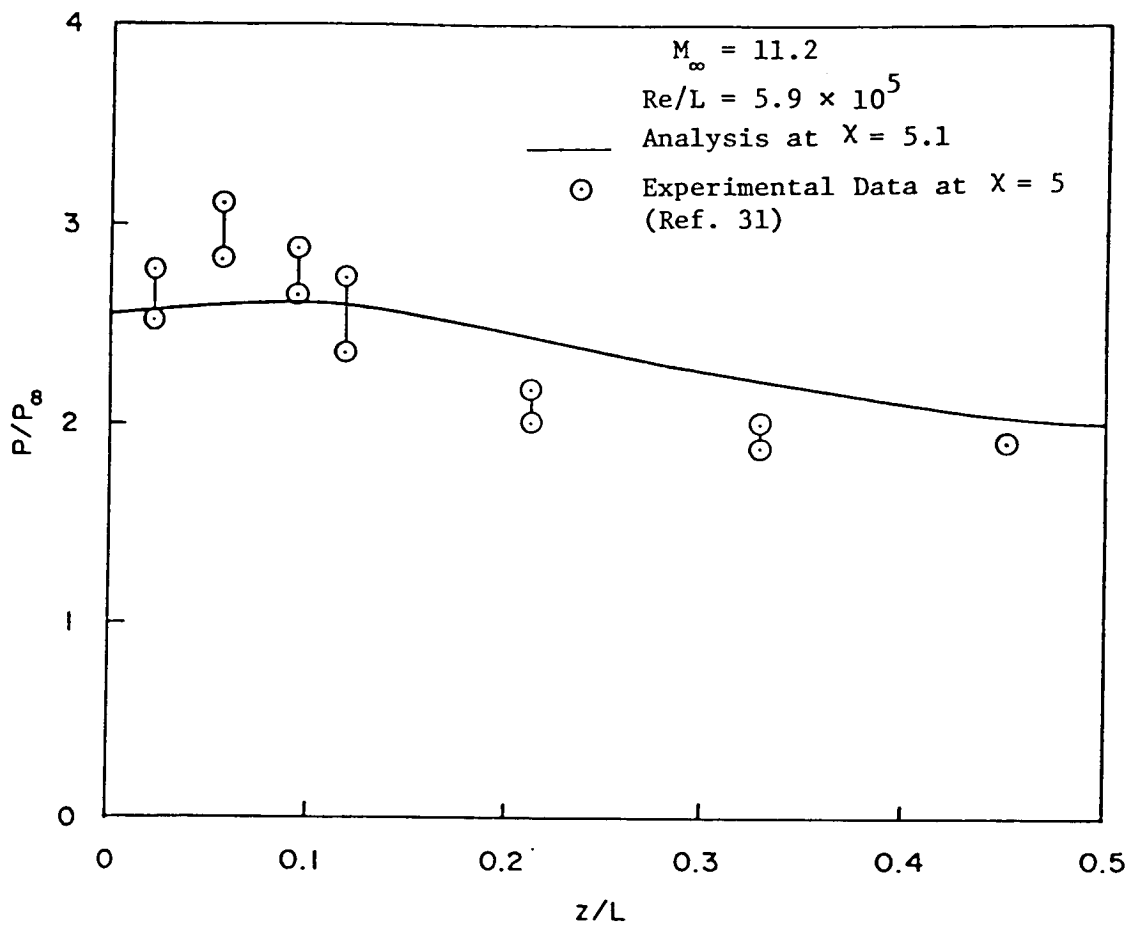


Figure 15. Hypersonic Corner Flow - Comparison of Pressure on a Spanwise Surface.

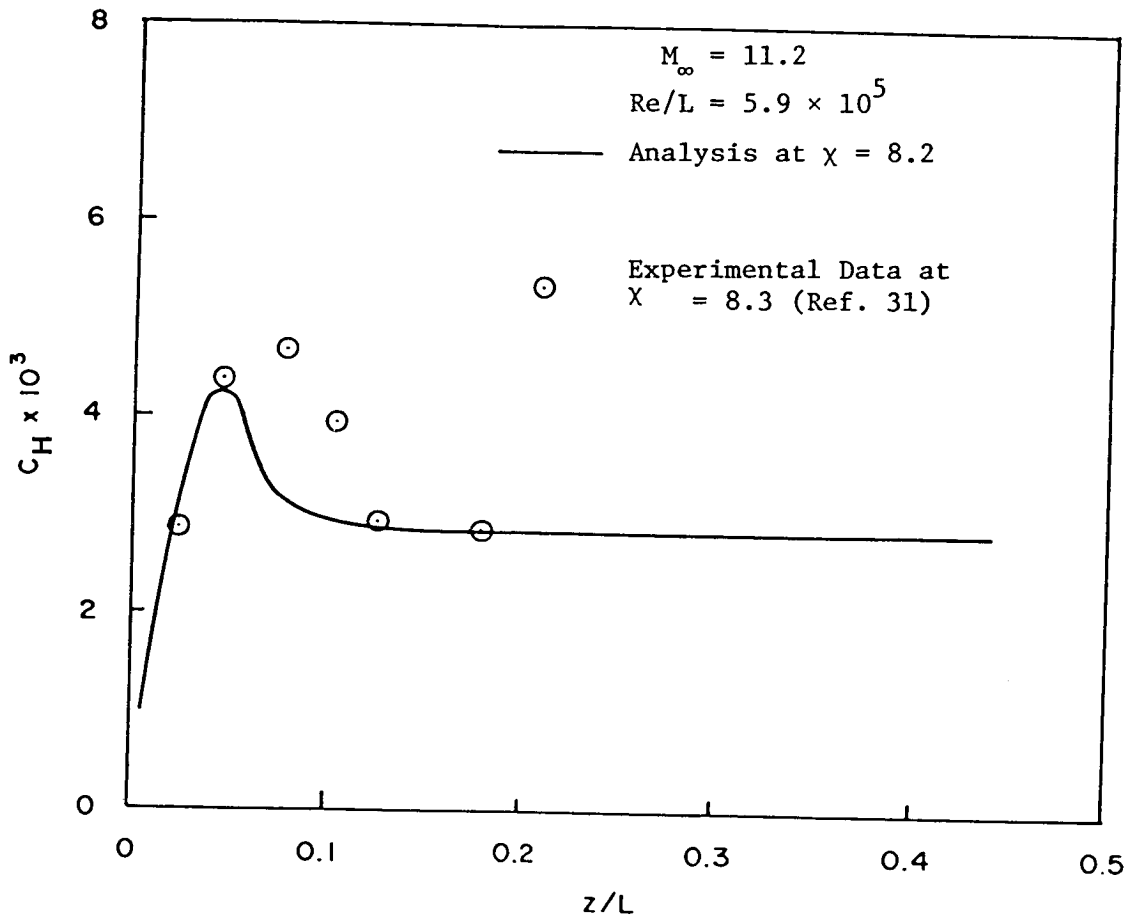


Figure 16. Hypersonic Corner Flow - Comparison of Heat Transfer Coefficient on a Spanwise Surface.

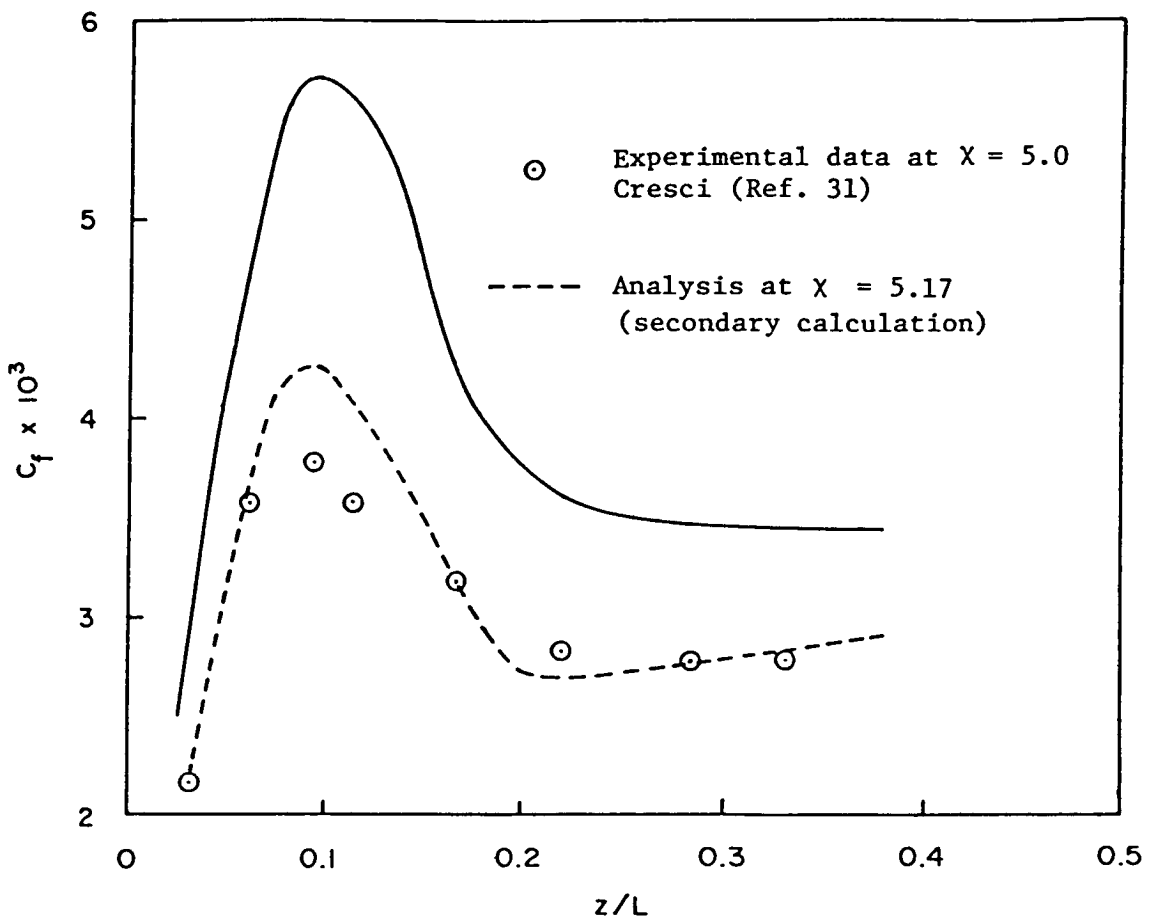


Figure 17. Hypersonic Corner Flow Comparison of Skin Friction Coefficients on a Spanwise Surface.

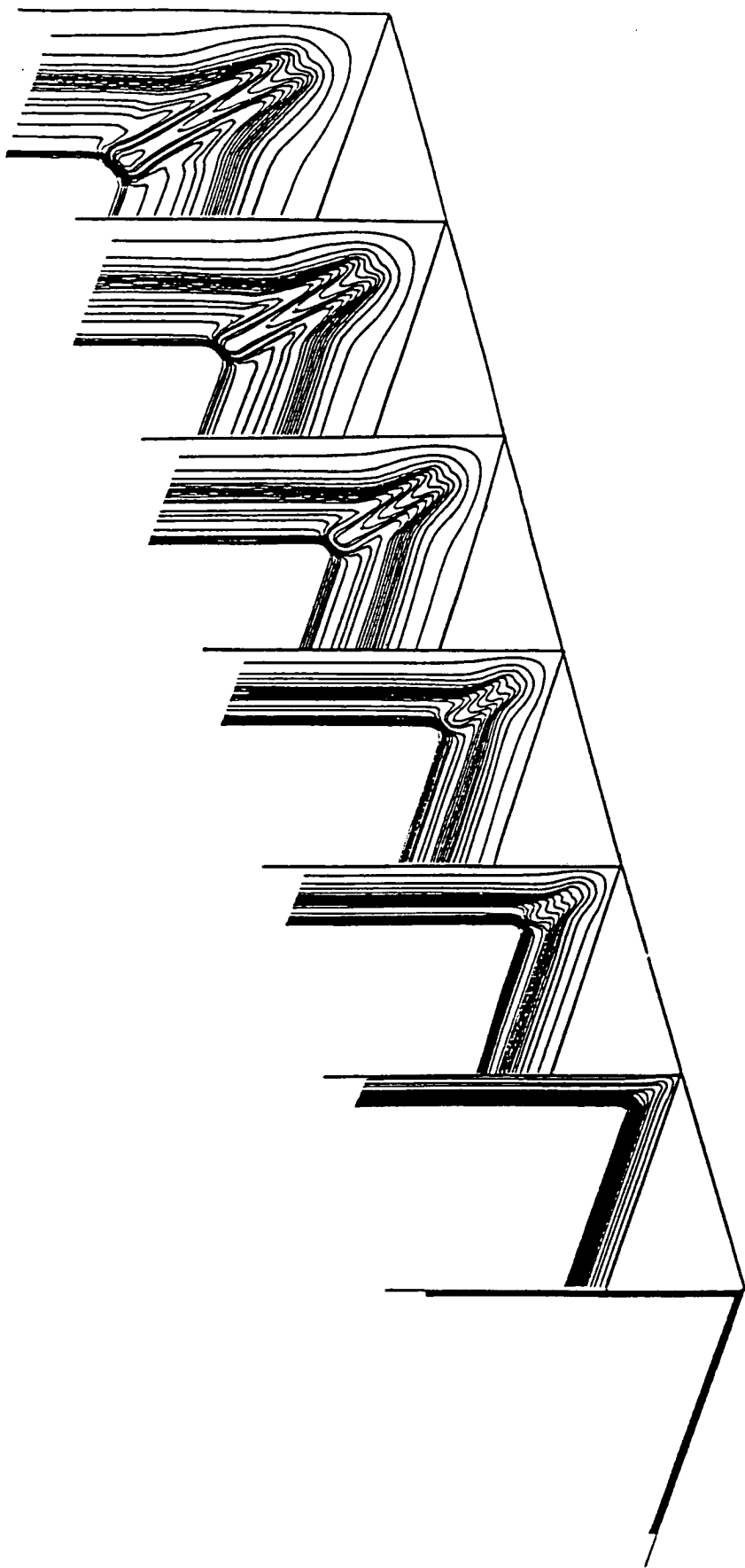


Figure 18. Hypersonic Corner Flow - Streamwise Development of the Stagnation Pressure Isobars.

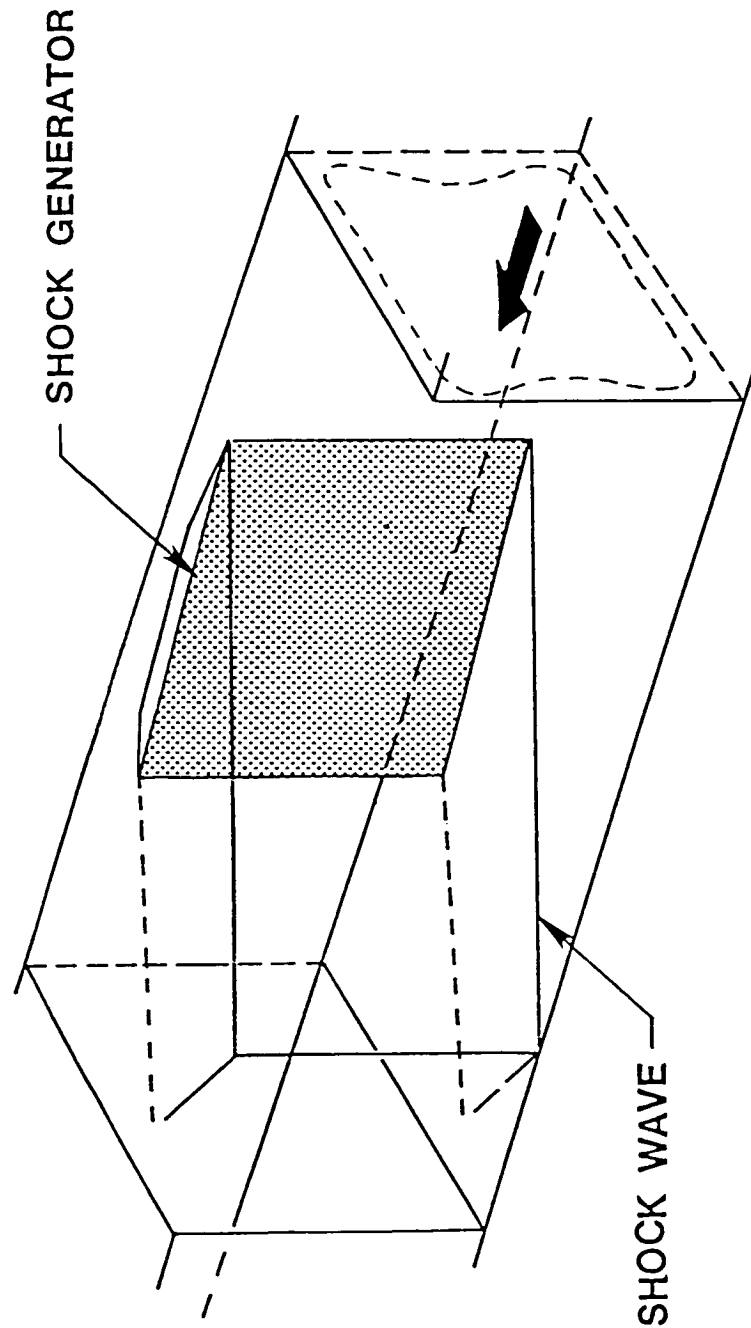


Figure 19. Glancing Shock Wave-Boundary Layer Interaction.
Schematic of Experimental Facility

INSTRUMENTATION AT $X =$ (INCHES)

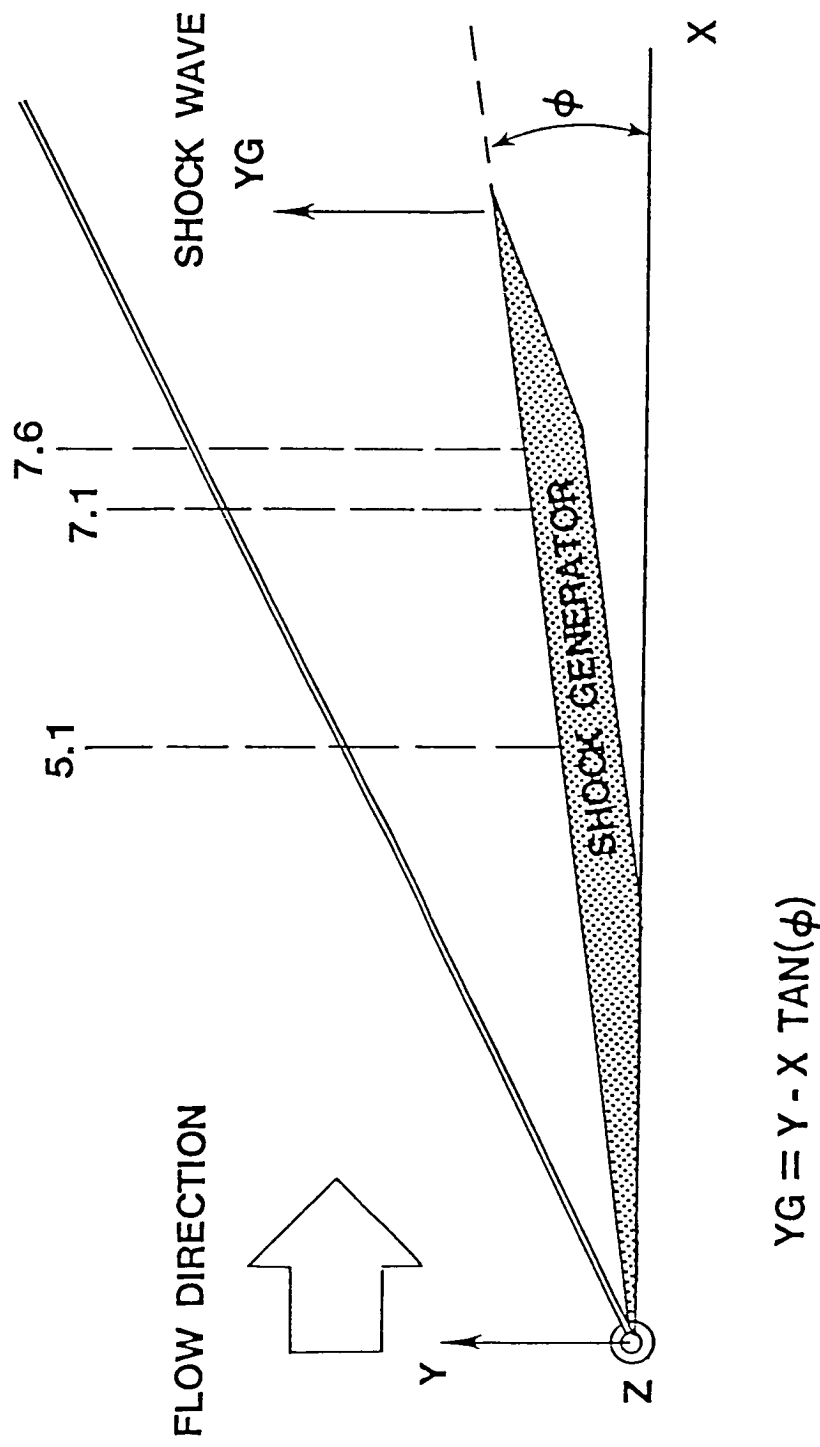


Figure 20. Glancing Shock Wave-Boundary Layer Interaction.
Coordinates for Data Acquisition

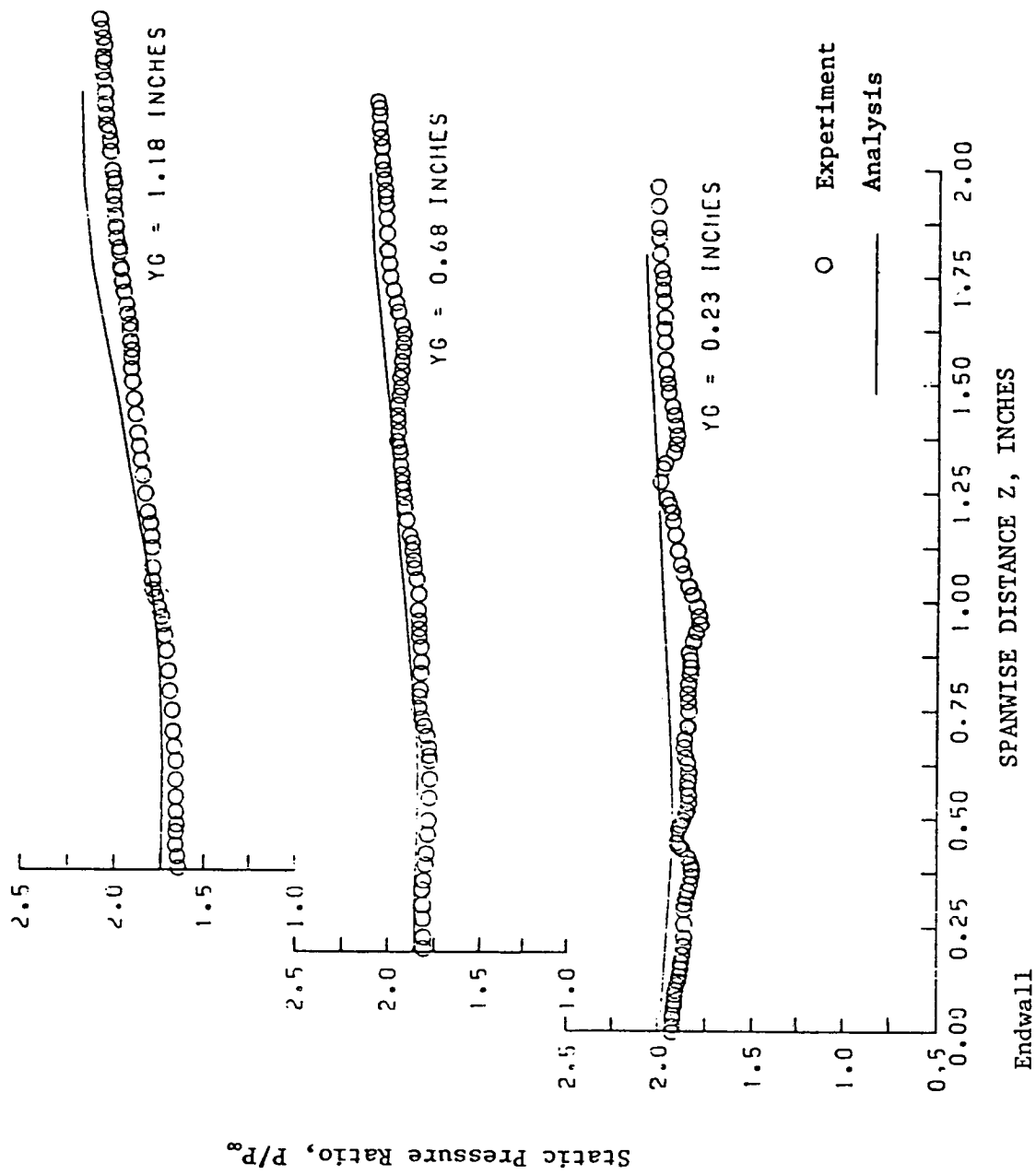


Figure 21 - Glancing Shock Wave - Boundary Layer Interaction -
Static Pressure at $X = 5.1$.

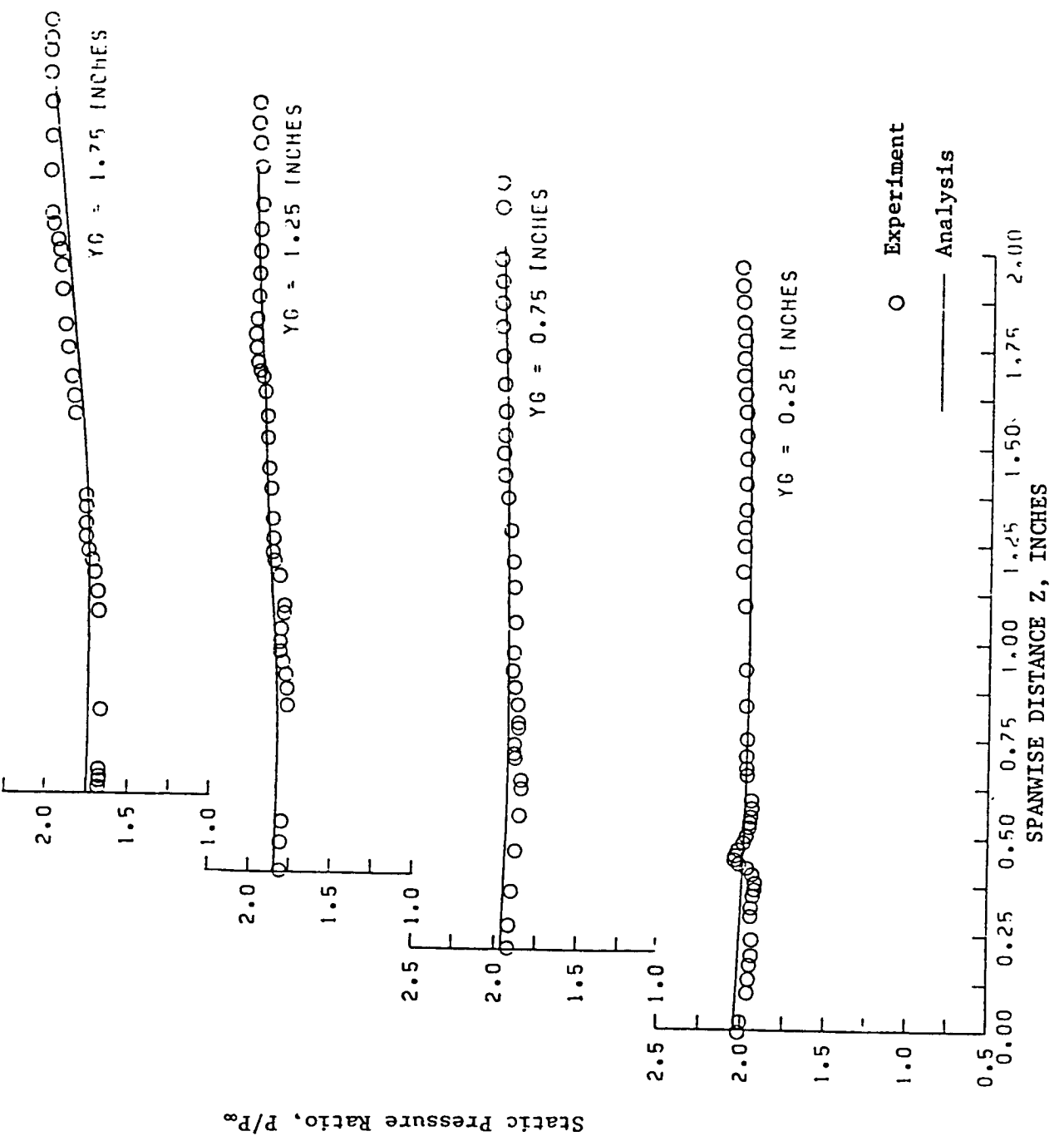


Figure 22 (a) - Glancing Shock Wave - Boundary Layer Interaction -
Static Pressure at $X = 7.6$.

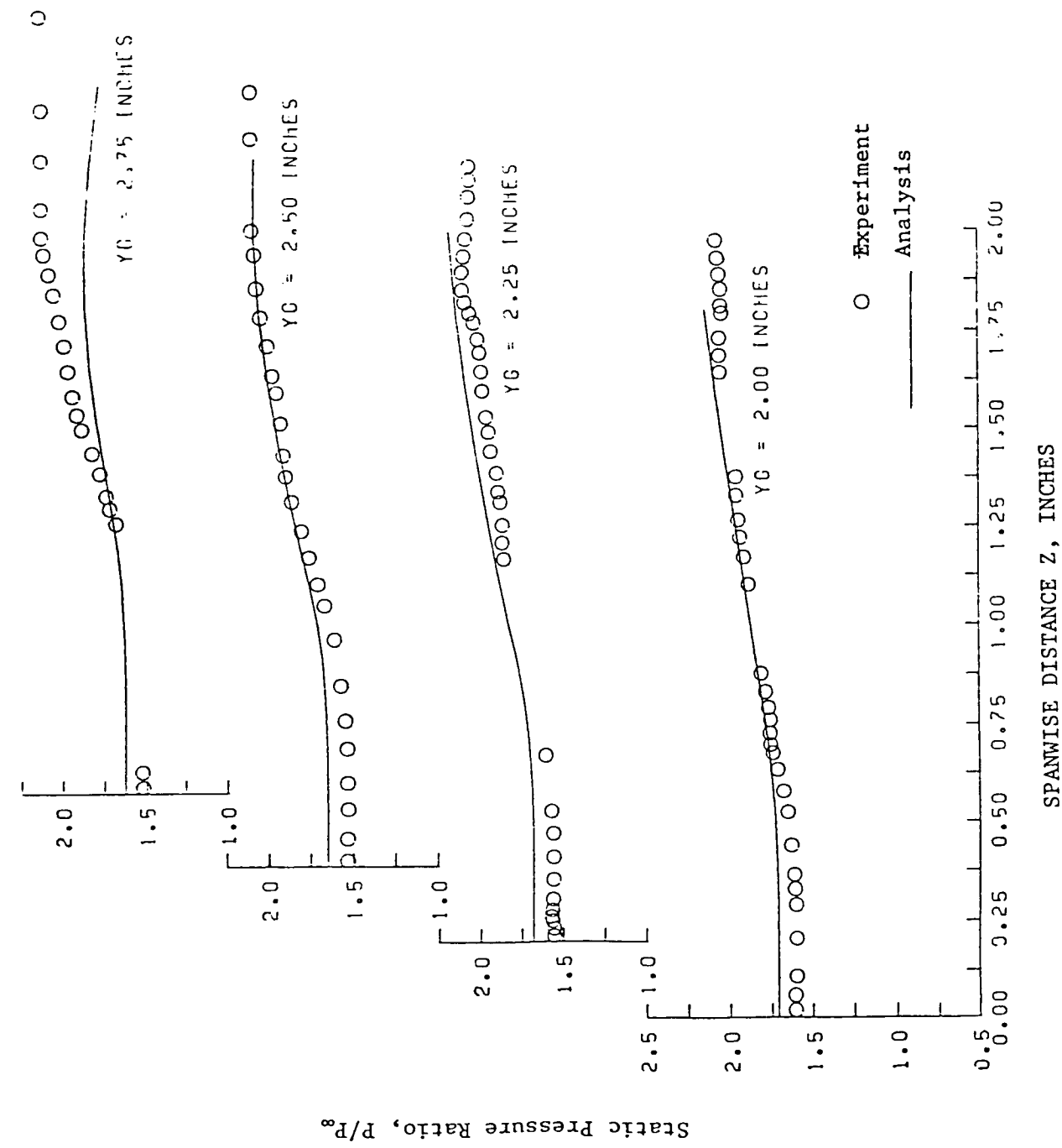


Figure 22(b) - Glancing Shock Wave - Boundary Layer Interaction -
Static Pressure at $X = 7.6$.

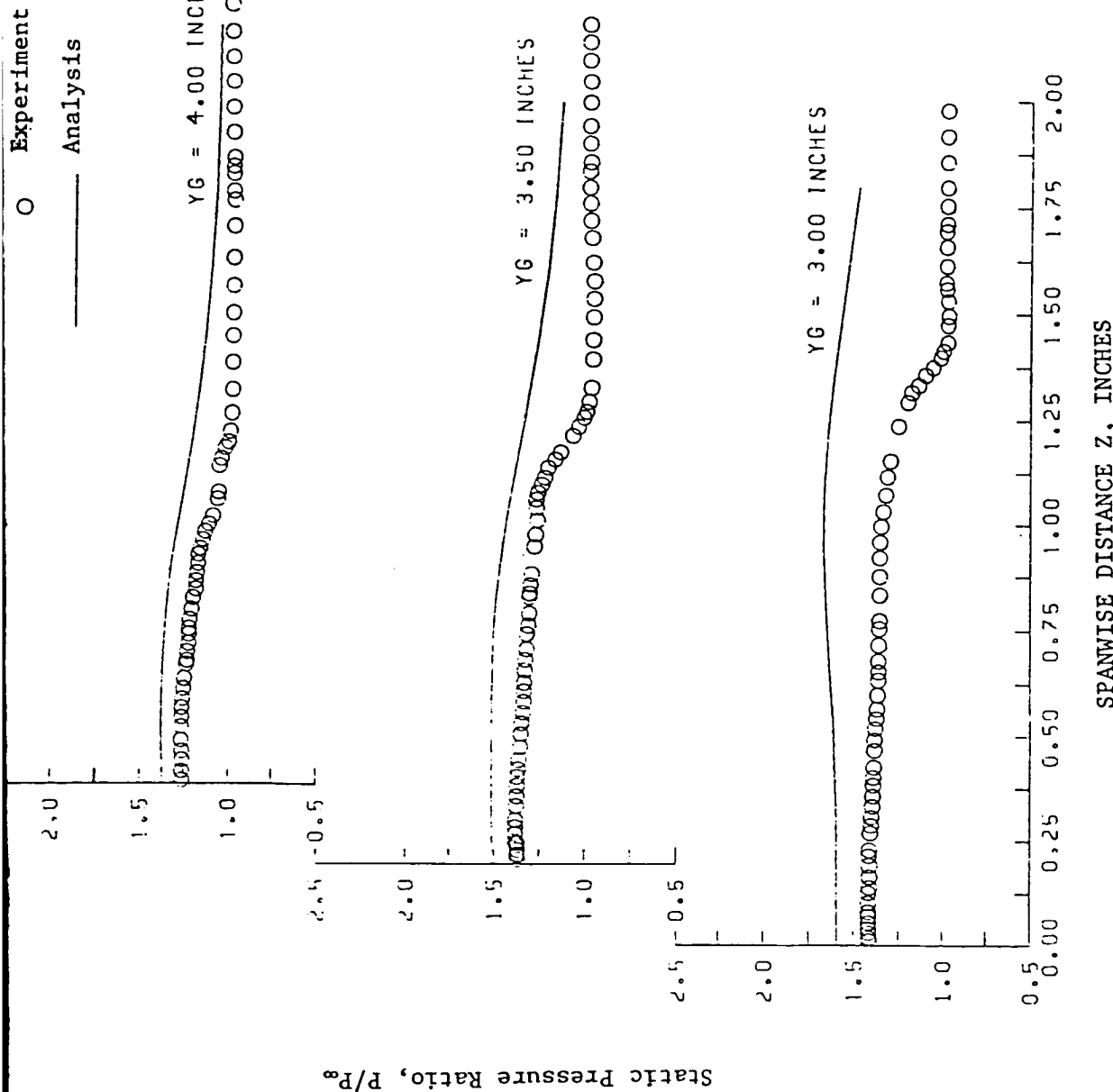


Figure 22 (c) - Glancing Shock Wave - Boundary Layer Interaction -
Static Pressure at $X = 7.6$.

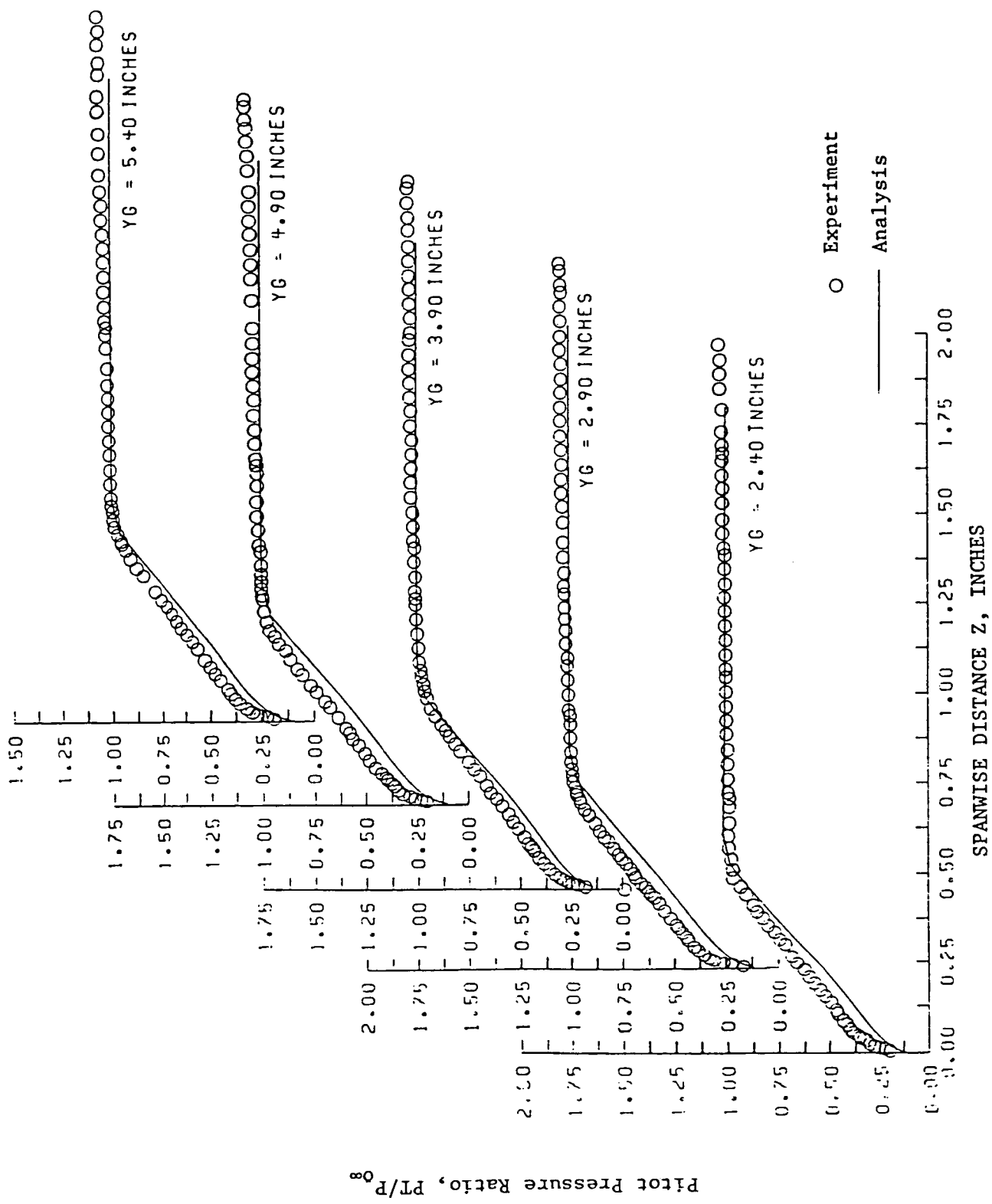


Figure 23 - Glancing Shock Wave - Boundary Layer Interaction -
Pitot Pressure at $X = 3.56$.

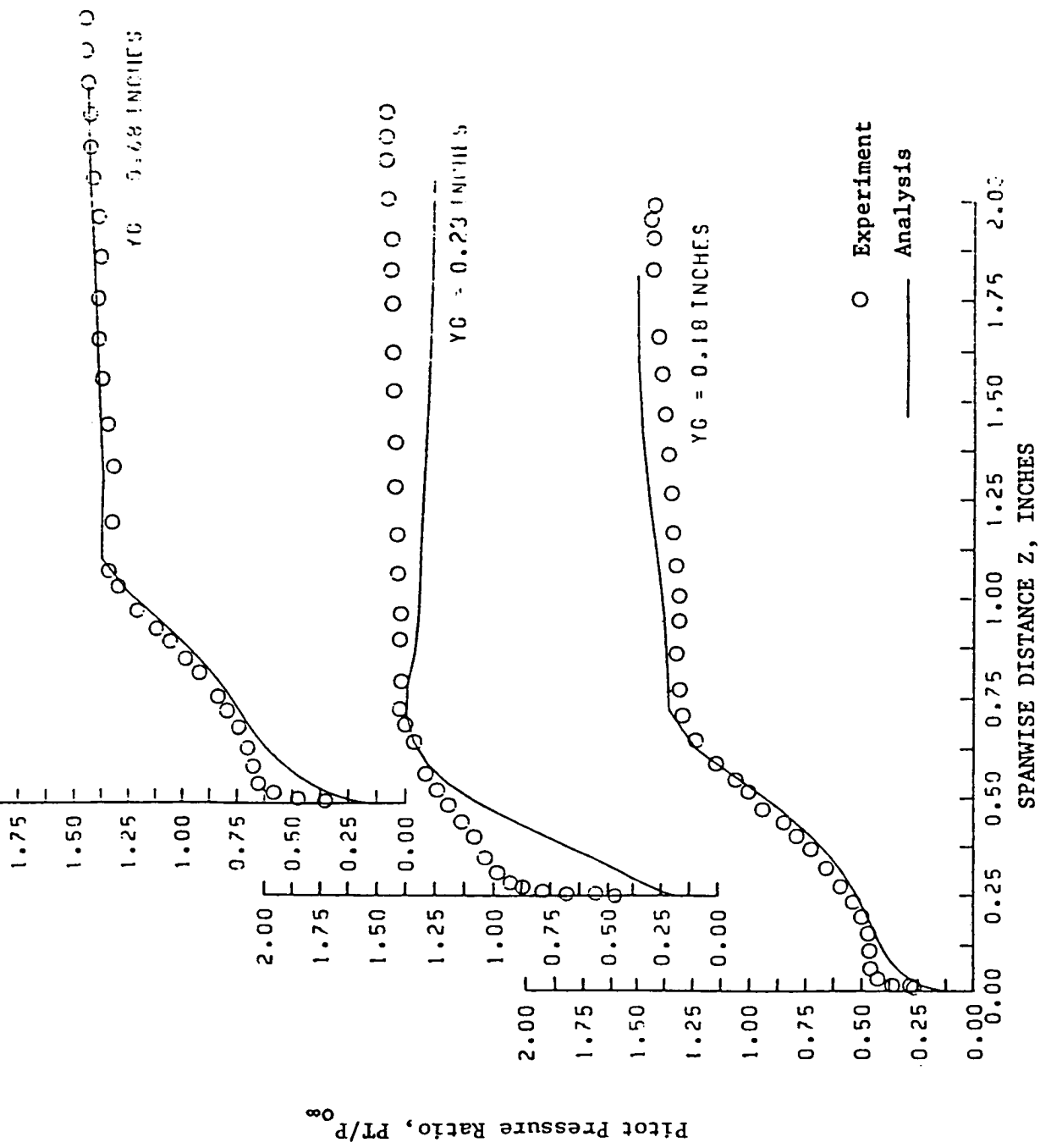


Figure 24 - Glancing Shock Wave - Boundary Layer Interaction -
Pitot Pressure at $X = 5.1$.

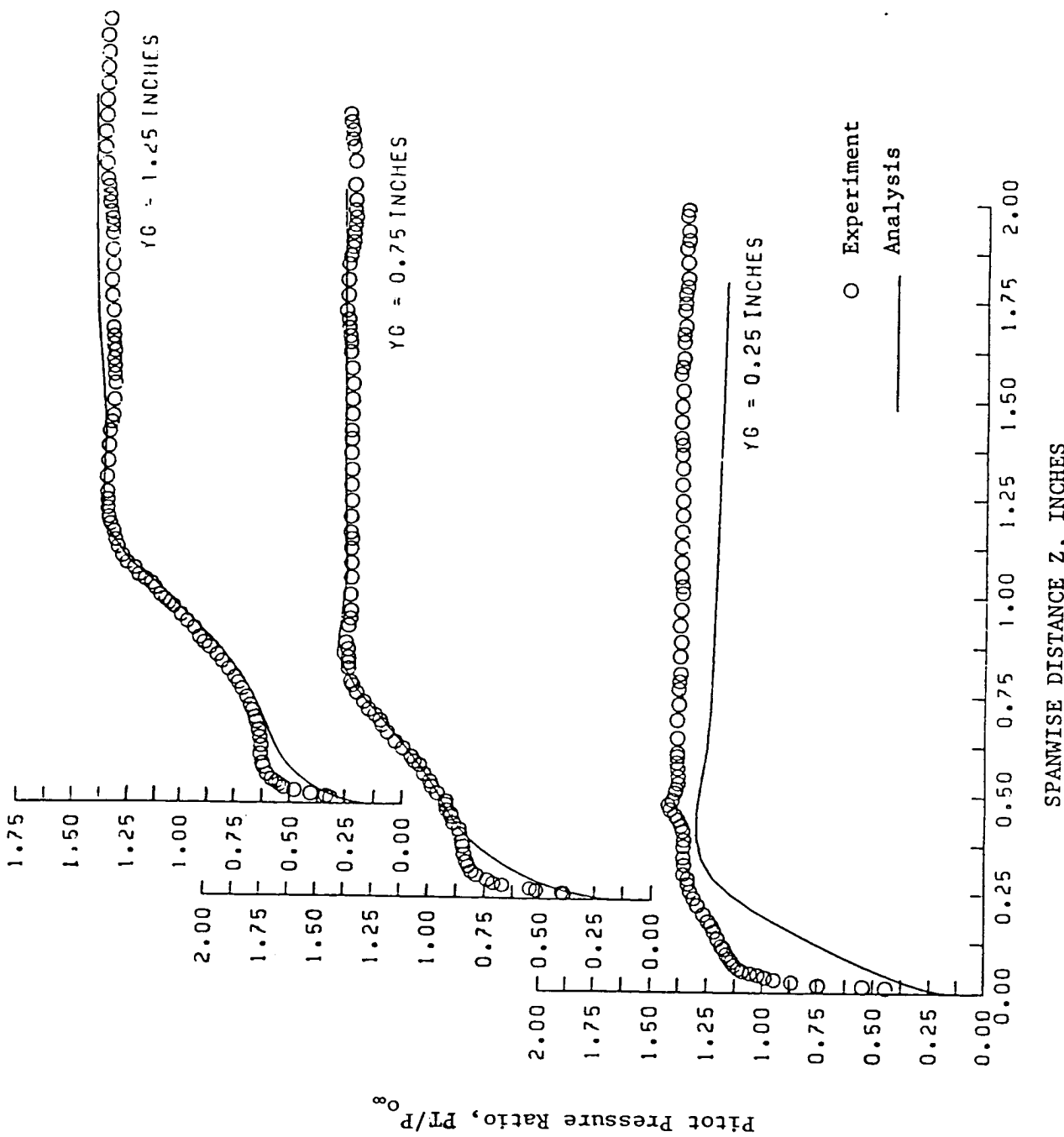


Figure 25 - Glancing Shock Wave - Boundary Layer Interaction -
Pitot Pressure at $X = 7.1$.

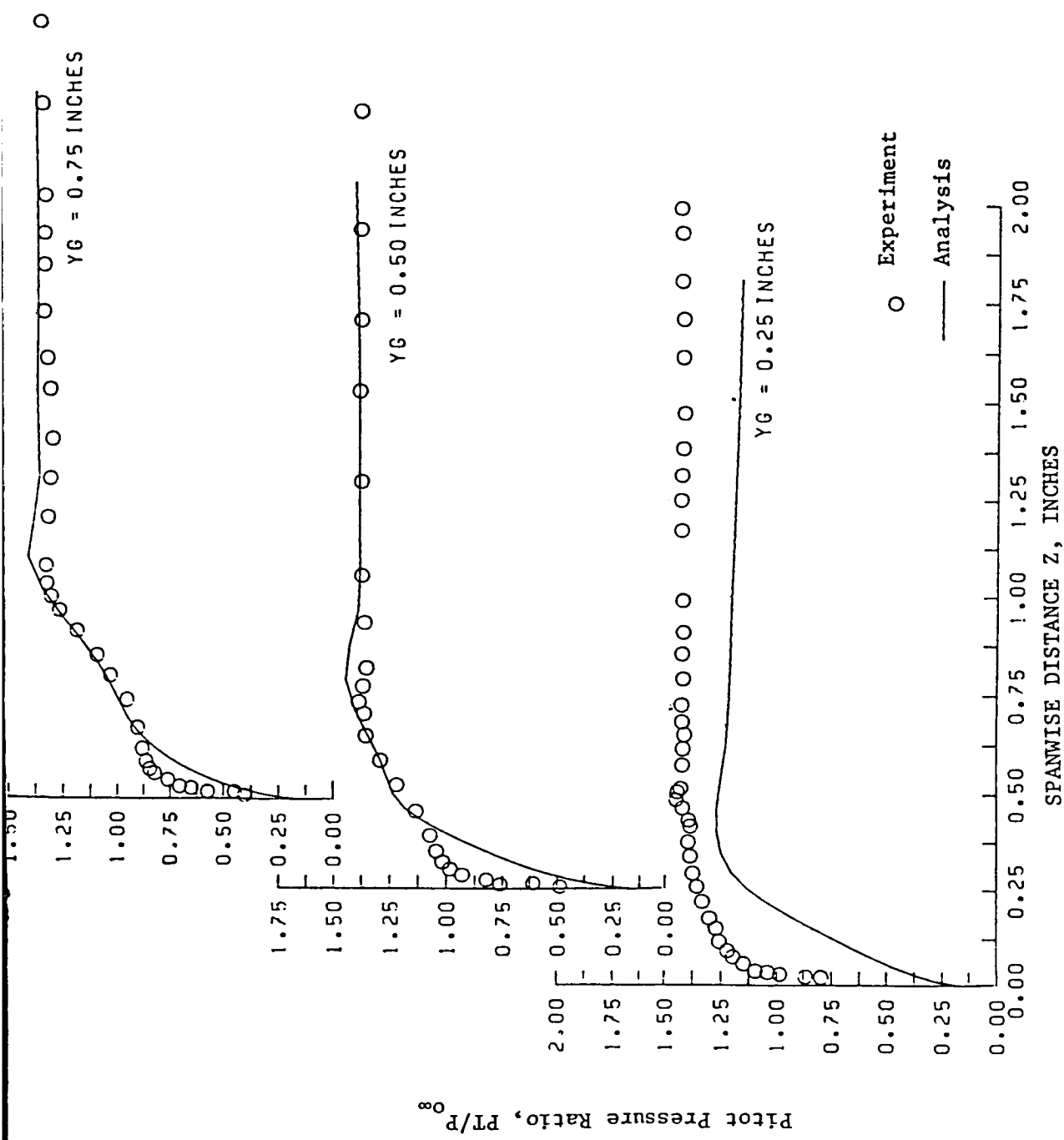


Figure 26(a) - Glancing Shock Wave - Boundary Layer Interaction -
Pitot Pressure at $X = 7.6$.

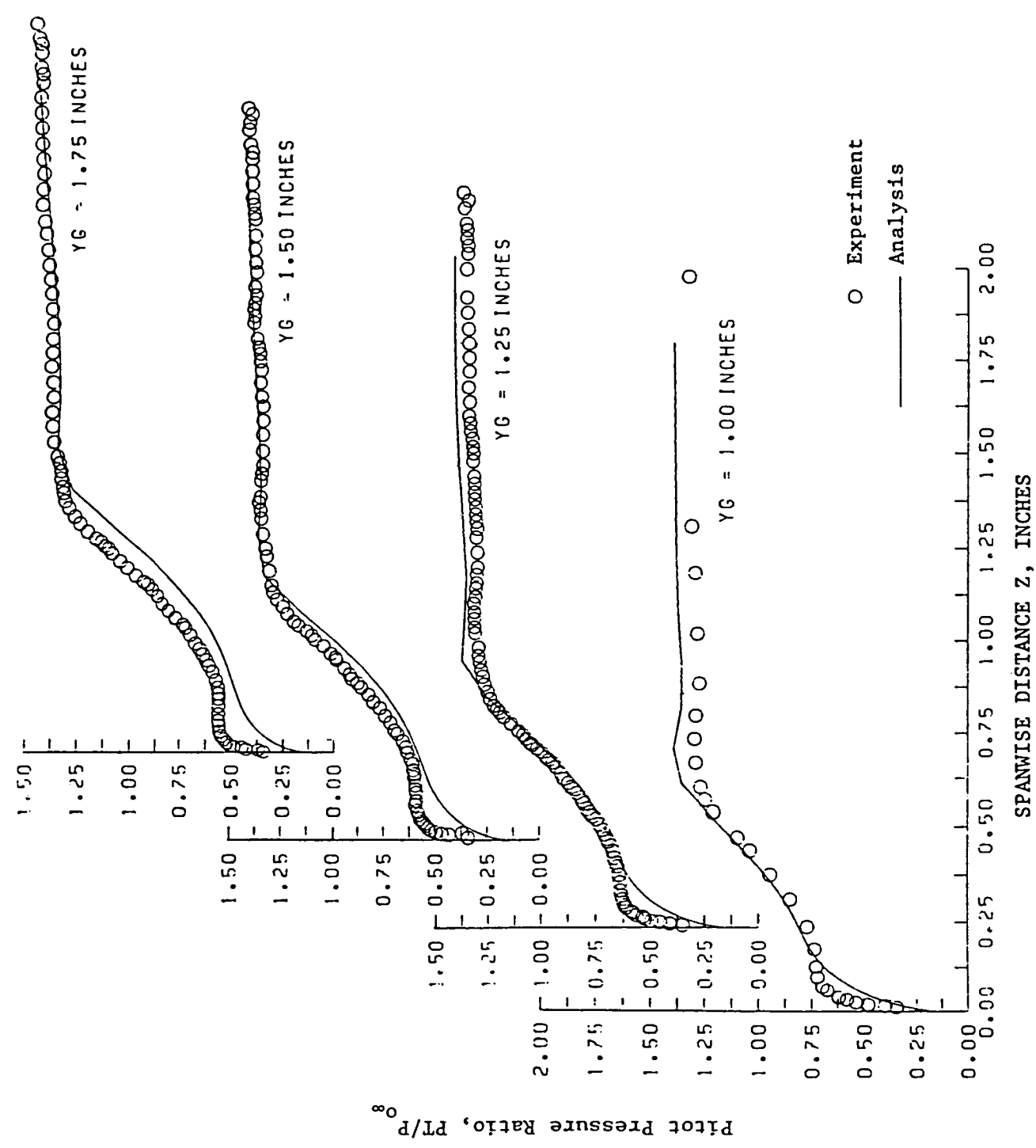


Figure 26(b) - Glancing Shock Wave - Boundary Layer Interaction -
Pitot Pressure at $Y = 7.6$

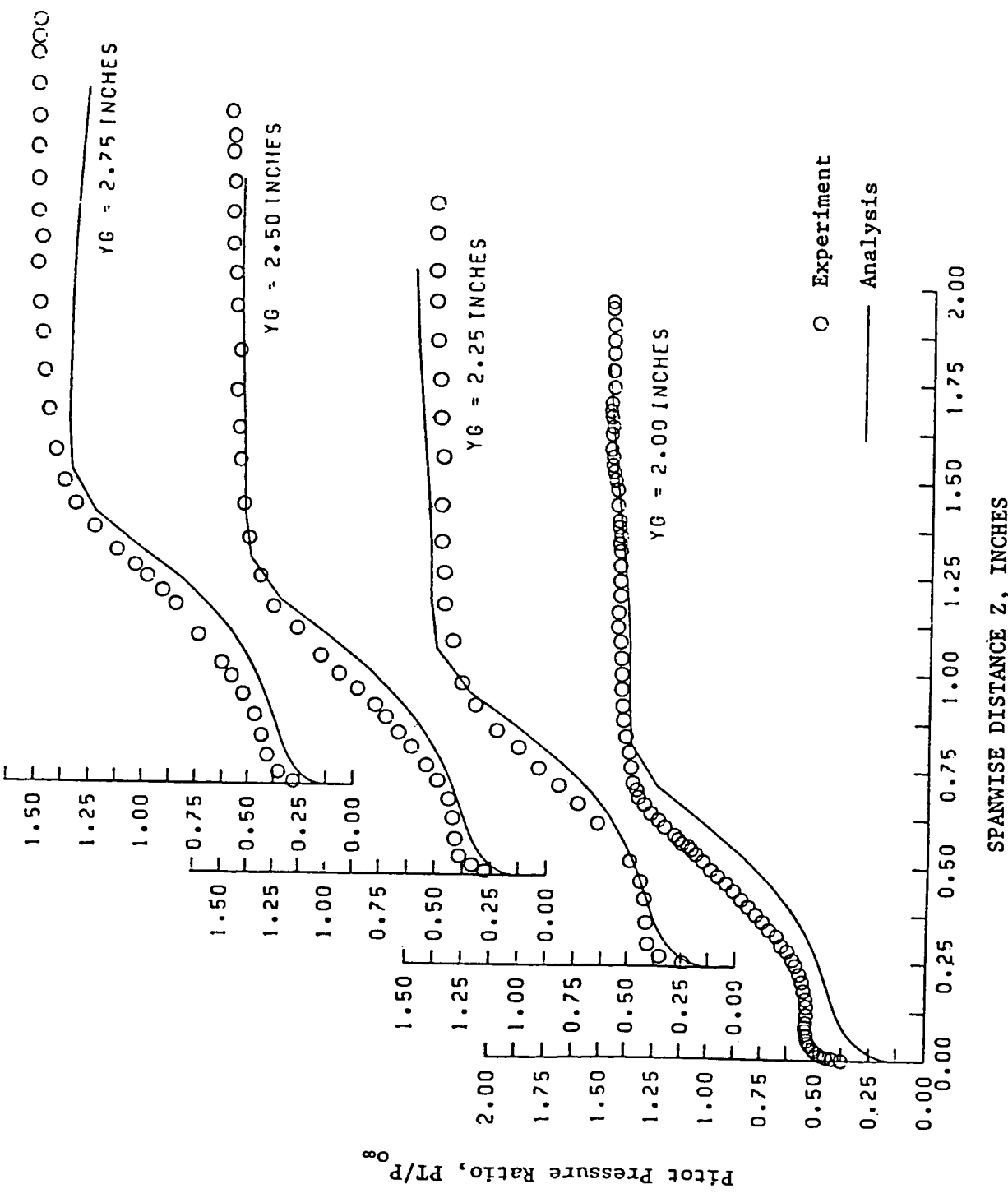


Figure 26(c) - Glancing Shock Wave - Boundary Layer Interaction -
Pitot Pressure at $X = 7.6$.

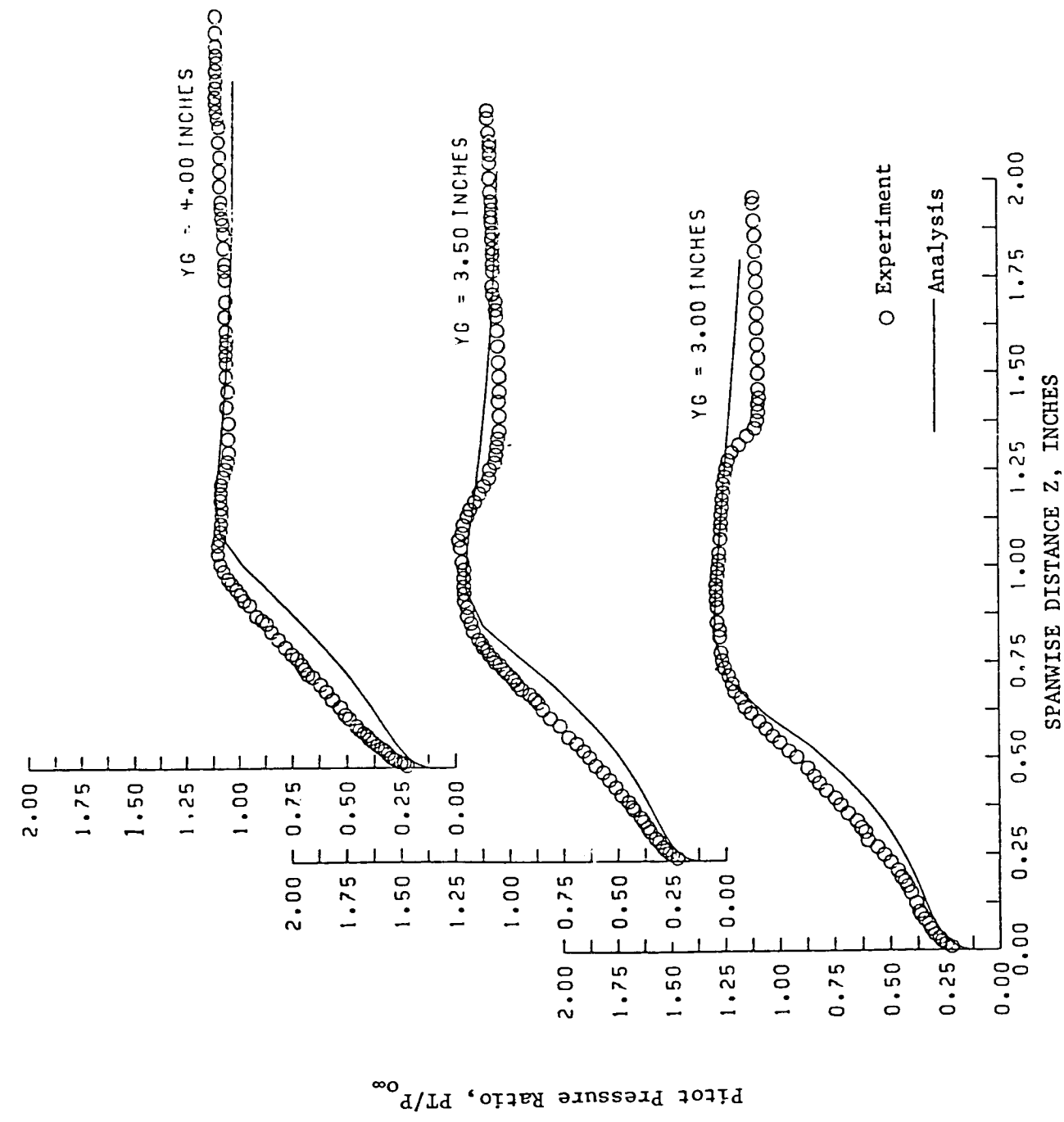


Figure 26(d) - Glancing Shock Wave - Boundary Layer Interaction -

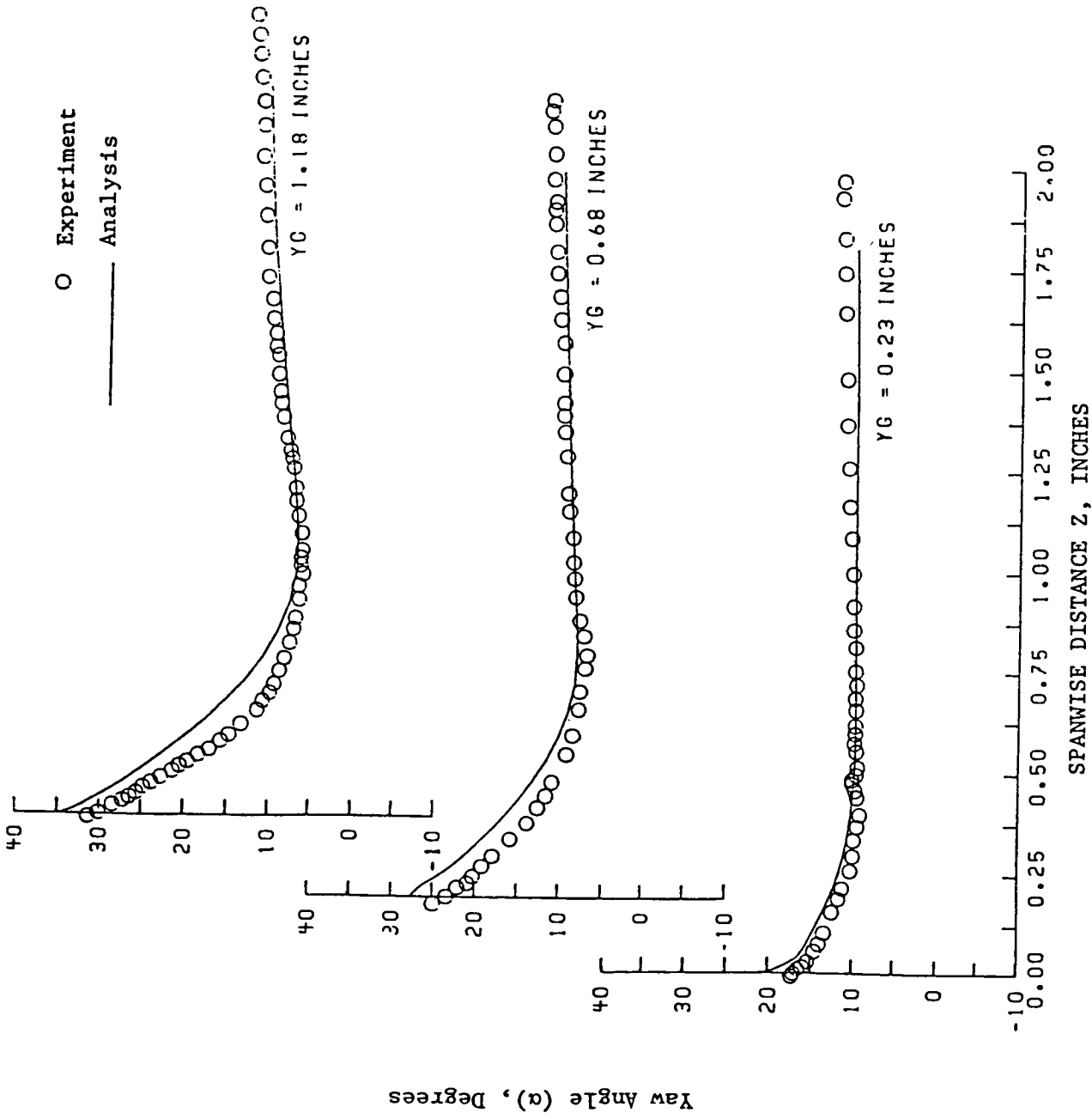


Figure 27 - Glancing Shock Wave - Boundary Layer Interaction -
Yaw Angle at $X = 5.1$.

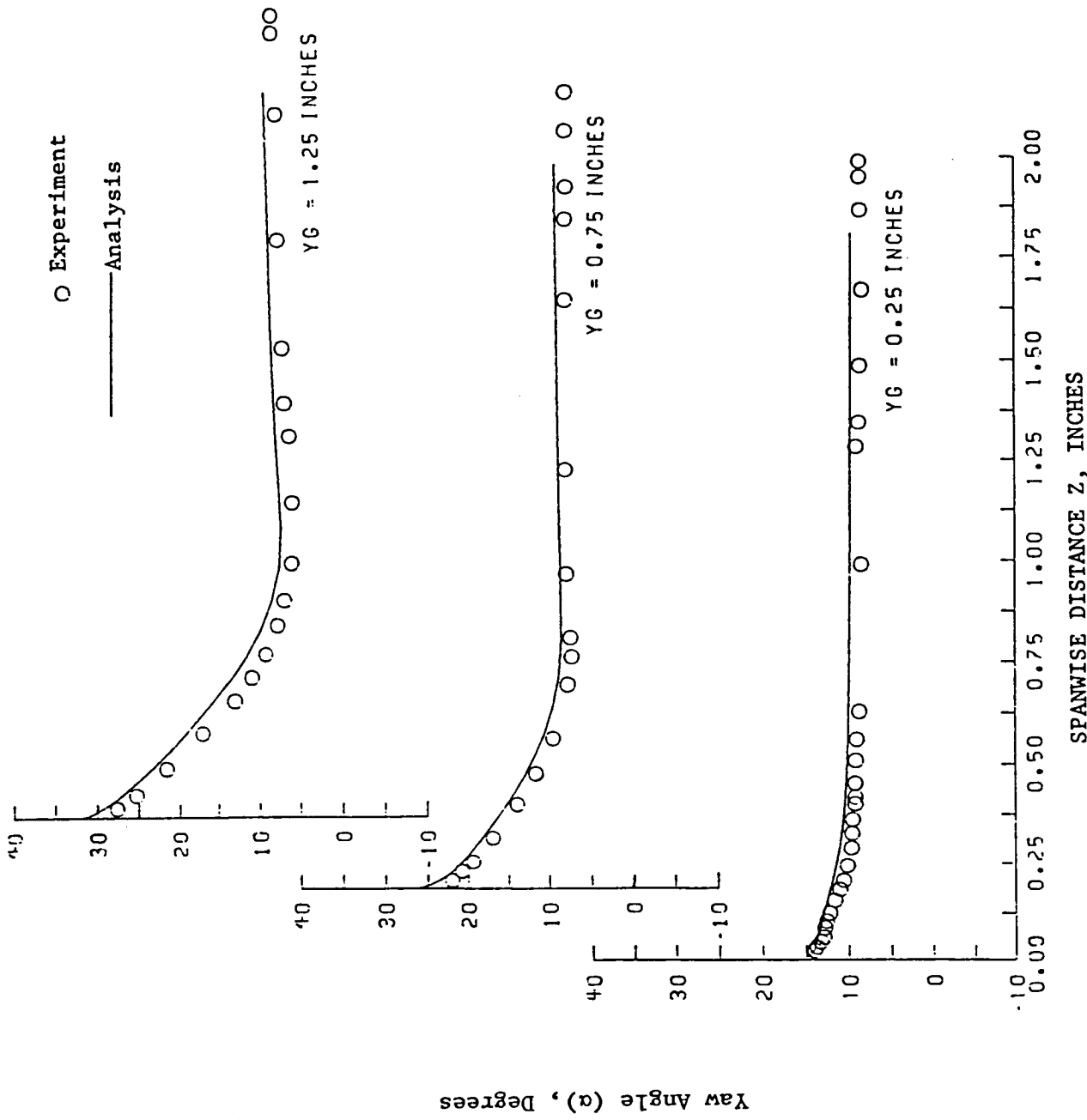


Figure 28 - Glancing Shock Wave - Boundary Layer Interaction -
Yaw Angle at $X = 7.1$.

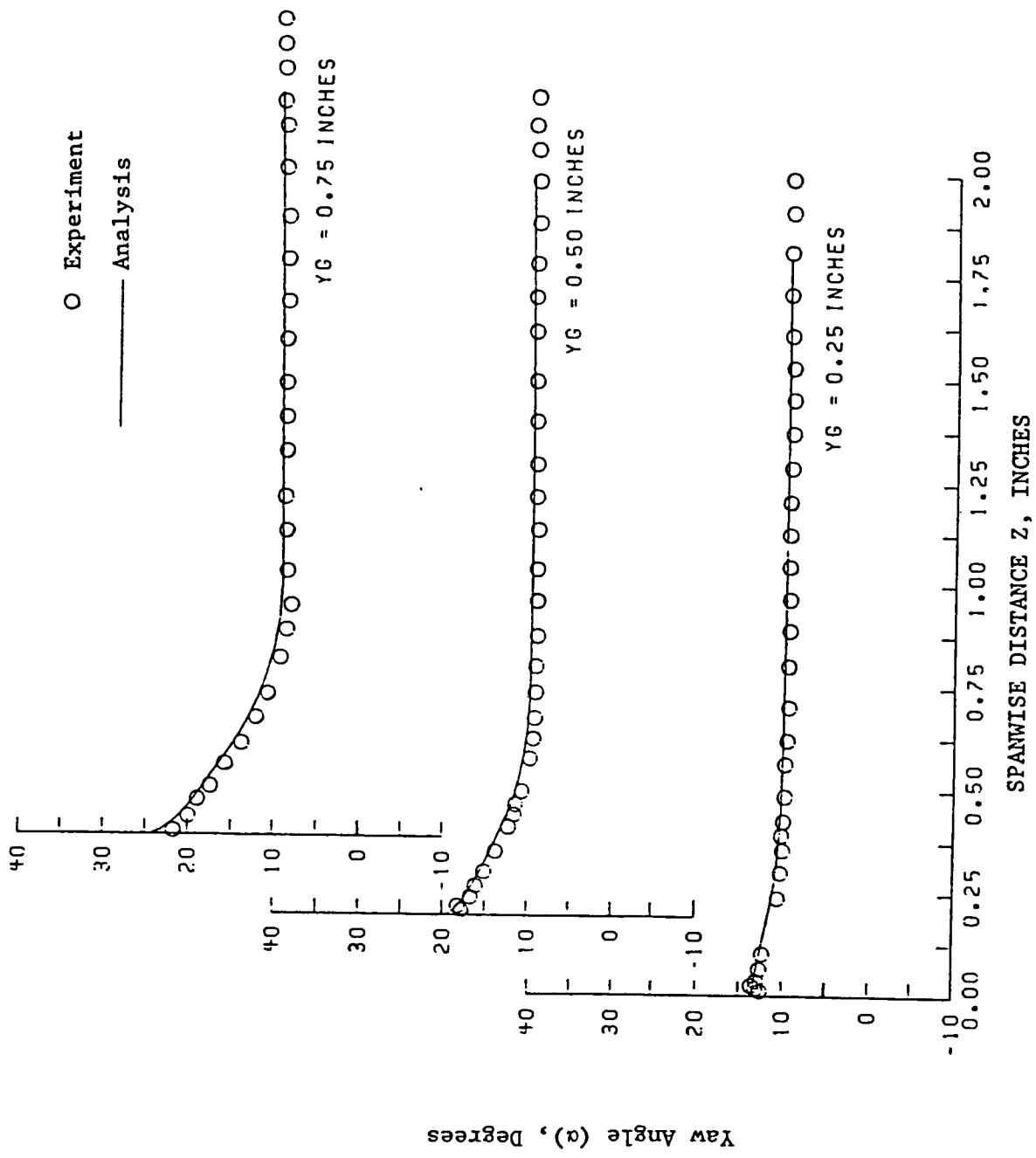


Figure 29(a) – Glancing Shock Wave – Boundary Layer Interaction –
Yaw Angle at $X = 7.6$.

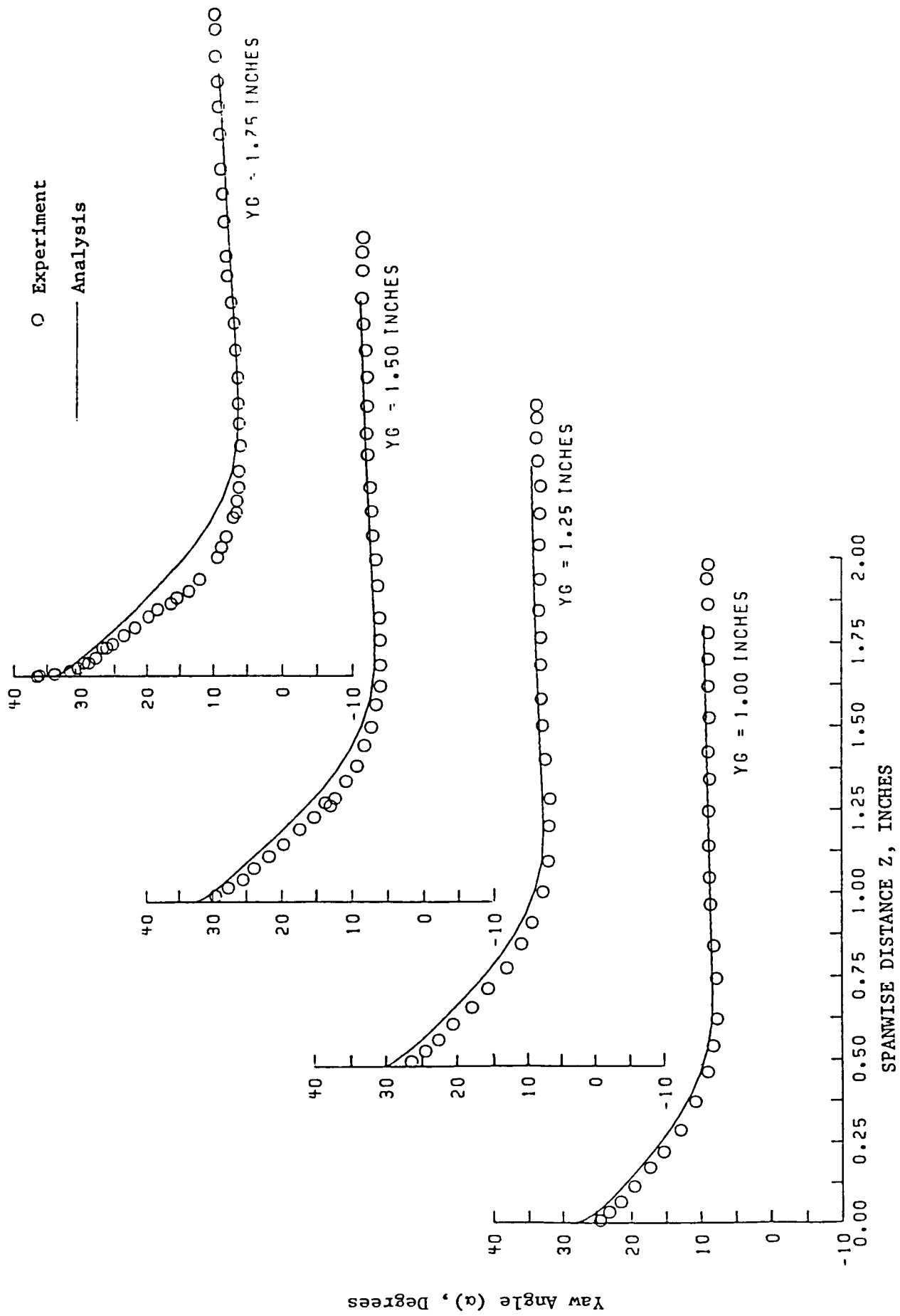


Figure 29(b) - Glancing Shock Wave - Boundary Layer Interaction -
Yaw Angle at $X = 7.6$.

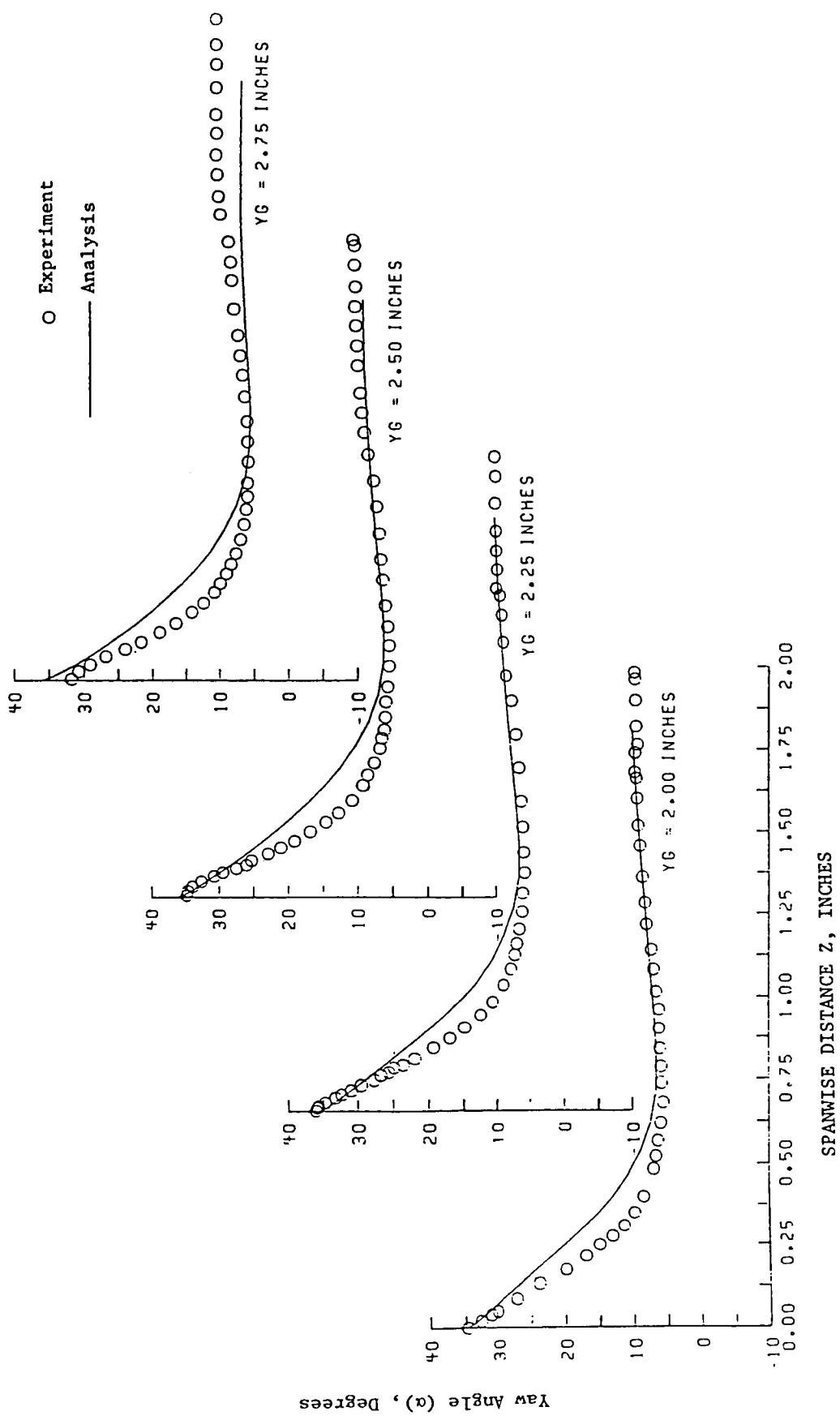


Figure 29(c) - Glancing Shock Wave - Boundary Layer Interaction -
Yaw Angle at $X = 7.6$.

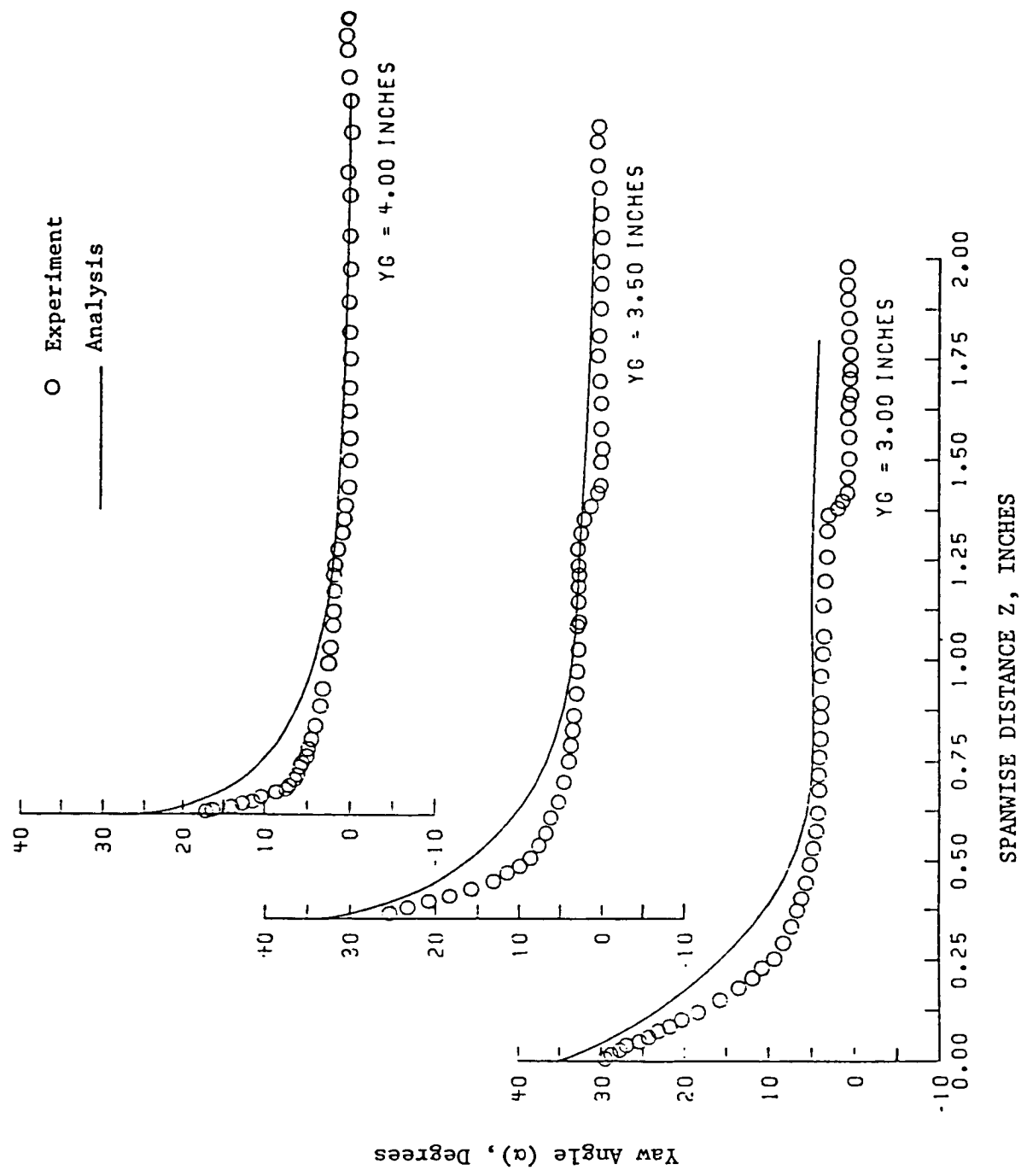


Figure 29(d) – Glancing Shock Wave – Boundary Layer Interaction –
Yaw Angle at $X = 7.6$.

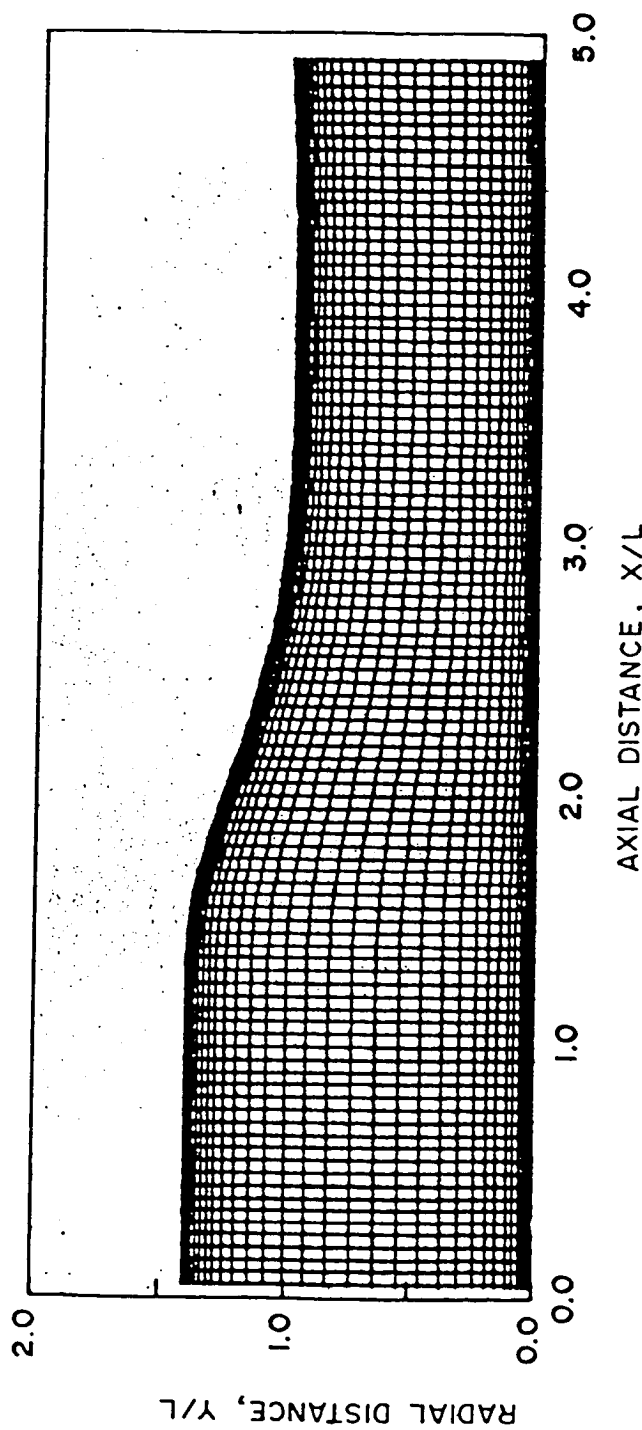


Figure 30 - Nonorthogonal Channel Flow - Computational Mesh.

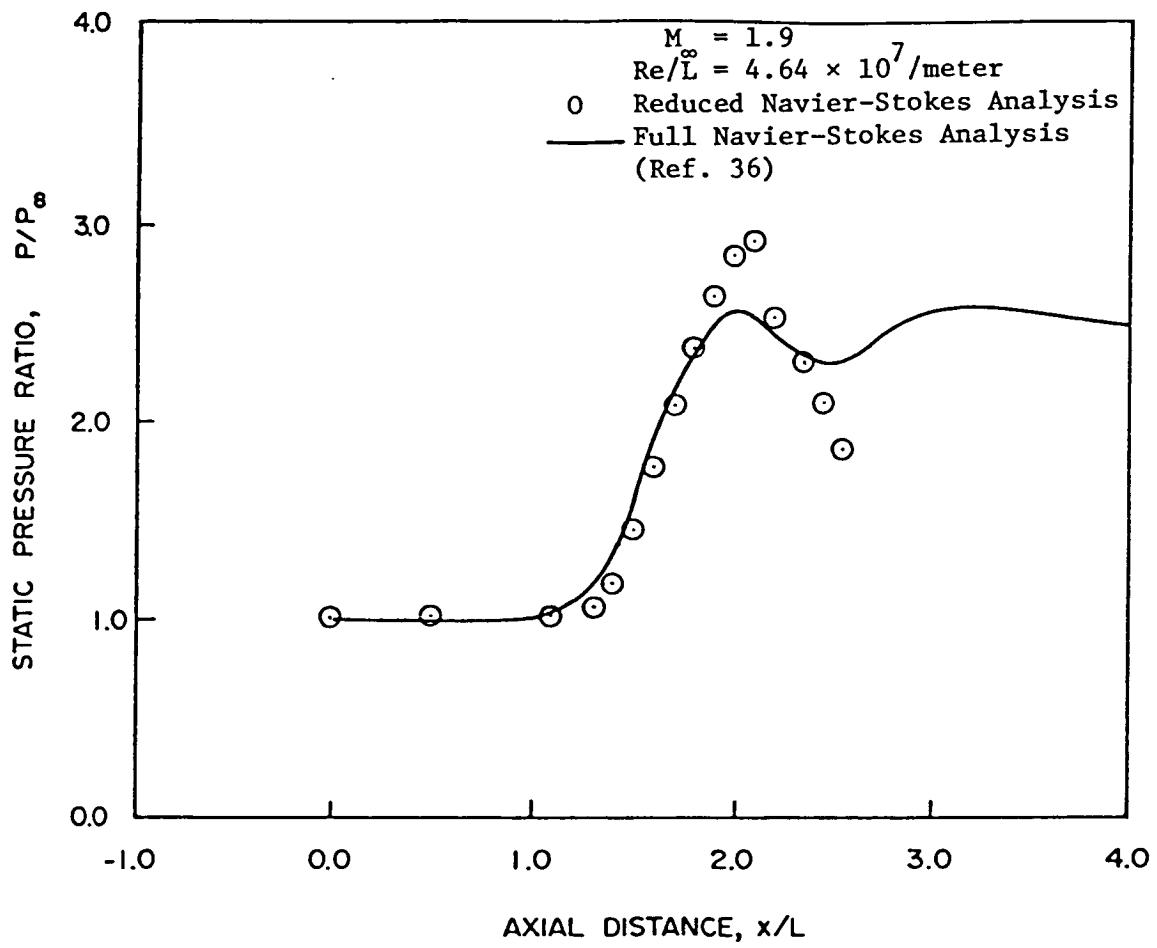


Figure 31 - Comparison of Computed Pressure Distribution on Upper Wall.

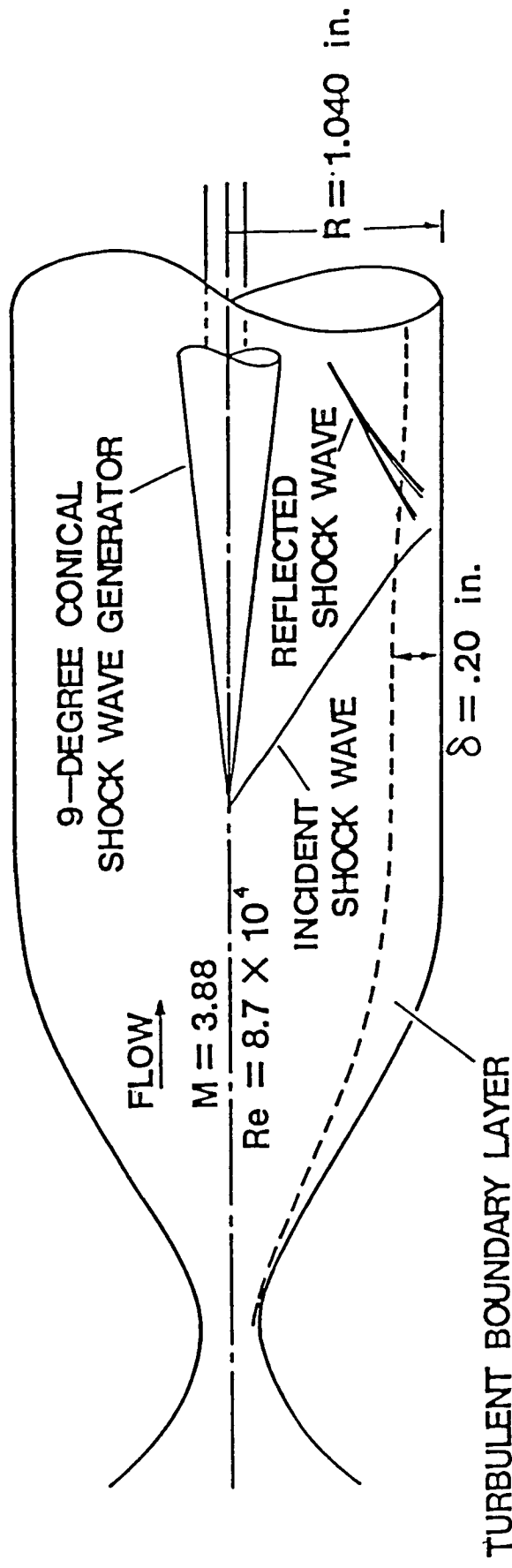


Figure 32 - Supersonic Turbulent Shock Wave-Boundary Layer Interaction - Schematic of Experimental Facility.

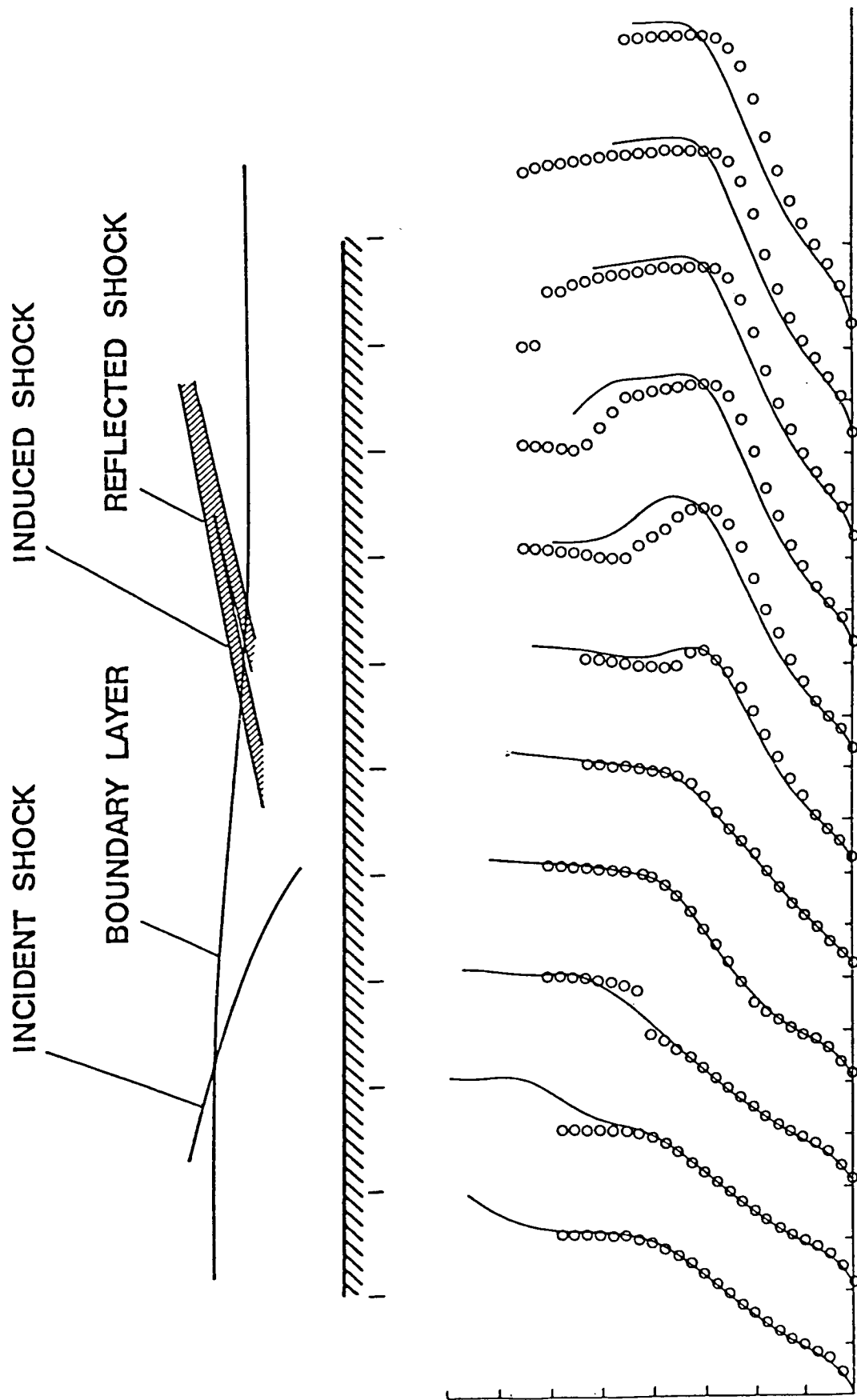


Figure 33 - Supersonic Turbulent Shock Wave-Boundary Layer Interaction - Stagnation Pressure.

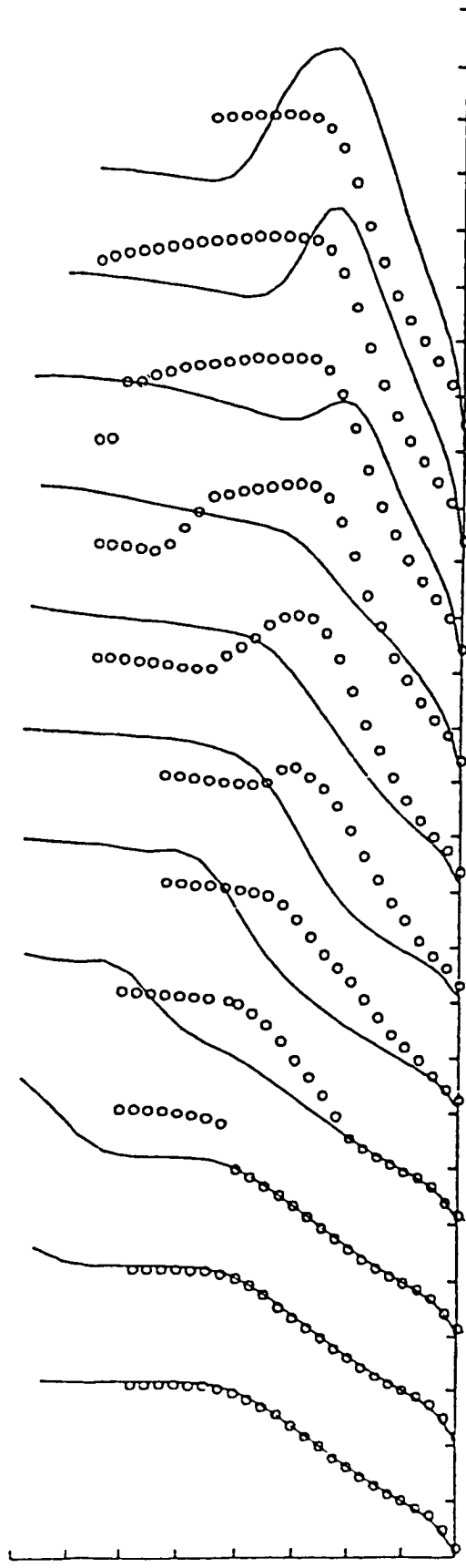
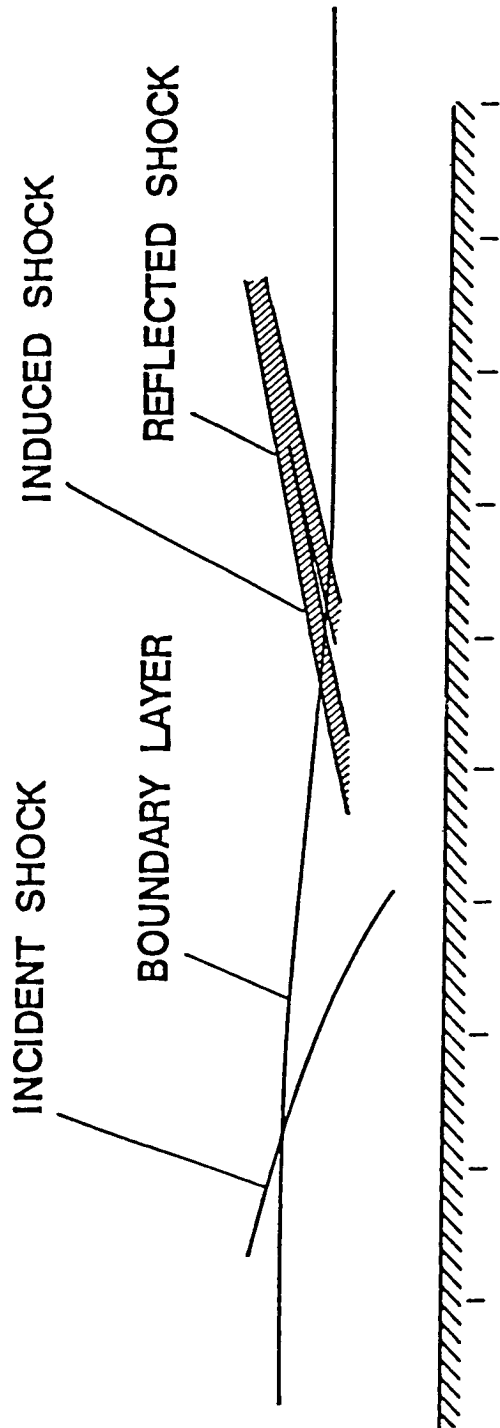


Figure 34 - Supersonic Turbulent Shock Wave-Boundary Layer Interaction - Stagnation Pressure (Rudman & Rubin).

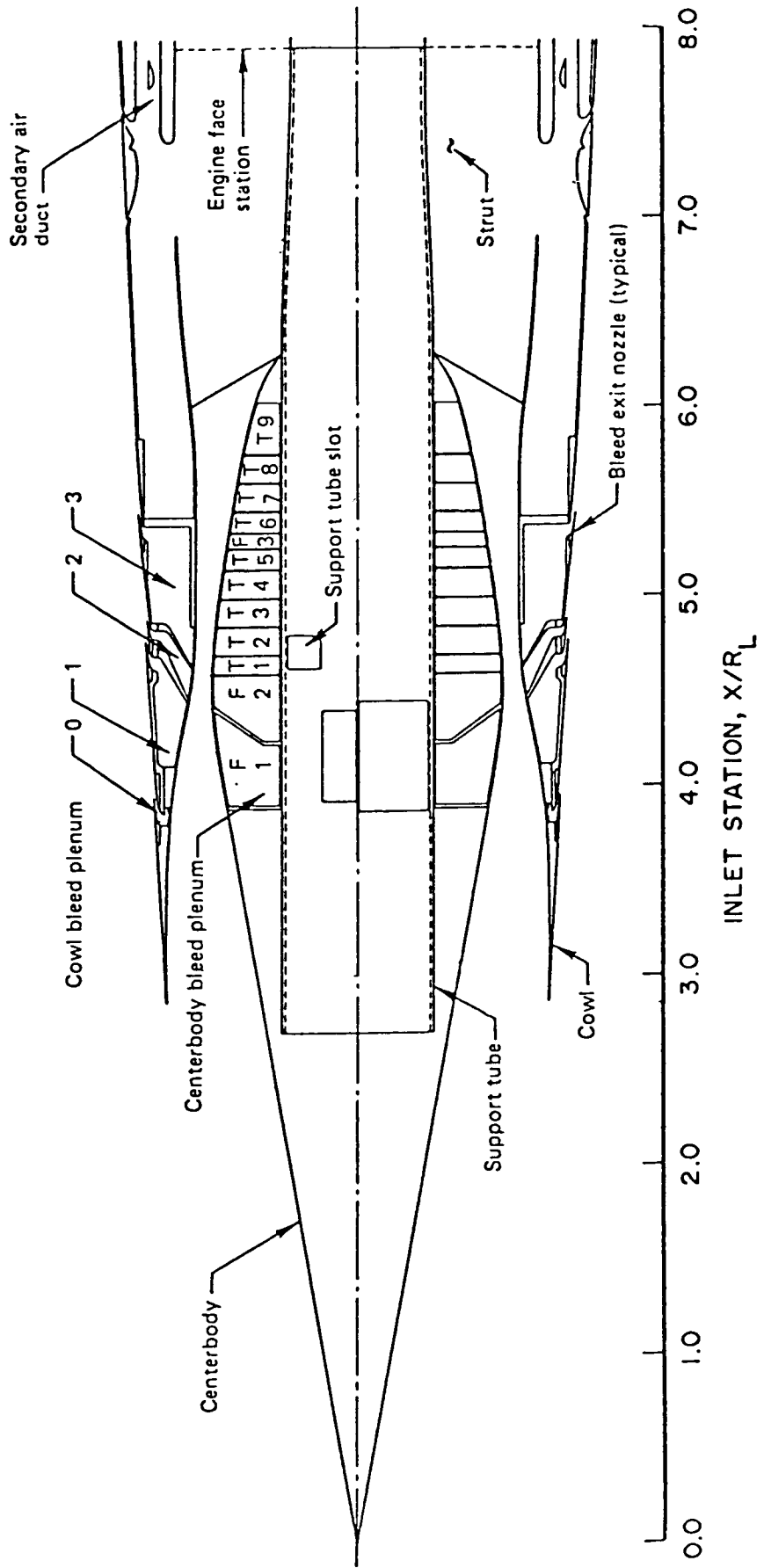


Figure 35 – Axisymmetric Inlet – Mach 3.5 Inlet Model Schematic.

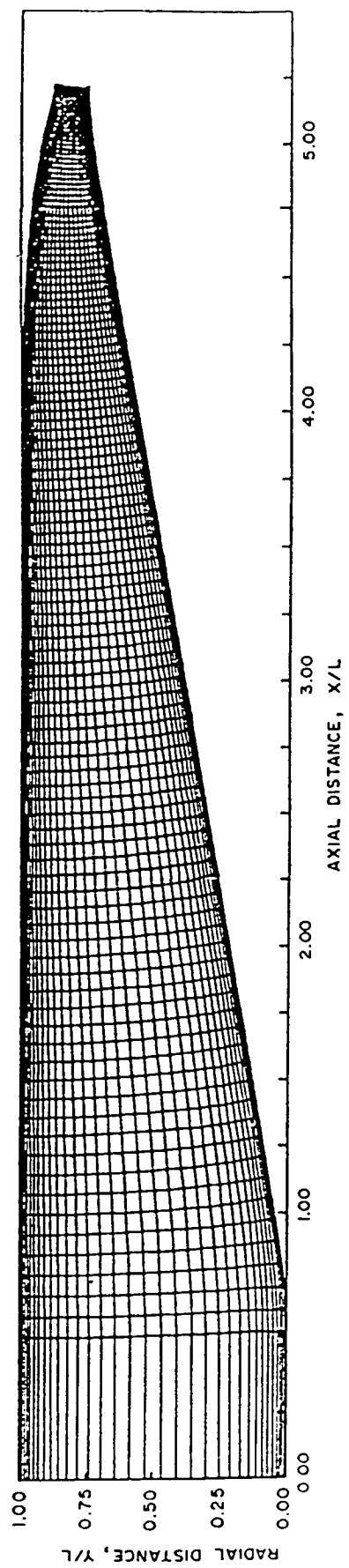


Figure 36 - Axisymmetric Inlet - Computation Mesh.

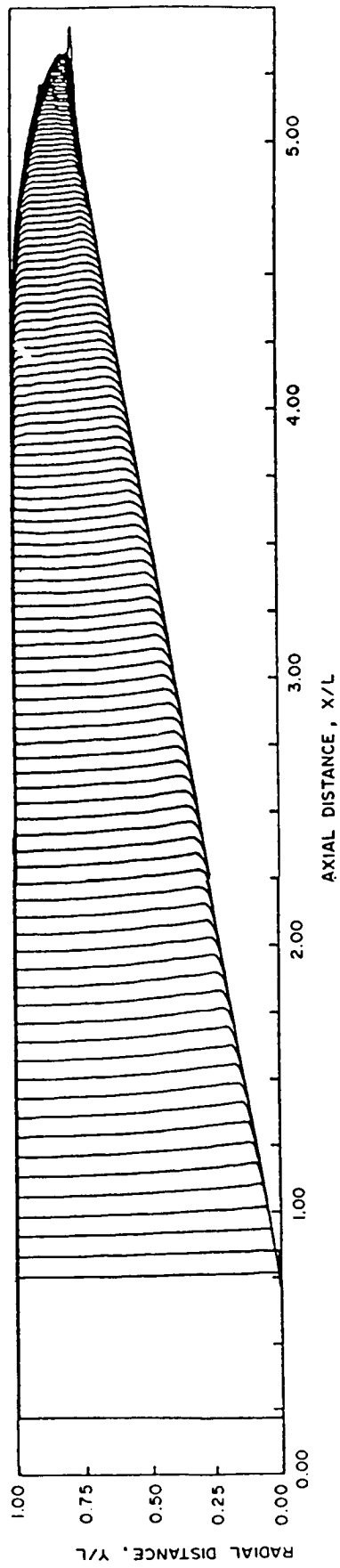
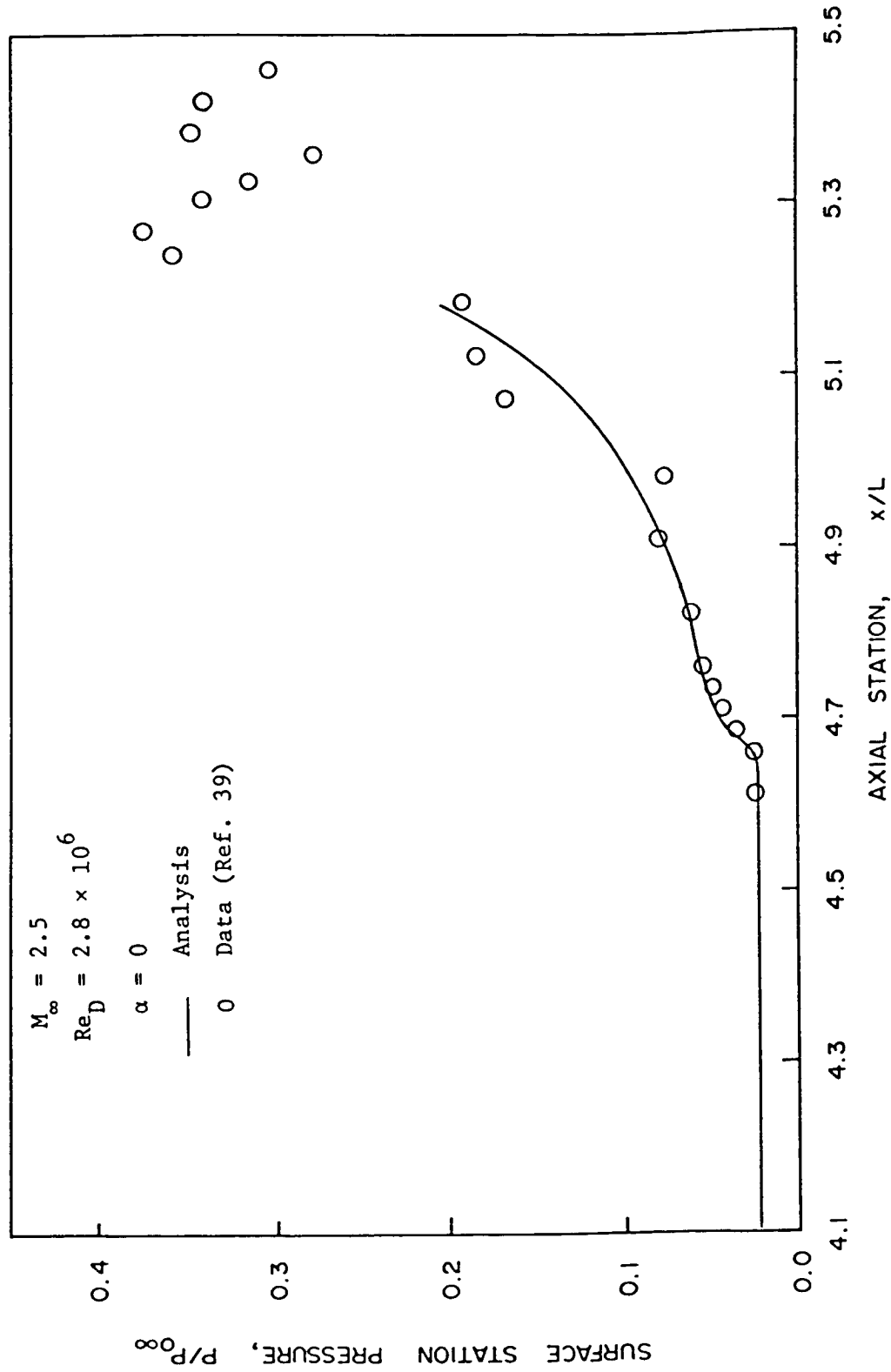


Figure 37 - Axisymmetric Inlet - Streamwise Development of Axial Mach Number Profiles.



Figure 38 - Axisymmetric Inlet - Streamwise Development of Axial Mach Number Profiles.



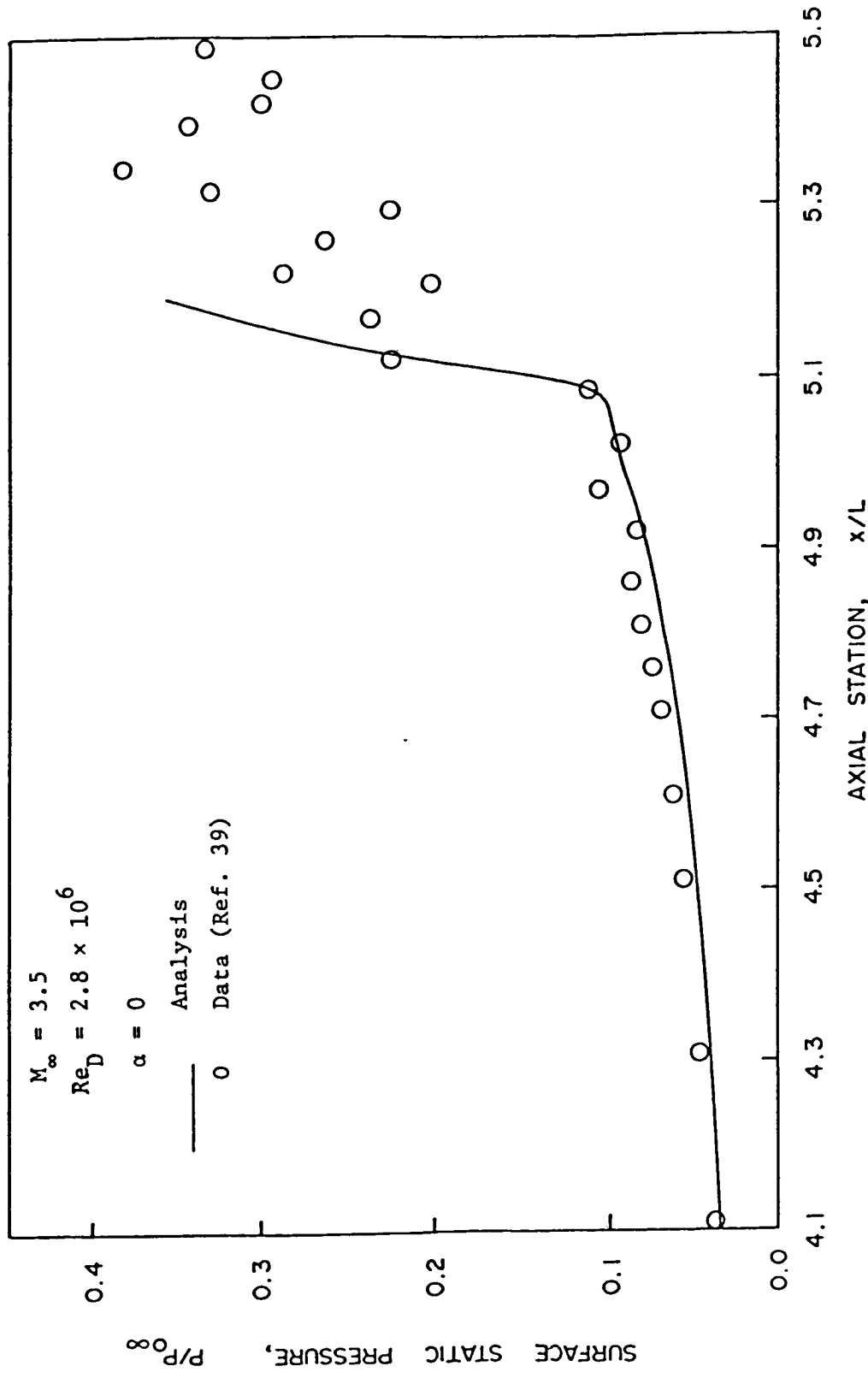


Figure 40 - Axisymmetric Inlet - Comparison of Cowl Static Pressure.

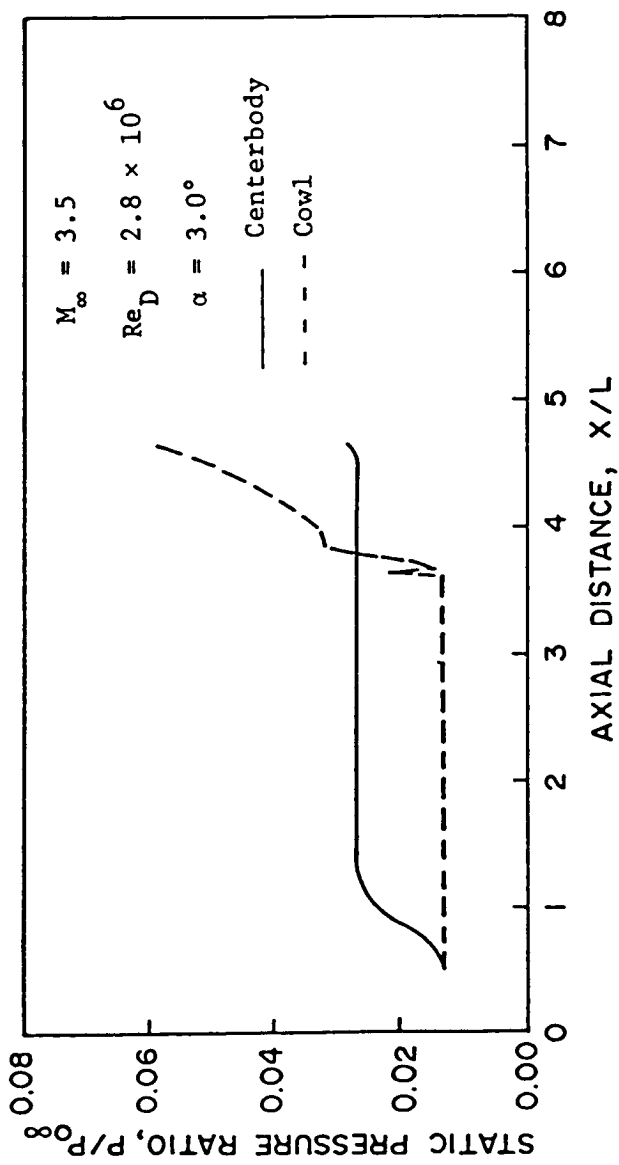


Figure 41 - Axisymmetric Inlet at Angle of Attack - Streamwise Static Pressure Distribution on both Centerbody and Cowl on Windward Ray.

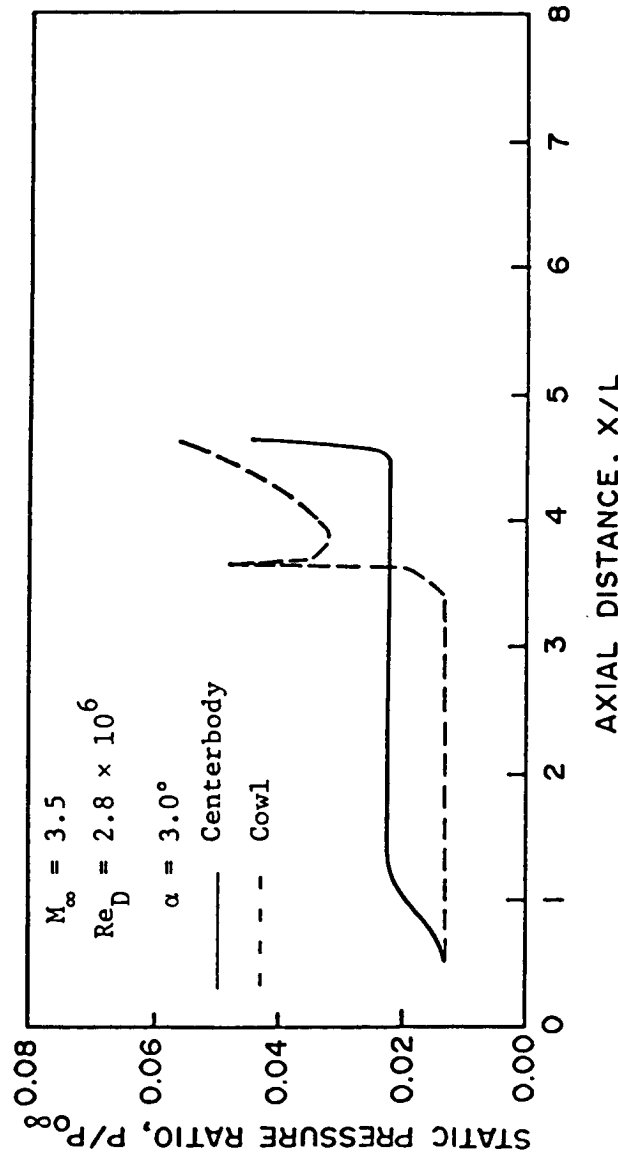


Figure 42 - Axisymmetric Inlet at Angle of Attack - Streamwise Static Pressure Distribution on Both Centerbody and Cowl on Waterline Ray.

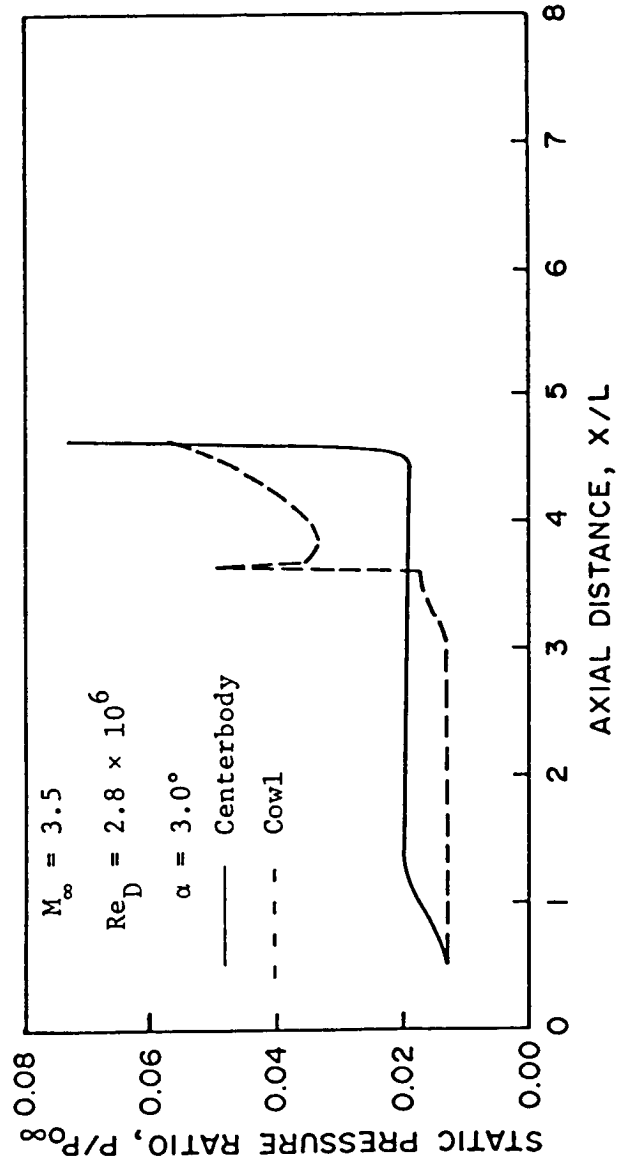


Figure 43 - Axisymmetric Inlet Angle of Attack Streamwise Static Pressure Distribution on Both Centerbody and Cowl on Leeward Ray.

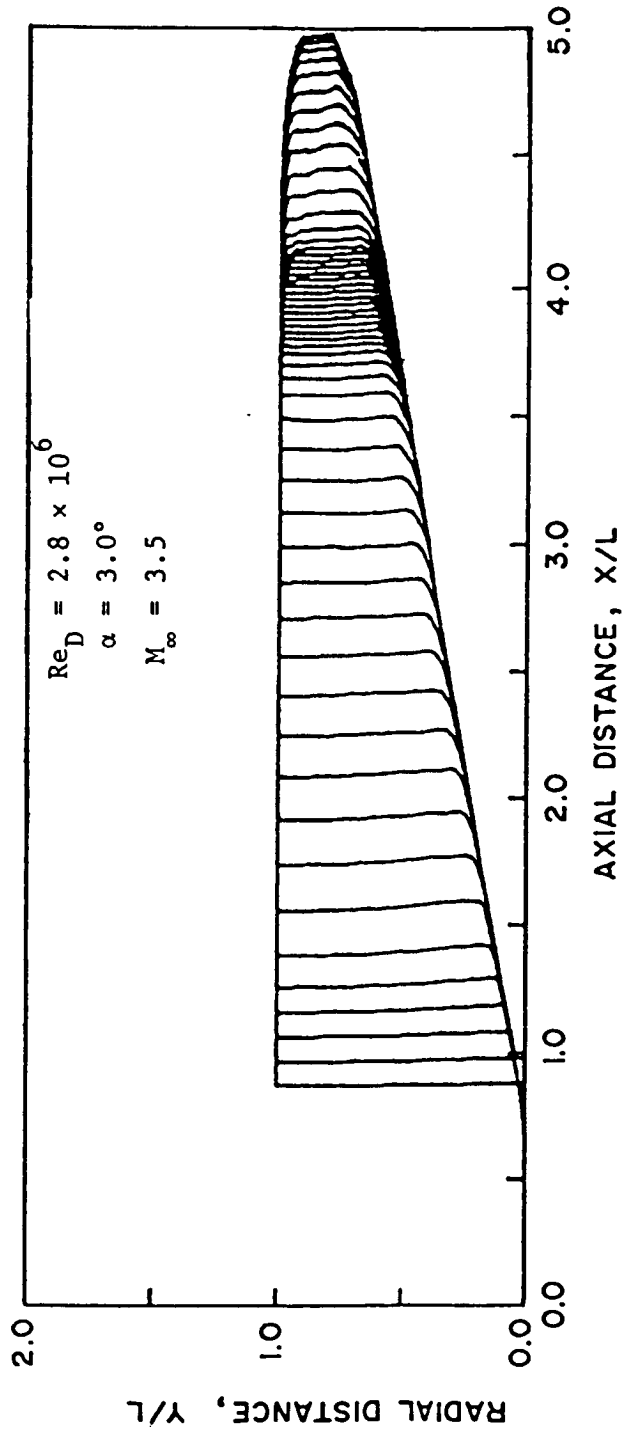


Figure 44 - Axisymmetric Inlet of Angle of Attack - Streamwise Development of Axial - Mach Number Profiles on Windward Ray.

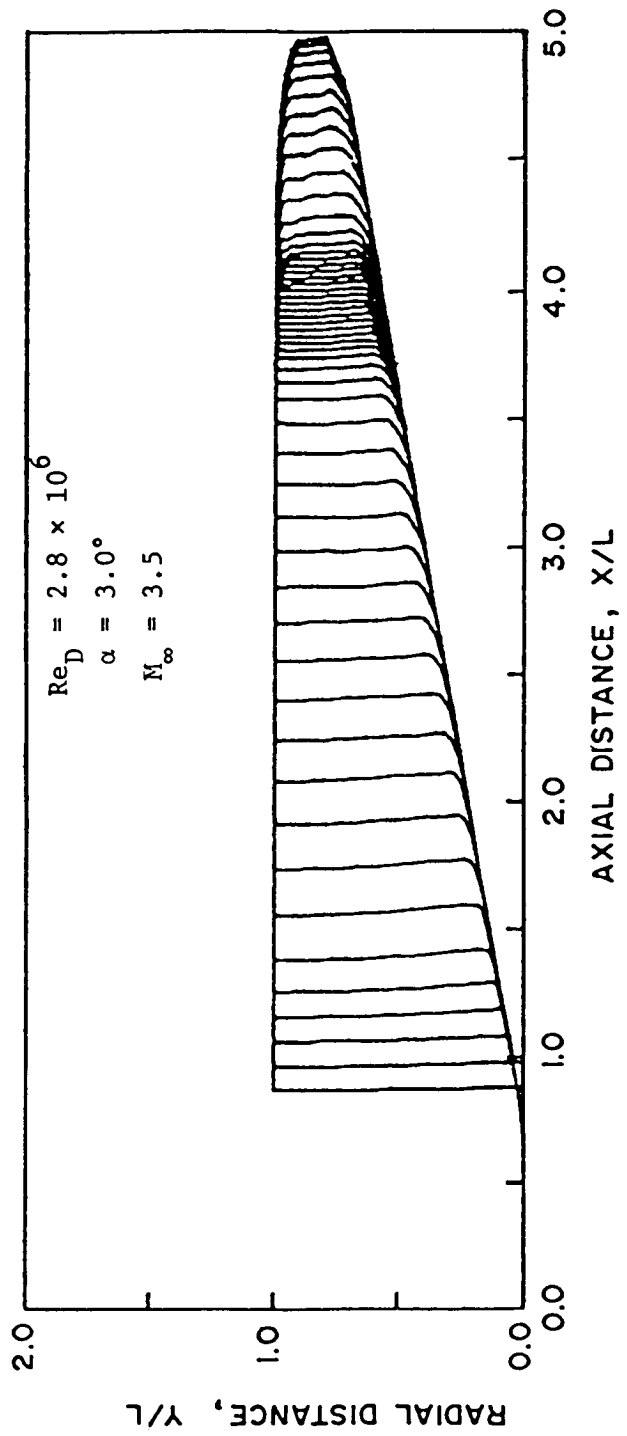


Figure 45 - Axisymmetric Inlet of Angle of Attack - Streamwise Development of Mach Number Profiles on Waterline Ray.

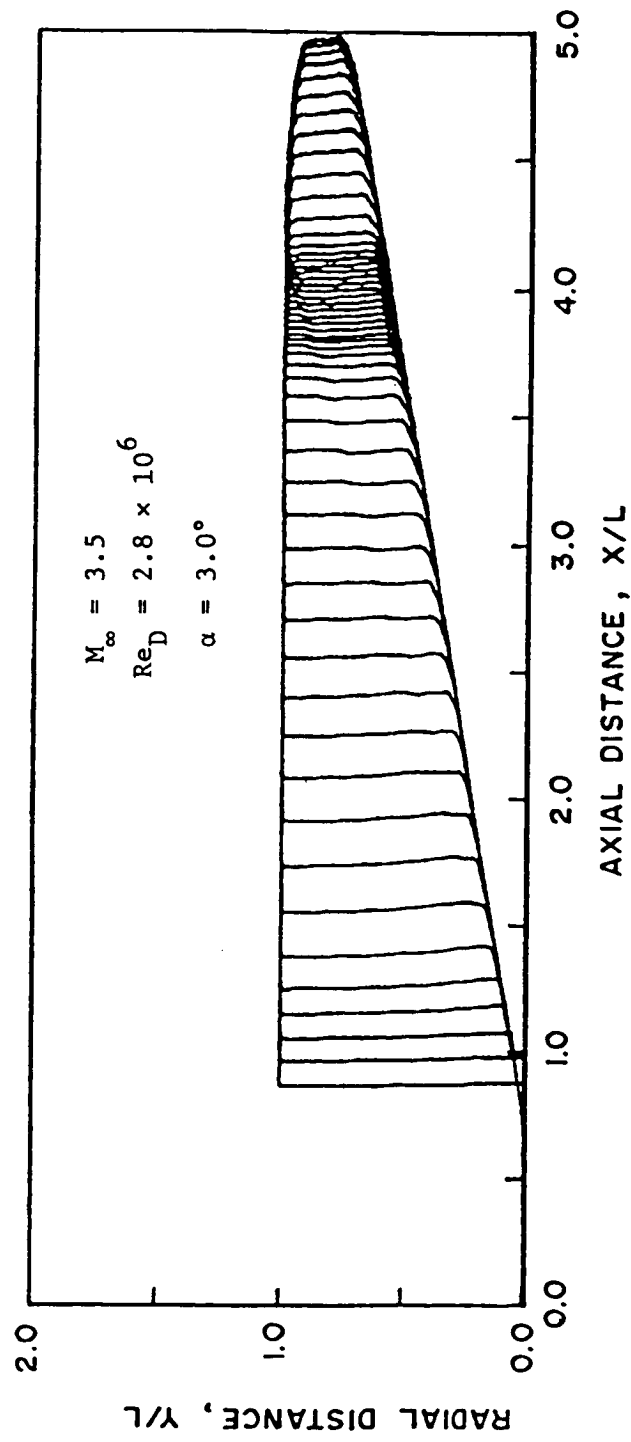


Figure 46 - Axisymmetric Inlet at Angle of Attack - Streamwise Development of Mach Number Profiles on Leeward Ray.

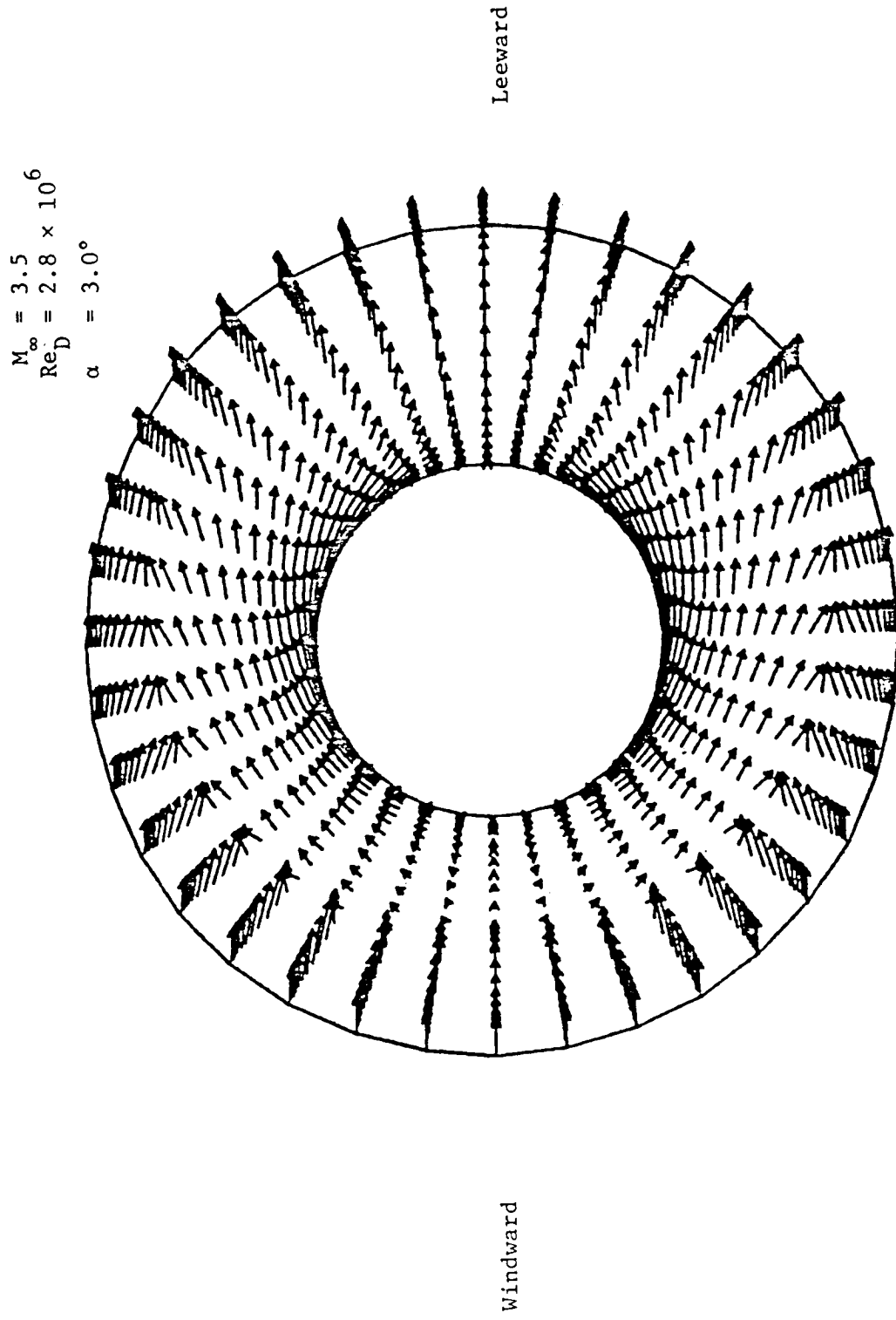


Figure 47 - Axisymmetric Inlet of Angle of Attack - Typical Secondary Velocity Vectors in the Cross Section - Axial Location - $X/R_1 = 2.45$

$$M_{\infty} = 3.5$$

$$Re_D = 2.8 \times 10^6$$

$$\alpha = 3.0^\circ$$

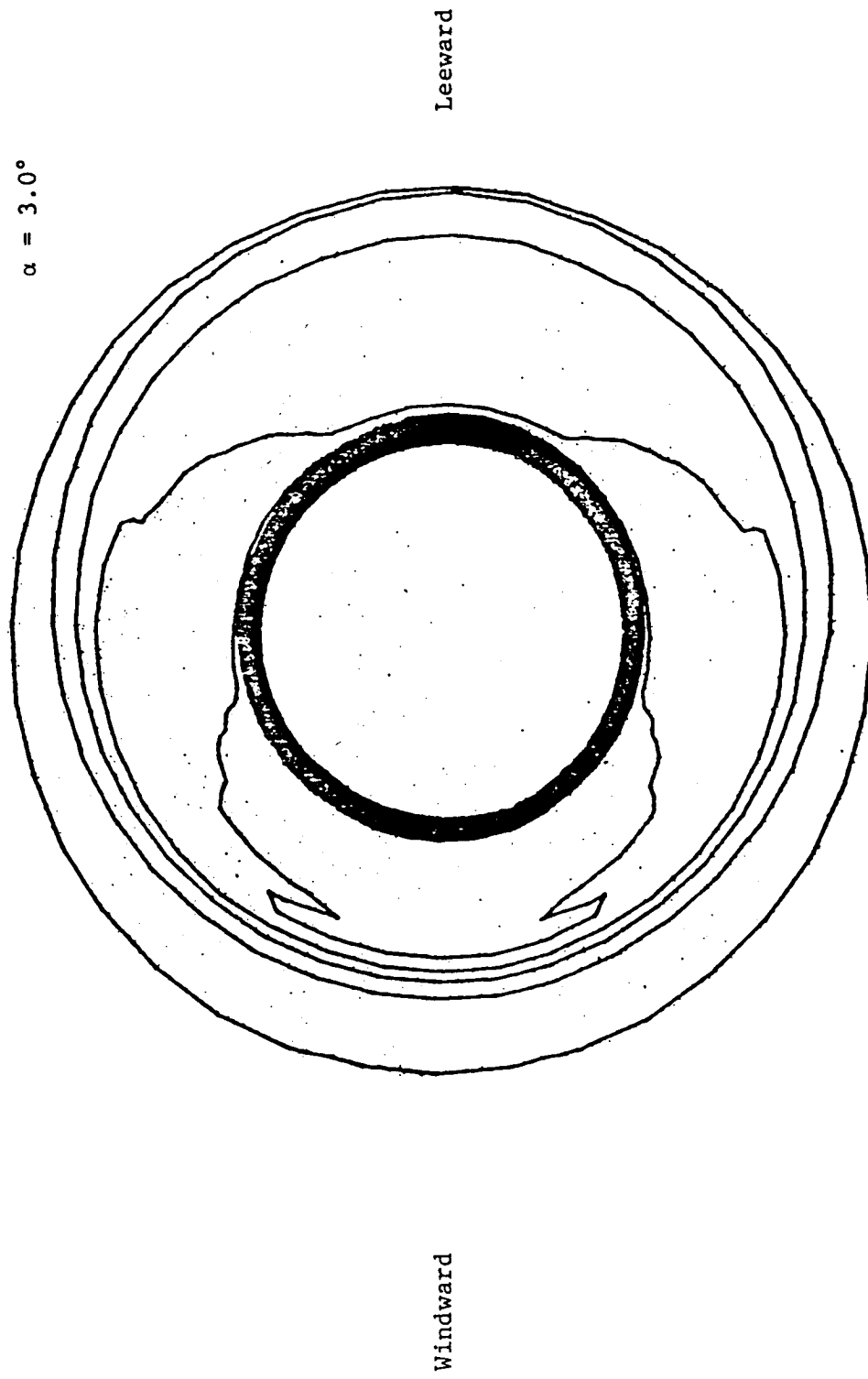


Figure 48 - Axisymmetric Inlet of Angle of Attack - Mach Number Contours for
Axisymmetric Cone at Angle of Attack - Axial Location - $X/R_1 = 2.45$

Table 1 - Inlet Contours

X/R_L	R/R_L	Slope
Centerbody		
0.0	0.0	0.17633
4.0	0.70532	0.17633
4.1	0.7228	
4.2	0.7387	0.144
4.3	0.7512	
4.4	0.759	0.052
4.5	0.7625	
4.55	0.763	0.0
4.6	0.7625	
4.65	0.7611	
4.7	0.7585	-0.0646
4.8	0.7504	
4.9	0.7391	-0.1295
5.1	0.7120	
5.3	0.6829	
5.5	0.6525	-0.153
5.6	0.6362	
5.7	0.618	
5.8	0.5973	
5.9	0.5744	
6.0	0.5467	
6.1	0.5093	
6.2	0.4564	
6.28	0.4	-0.794
Cowl		
2.86	1.0	0.01745
3.1	1.004188	0.01745
3.2	1.0054	
3.4	1.0051	-0.011
3.6	0.99996	
3.8	0.9882	
4.0	0.9681	-0.124
4.1	0.954	
4.2	0.9364	-0.1942
4.25	0.9261	
4.3	0.9154	-0.213
4.4	0.8949	
4.5	0.8768	-0.163
4.55	0.8695	
4.6	0.864	-0.093
4.65	0.86	
4.7	0.8572	-0.0485
4.8	0.8533	
4.9	0.8511	

Table 1 - (Concluded)

X/R_L	R/R_L	Slope
Cowl		
5.0	0.8502	
5.1	0.85	0.0
5.6	0.85	
5.8	0.8574	
5.9	0.8646	
6.0	0.8735	
6.1	0.8839	0.107
6.2	0.8946	
6.3	0.9050	
6.4	0.9145	
6.5	0.9227	0.0729
6.6	0.9299	
6.7	0.9368	
6.8	0.9435	
6.9	0.95	0.065

Table 1 - Surface contours of the centerbody and cowl

TABLE II - Sample Two-Dimensional Input

TOP RECORD
****ROSE CASE****

```

01 1.0
&REST
ICOMP = 3,
IRESTIN = 0, NFILE = 0, NSAVED = 0,
IRSTOT = 200,
JRSTOT = 17,
&END
&LIST1
IHSTAG = 1,
IBOUND = 2,1,2,2,
IEQBC(1,1) = 2,2,13,13,
IEQBC(1,2) = 2,2,13,13,
IEQBC(1,3) = 2,2,2,2,
IEQBC(1,4) = 16,16,16,16,
IEQBC(1,5) = 8,8,8,8,
JEQBC(1,1) = 44,21,11,11,
JEQBC(1,2) = 45,12,11,11,
JEQBC(1,3) = 12,12,2,2,
JEQBC(1,4) = 46,12,14,14,
JEQBC(1,5) = 47,17,17,17,
ASW(1) = .5618,
TWALL(1) = 2*3.651111439,
&END
&LIST2
LREF = .08666667,
REPL = 5,22E+06,
MINF = 3.88,
PINF = 59.1870527
PR = 0.710,
IUNITS = 1,
&END
&LIST3
XOB(1) = 0.5618,
TWOD = .TRUE.,
TT1 = -0.80, 0.0,
TT2 = 0.95, 0.0,
YS(1,1) = 1.0E-03,
NE(1) = 99,
IGEOM = 11,
DELX = 0.01,
NS = 200,
XENTR = 0.2,
&END
&LIST4
IDIRP = 2,IBCP = 2,
DELTAP(2) = 0.130, CFP(2) = 1.72E-03,
IVISC = 3,

```

TABLE II - Sample Two-Dimensional Input (Continued)

```
IPROF = 4,  
DELTAB(1) = 2*0.130,  
IMIXL = 1,  
&END  
&LIST5  
IPRINT = 10,  
IPLOT = 2,  
&END
```

**ORIGINAL PAGE IS
OF POOR QUALITY**

Table III - Sample Two-Dimensional Output

**ORIGINAL PAGE IS
OF POOR QUALITY**

```

INND = 9
INIU = 10
INUT = 10
INUFF = 11
ITAUU = 11
ILIL = 7
ISSE = 12
IPL = 1
ITLL = 12
IWNL = 1
INDL = 1
IWUL = 1
IFFL = 1

```

```

TITLE = 2
MLL = 1
OLF = 1
NSL = 2
IUPY2 = 4C+1
IUPY2 = 42+1
NPSX = 4+0
NPTY2 = 60+0
XYM0 = 60+0
YZW0 = 700+0
YD0 = 90+0
DT0N = 4+0
T4SLU = 2+0
PRES = 2+0
NN = 100
M2WARE = 12
NLEVEL = 12
NEOS = 7
NDIFM = 3
NIT = 0
END
ALIS12
NYINF = 28+0
RINF = 3+20
UINF = 22+25
TINF = 736992+875
PINF = 59+81705270
RHINF = 1+70541569+67
CPINF = 0+25444480101510-03
H1INF = 32996+20+46704
RCPL = 522000+0
HUIINF = 0+1085105871068C-06
PZERO = 7729+7270093H2
TZERO = 549+7073837739
GAMA = 1+399996185303
HFORM = 0+0
RGAS = 1714+99527234
URFE = 0+166666700-1
YREF = 2+96598x151P0
URFF = 32240+7369921875
PRFF = 1+34954156680+674
TRFF = 1+349541488870+674
QRREF = 35115+60308652
HREF = 4+953005+15839
YREF = 4+0+085105817068C-06
REF = 4+2400+01740
REF = 0+22143315989+010-05
RC12 = 0+1
PRT = 0+1
CTWO = 1+0+6666666RA653488
UNITS = 1
END
ALIST3
TCOM4 = 11
NSV = 0+20
T20 = 0+20
T30 = 0+40
T40 = 0+60
T50 = 0+80
T60 = 0+100
T70 = 0+120
T80 = 0+140
T90 = 0+160
T100 = 0+180
T110 = 0+200
T120 = 0+220
T130 = 0+240
T140 = 0+260
T150 = 0+280
T160 = 0+300
T170 = 0+320
T180 = 0+340
T190 = 0+360
T200 = 0+380
T210 = 0+400
T220 = 0+420
T230 = 0+440
T240 = 0+460
T250 = 0+480
T260 = 0+500
T270 = 0+520
T280 = 0+540
T290 = 0+560
T300 = 0+580
T310 = 0+600
T320 = 0+620
T330 = 0+640
T340 = 0+660
T350 = 0+680
T360 = 0+700
T370 = 0+720
T380 = 0+740
T390 = 0+760
T400 = 0+780
T410 = 0+800
T420 = 0+820
T430 = 0+840
T440 = 0+860
T450 = 0+880
T460 = 0+900
T470 = 0+920
T480 = 0+940
T490 = 0+960
T500 = 0+980
T510 = 0+1000
T520 = 0+1020
T530 = 0+1040
T540 = 0+1060
T550 = 0+1080
T560 = 0+1100
T570 = 0+1120
T580 = 0+1140
T590 = 0+1160
T600 = 0+1180
T610 = 0+1200
T620 = 0+1220
T630 = 0+1240
T640 = 0+1260
T650 = 0+1280
T660 = 0+1300
T670 = 0+1320
T680 = 0+1340
T690 = 0+1360
T700 = 0+1380
T710 = 0+1400
T720 = 0+1420
T730 = 0+1440
T740 = 0+1460
T750 = 0+1480
T760 = 0+1500
T770 = 0+1520
T780 = 0+1540
T790 = 0+1560
T800 = 0+1580
T810 = 0+1600
T820 = 0+1620
T830 = 0+1640
T840 = 0+1660
T850 = 0+1680
T860 = 0+1700
T870 = 0+1720
T880 = 0+1740
T890 = 0+1760
T900 = 0+1780
T910 = 0+1800
T920 = 0+1820
T930 = 0+1840
T940 = 0+1860
T950 = 0+1880
T960 = 0+1900
T970 = 0+1920
T980 = 0+1940
T990 = 0+1960
T1000 = 0+1980
T1010 = 0+2000
T1020 = 0+2020
T1030 = 0+2040
T1040 = 0+2060
T1050 = 0+2080
T1060 = 0+2100
T1070 = 0+2120
T1080 = 0+2140
T1090 = 0+2160
T1100 = 0+2180
T1110 = 0+2200
T1120 = 0+2220
T1130 = 0+2240
T1140 = 0+2260
T1150 = 0+2280
T1160 = 0+2300
T1170 = 0+2320
T1180 = 0+2340
T1190 = 0+2360
T1200 = 0+2380
T1210 = 0+2400
T1220 = 0+2420
T1230 = 0+2440
T1240 = 0+2460
T1250 = 0+2480
T1260 = 0+2500
T1270 = 0+2520
T1280 = 0+2540
T1290 = 0+2560
T1300 = 0+2580
T1310 = 0+2600
T1320 = 0+2620
T1330 = 0+2640
T1340 = 0+2660
T1350 = 0+2680
T1360 = 0+2700
T1370 = 0+2720
T1380 = 0+2740
T1390 = 0+2760
T1400 = 0+2780
T1410 = 0+2800
T1420 = 0+2820
T1430 = 0+2840
T1440 = 0+2860
T1450 = 0+2880
T1460 = 0+2900
T1470 = 0+2920
T1480 = 0+2940
T1490 = 0+2960
T1500 = 0+2980
T1510 = 0+3000
T1520 = 0+3020
T1530 = 0+3040
T1540 = 0+3060
T1550 = 0+3080
T1560 = 0+3100
T1570 = 0+3120
T1580 = 0+3140
T1590 = 0+3160
T1600 = 0+3180
T1610 = 0+3200
T1620 = 0+3220
T1630 = 0+3240
T1640 = 0+3260
T1650 = 0+3280
T1660 = 0+3300
T1670 = 0+3320
T1680 = 0+3340
T1690 = 0+3360
T1700 = 0+3380
T1710 = 0+3400
T1720 = 0+3420
T1730 = 0+3440
T1740 = 0+3460
T1750 = 0+3480
T1760 = 0+3500
T1770 = 0+3520
T1780 = 0+3540
T1790 = 0+3560
T1800 = 0+3580
T1810 = 0+3600
T1820 = 0+3620
T1830 = 0+3640
T1840 = 0+3660
T1850 = 0+3680
T1860 = 0+3700
T1870 = 0+3720
T1880 = 0+3740
T1890 = 0+3760
T1900 = 0+3780
T1910 = 0+3800
T1920 = 0+3820
T1930 = 0+3840
T1940 = 0+3860
T1950 = 0+3880
T1960 = 0+3900
T1970 = 0+3920
T1980 = 0+3940
T1990 = 0+3960
T2000 = 0+3980
T2010 = 0+4000
T2020 = 0+4020
T2030 = 0+4040
T2040 = 0+4060
T2050 = 0+4080
T2060 = 0+4100
T2070 = 0+4120
T2080 = 0+4140
T2090 = 0+4160
T2100 = 0+4180
T2110 = 0+4200
T2120 = 0+4220
T2130 = 0+4240
T2140 = 0+4260
T2150 = 0+4280
T2160 = 0+4300
T2170 = 0+4320
T2180 = 0+4340
T2190 = 0+4360
T2200 = 0+4380
T2210 = 0+4400
T2220 = 0+4420
T2230 = 0+4440
T2240 = 0+4460
T2250 = 0+4480
T2260 = 0+4500
T2270 = 0+4520
T2280 = 0+4540
T2290 = 0+4560
T2300 = 0+4580
T2310 = 0+4600
T2320 = 0+4620
T2330 = 0+4640
T2340 = 0+4660
T2350 = 0+4680
T2360 = 0+4700
T2370 = 0+4720
T2380 = 0+4740
T2390 = 0+4760
T2400 = 0+4780
T2410 = 0+4800
T2420 = 0+4820
T2430 = 0+4840
T2440 = 0+4860
T2450 = 0+4880
T2460 = 0+4900
T2470 = 0+4920
T2480 = 0+4940
T2490 = 0+4960
T2500 = 0+4980
T2510 = 0+5000
T2520 = 0+5020
T2530 = 0+5040
T2540 = 0+5060
T2550 = 0+5080
T2560 = 0+5100
T2570 = 0+5120
T2580 = 0+5140
T2590 = 0+5160
T2600 = 0+5180
T2610 = 0+5200
T2620 = 0+5220
T2630 = 0+5240
T2640 = 0+5260
T2650 = 0+5280
T2660 = 0+5300
T2670 = 0+5320
T2680 = 0+5340
T2690 = 0+5360
T2700 = 0+5380
T2710 = 0+5400
T2720 = 0+5420
T2730 = 0+5440
T2740 = 0+5460
T2750 = 0+5480
T2760 = 0+5500
T2770 = 0+5520
T2780 = 0+5540
T2790 = 0+5560
T2800 = 0+5580
T2810 = 0+5600
T2820 = 0+5620
T2830 = 0+5640
T2840 = 0+5660
T2850 = 0+5680
T2860 = 0+5700
T2870 = 0+5720
T2880 = 0+5740
T2890 = 0+5760
T2900 = 0+5780
T2910 = 0+5800
T2920 = 0+5820
T2930 = 0+5840
T2940 = 0+5860
T2950 = 0+5880
T2960 = 0+5900
T2970 = 0+5920
T2980 = 0+5940
T2990 = 0+5960
T3000 = 0+5980
T3010 = 0+6000
T3020 = 0+6020
T3030 = 0+6040
T3040 = 0+6060
T3050 = 0+6080
T3060 = 0+6100
T3070 = 0+6120
T3080 = 0+6140
T3090 = 0+6160
T3100 = 0+6180
T3110 = 0+6200
T3120 = 0+6220
T3130 = 0+6240
T3140 = 0+6260
T3150 = 0+6280
T3160 = 0+6300
T3170 = 0+6320
T3180 = 0+6340
T3190 = 0+6360
T3200 = 0+6380
T3210 = 0+6400
T3220 = 0+6420
T3230 = 0+6440
T3240 = 0+6460
T3250 = 0+6480
T3260 = 0+6500
T3270 = 0+6520
T3280 = 0+6540
T3290 = 0+6560
T3300 = 0+6580
T3310 = 0+6600
T3320 = 0+6620
T3330 = 0+6640
T3340 = 0+6660
T3350 = 0+6680
T3360 = 0+6700
T3370 = 0+6720
T3380 = 0+6740
T3390 = 0+6760
T3400 = 0+6780
T3410 = 0+6800
T3420 = 0+6820
T3430 = 0+6840
T3440 = 0+6860
T3450 = 0+6880
T3460 = 0+6900
T3470 = 0+6920
T3480 = 0+6940
T3490 = 0+6960
T3500 = 0+6980
T3510 = 0+7000
T3520 = 0+7020
T3530 = 0+7040
T3540 = 0+7060
T3550 = 0+7080
T3560 = 0+7100
T3570 = 0+7120
T3580 = 0+7140
T3590 = 0+7160
T3600 = 0+7180
T3610 = 0+7200
T3620 = 0+7220
T3630 = 0+7240
T3640 = 0+7260
T3650 = 0+7280
T3660 = 0+7300
T3670 = 0+7320
T3680 = 0+7340
T3690 = 0+7360
T3700 = 0+7380
T3710 = 0+7400
T3720 = 0+7420
T3730 = 0+7440
T3740 = 0+7460
T3750 = 0+7480
T3760 = 0+7500
T3770 = 0+7520
T3780 = 0+7540
T3790 = 0+7560
T3800 = 0+7580
T3810 = 0+7600
T3820 = 0+7620
T3830 = 0+7640
T3840 = 0+7660
T3850 = 0+7680
T3860 = 0+7700
T3870 = 0+7720
T3880 = 0+7740
T3890 = 0+7760
T3900 = 0+7780
T3910 = 0+7800
T3920 = 0+7820
T3930 = 0+7840
T3940 = 0+7860
T3950 = 0+7880
T3960 = 0+7900
T3970 = 0+7920
T3980 = 0+7940
T3990 = 0+7960
T4000 = 0+7980
T4010 = 0+8000
T4020 = 0+8020
T4030 = 0+8040
T4040 = 0+8060
T4050 = 0+8080
T4060 = 0+8100
T4070 = 0+8120
T4080 = 0+8140
T4090 = 0+8160
T4100 = 0+8180
T4110 = 0+8200
T4120 = 0+8220
T4130 = 0+8240
T4140 = 0+8260
T4150 = 0+8280
T4160 = 0+8300
T4170 = 0+8320
T4180 = 0+8340
T4190 = 0+8360
T4200 = 0+8380
T4210 = 0+8400
T4220 = 0+8420
T4230 = 0+8440
T4240 = 0+8460
T4250 = 0+8480
T4260 = 0+8500
T4270 = 0+8520
T4280 = 0+8540
T4290 = 0+8560
T4300 = 0+8580
T4310 = 0+8600
T4320 = 0+8620
T4330 = 0+8640
T4340 = 0+8660
T4350 = 0+8680
T4360 = 0+8700
T4370 = 0+8720
T4380 = 0+8740
T4390 = 0+8760
T4400 = 0+8780
T4410 = 0+8800
T4420 = 0+8820
T4430 = 0+8840
T4440 = 0+8860
T4450 = 0+8880
T4460 = 0+8900
T4470 = 0+8920
T4480 = 0+8940
T4490 = 0+8960
T4500 = 0+8980
T4510 = 0+9000
T4520 = 0+9020
T4530 = 0+9040
T4540 = 0+9060
T4550 = 0+9080
T4560 = 0+9100
T4570 = 0+9120
T4580 = 0+9140
T4590 = 0+9160
T4600 = 0+9180
T4610 = 0+9200
T4620 = 0+9220
T4630 = 0+9240
T4640 = 0+9260
T4650 = 0+9280
T4660 = 0+9300
T4670 = 0+9320
T4680 = 0+9340
T4690 = 0+9360
T4700 = 0+9380
T4710 = 0+9400
T4720 = 0+9420
T4730 = 0+9440
T4740 = 0+9460
T4750 = 0+9480
T4760 = 0+9500
T4770 = 0+9520
T4780 = 0+9540
T4790 = 0+9560
T4800 = 0+9580
T4810 = 0+9600
T4820 = 0+9620
T4830 = 0+9640
T4840 = 0+9660
T4850 = 0+9680
T4860 = 0+9700
T4870 = 0+9720
T4880 = 0+9740
T4890 = 0+9760
T4900 = 0+9780
T4910 = 0+9800
T4920 = 0+9820
T4930 = 0+9840
T4940 = 0+9860
T4950 = 0+9880
T4960 = 0+9900
T4970 = 0+9920
T4980 = 0+9940
T4990 = 0+9960
T5000 = 0+9980
T5010 = 0+10000

```

ORIGINAL PAGE IS
OF POOR QUALITY

ISMTH 0
 CRITURE 0.500-01
 IF FLARE = n
 END
 NLISTS
 MLINE 5
 ROUTE 6
 MASS1 = p
 MASS2 = q
 JORURH = 11
 LDORUM = 13
 JUNCCR = 14
 SD005 = 15
 LADPR = 5.11, 2.0, 3.1, 7.0, 1, 0, 1, 0, 1, 3.0
 LLOT = 2
 MPY = 0
 DMPZ = 0
 GDMZ = 0
 ISY = 1
 JUNE = 5*, 1
 UPRINT = 1
 JXDUMP = 2
 JXDUMPN

ORIGINAL PAGE IS
OF POOR QUALITY

A decorative border consisting of a repeating pattern of small circles and dots, creating a scalloped or wavy effect along the inner edge.

A decorative horizontal border consisting of a repeating pattern of small circles and dots. The pattern alternates between a circle-dot combination and a dot-circle combination, creating a rhythmic visual texture. The border is composed of two rows of these units, one above the other.

STREAMWISE LOCATION X(1) = 2.0000E-01

The image consists of a dense, repeating pattern of binary digits (0s and 1s) arranged in a grid. The pattern is mostly composed of 0s, with occasional 1s appearing in a specific sequence. This sequence of 1s forms a large, faint watermark or logo that is oriented vertically and slightly tilted. The watermark appears to be a stylized letter 'M' or a similar shape, though it is very faint due to the high density of 0s. The overall effect is that of a digital watermark or a complex binary code representation.

ORIGINAL PAGE IS
OF POOR QUALITY

STREAMWISE LOCATION X(1) = 2.0000E-01
LEVEL = 1

ORIGINAL PAGE IS
OF POOR QUALITY

14. 15. 16. 17. 18. 19. 20. 21. 22. 23. 24. 25. 26. 27. 28. 29. 30. 31. 32. 33. 34. 35. 36. 37. 38. 39. 40. 41. 42. 43. 44. 45. 46. 47. 48. 49. 50. 51. 52. 53. 54. 55. 56. 57. 58. 59. 60. 61. 62. 63. 64. 65. 66. 67. 68. 69. 70. 71. 72. 73. 74. 75. 76. 77. 78. 79. 80. 81. 82. 83. 84. 85. 86. 87. 88. 89. 90. 91. 92. 93. 94. 95. 96. 97. 98. 99. 100.

6.02385

ORIGINAL PAGE IS
OF POOR QUALITY

STREAMWISE LOCATION X (10) = 2.9000E-01
LEVEL = 1

**ORIGINAL PAGE IS
OF POOR QUALITY**

| | | | | | | | | |
|---|------------|------------|------------|------------|------------|------------|-----------|------------|
| 1 | 1-3932E-02 | 3-0000E+00 | 6-1312E+00 | 1-1952E+05 | 1-0001E+00 | 1-1700E+02 | 9-508E-04 | 1-9006E+00 |
| 2 | 1-2000E-03 | 3-0000E+00 | 6-1312E+00 | 1-1952E+05 | 1-0001E+00 | 1-1700E+02 | 7-612E-04 | 1-539E-01 |
| 3 | 1-2000E-03 | 3-0000E+00 | 6-1312E+00 | 1-1952E+05 | 1-0001E+00 | 1-1700E+02 | 7-612E-04 | 1-539E-01 |
| 4 | 1-2000E-03 | 3-0000E+00 | 6-1312E+00 | 1-1952E+05 | 1-0001E+00 | 1-1700E+02 | 7-612E-04 | 1-539E-01 |
| 5 | 1-2000E-03 | 3-0000E+00 | 6-1312E+00 | 1-1952E+05 | 1-0001E+00 | 1-1700E+02 | 7-612E-04 | 1-539E-01 |

STRENGTHENING LOCATIONAL POSITION = 2.9005-01

100

1 ISSN(1,1) 155(1,2) 180(1,1) JPOUNO(1,2)

| | | |
|-------------|----------------------------|-----|
| JXQUM = 10, | 1391 WORDS WRITTEN ON Urum | 15. |
| JXQUM = 12, | 1391 WORDS WRITTEN ON DRUM | 15. |
| JXQUM = 14, | 1391 WORDS WRITTEN ON CRUM | 15. |
| JXQUM = 16, | 1391 WORDS WRITTEN ON DRUM | 15. |

TABLE IV - Sample Three-Dimensional Input

TOP RECORD
BOG TEST CASE

```
1      1.0
&REST
ICOMP = 3,
IRSTIN = 350,
IRSTOT = 50,
JRSTOT = 17,
NFILE = 1,
NSAVED = 0,
&END
&LIST1
&END
&LIST2
&END
&LIST3
NS = 400,
IAP = 1,21,41,101,251,5*10000,
AP = 0.8,1.05,1.0,0.8,1.15,5*1.0,
DXMIN = 0.002,0.0,0.0,0.002,6*0.0,
DXMAX = 4*100000.0,0.005,5*100000.0,
&END
&LIST4
&END
&LIST5
&END
```

Table V - Sample Three-Dimensional Output

PAGE IS
OF POOR QUALITY

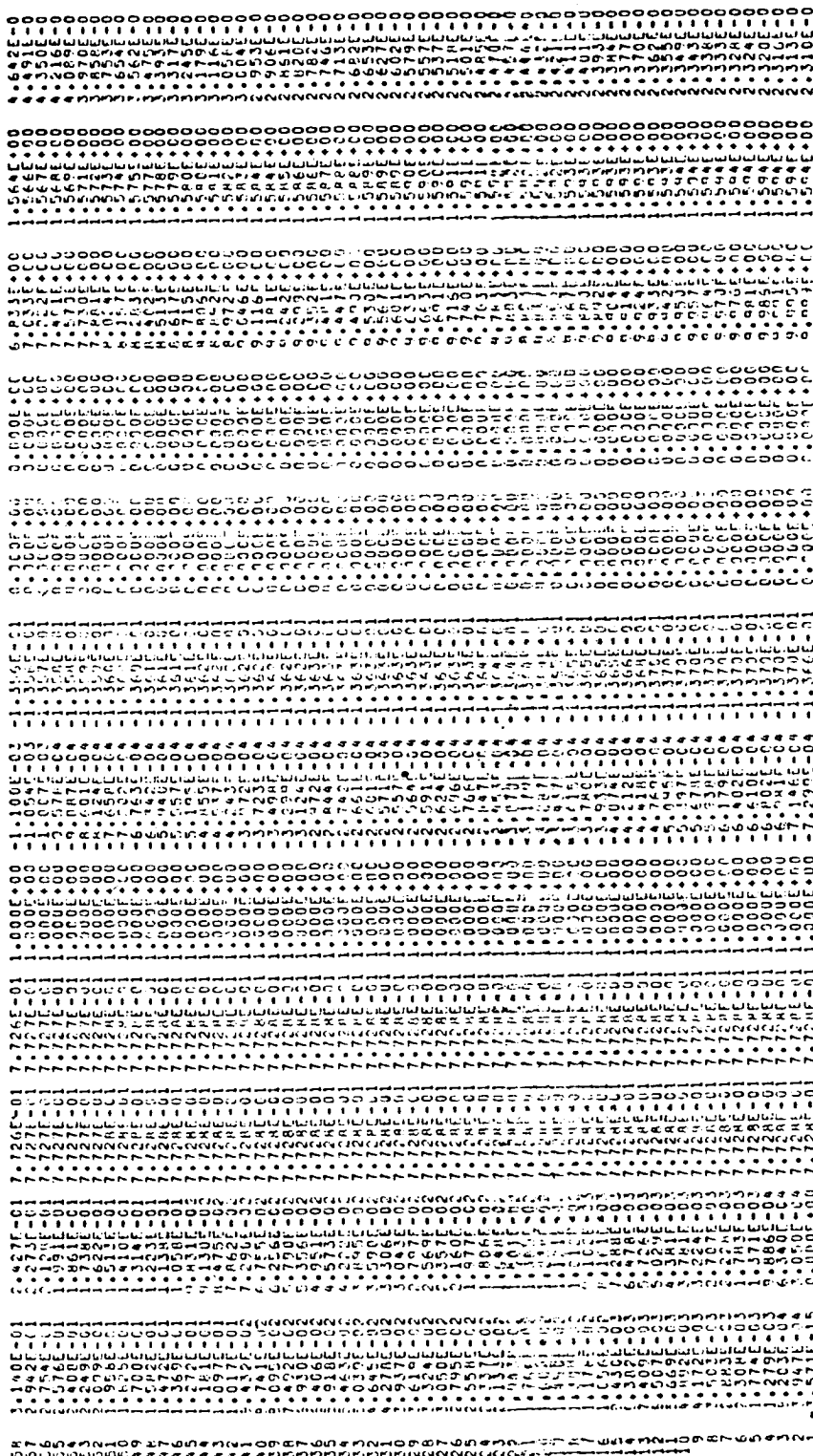
REINSTANT INFORMATION WRITTEN IN FILE 10 AT STATION 400 IN SEQUENCE NUMBER 6

CROSS PLANE DISTRIBUTION OF LEVEL

JSTREAMWISE LOCATION X(400) = 1.7199E+00
LEVEL = 1

| IVAR | JMAX | KMAX | CEU | CEV | CEW |
|------|------|------|--------|--------|--------|
| 1 | 69 | 11 | -2.604 | -0.5 | -0.5 |
| 1 | 69 | 10 | -2.614 | -0.5 | -0.5 |
| 1 | 69 | 12 | -2.620 | -0.5 | -0.5 |
| 2 | 55 | 10 | -1.384 | -0.2 | -0.2 |
| 2 | 55 | 12 | -1.386 | -0.2 | -0.2 |
| 2 | 55 | 14 | -1.386 | -0.2 | -0.2 |
| 3 | 45 | 10 | -0.766 | -0.1 | -0.1 |
| 3 | 45 | 12 | -0.766 | -0.1 | -0.1 |
| 3 | 45 | 14 | -0.766 | -0.1 | -0.1 |
| 4 | 35 | 10 | -0.384 | -0.05 | -0.05 |
| 4 | 35 | 12 | -0.384 | -0.05 | -0.05 |
| 4 | 35 | 14 | -0.384 | -0.05 | -0.05 |
| 5 | 25 | 10 | -0.192 | -0.02 | -0.02 |
| 5 | 25 | 12 | -0.192 | -0.02 | -0.02 |
| 5 | 25 | 14 | -0.192 | -0.02 | -0.02 |
| 6 | 15 | 10 | -0.096 | -0.01 | -0.01 |
| 6 | 15 | 12 | -0.096 | -0.01 | -0.01 |
| 6 | 15 | 14 | -0.096 | -0.01 | -0.01 |
| 7 | 10 | 10 | -0.048 | -0.005 | -0.005 |
| 7 | 10 | 12 | -0.048 | -0.005 | -0.005 |
| 7 | 10 | 14 | -0.048 | -0.005 | -0.005 |
| 8 | 5 | 10 | -0.024 | -0.002 | -0.002 |
| 8 | 5 | 12 | -0.024 | -0.002 | -0.002 |
| 8 | 5 | 14 | -0.024 | -0.002 | -0.002 |

MAX DELTAS

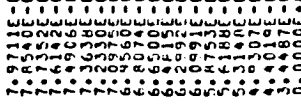
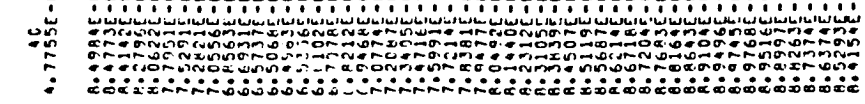
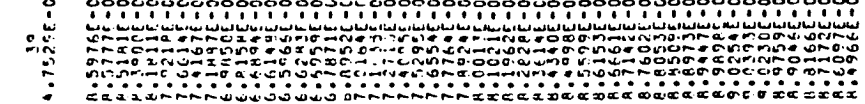
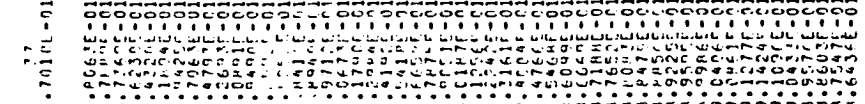
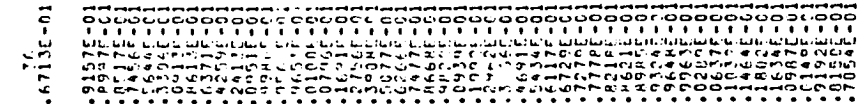
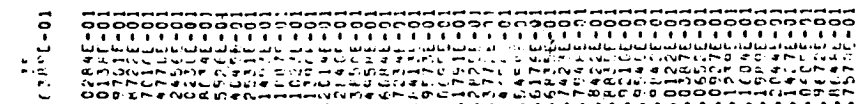
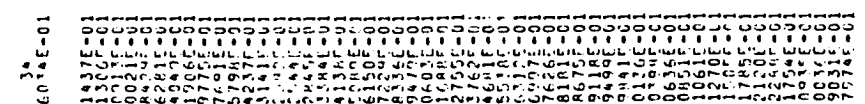
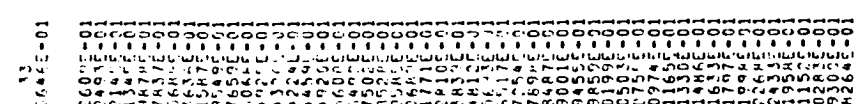
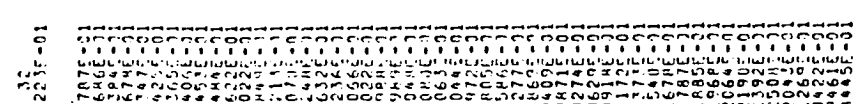


**CHART PAGE IS
OF POOR QUALITY**

A scatter plot showing the relationship between two variables. The x-axis ranges from $-1.0E-02$ to $2.0E-02$, and the y-axis ranges from $0.000E+00$ to $1.2E-02$. The data points form a dense, roughly triangular cluster centered near the origin, with a slight upward trend as the x-value increases.

| x | y |
|-----------|-----------|
| 0.000E+00 | 0.000E+00 |
| 1.000E-02 | 1.000E-02 |
| 2.000E-02 | 2.000E-02 |
| 3.000E-02 | 3.000E-02 |
| 4.000E-02 | 4.000E-02 |
| 5.000E-02 | 5.000E-02 |
| 6.000E-02 | 6.000E-02 |
| 7.000E-02 | 7.000E-02 |
| 8.000E-02 | 8.000E-02 |
| 9.000E-02 | 9.000E-02 |
| 1.000E-01 | 1.000E-01 |
| 1.100E-01 | 1.100E-01 |
| 1.200E-01 | 1.200E-01 |
| 1.300E-01 | 1.300E-01 |
| 1.400E-01 | 1.400E-01 |
| 1.500E-01 | 1.500E-01 |
| 1.600E-01 | 1.600E-01 |
| 1.700E-01 | 1.700E-01 |
| 1.800E-01 | 1.800E-01 |
| 1.900E-01 | 1.900E-01 |
| 2.000E-01 | 2.000E-01 |

**ORIGINAL PAGE IS
OF POOR QUALITY**

| | | |
|----|--------------|--|
| 1 | $4.7755E-0$ |  |
| 2 | $4.7529E-01$ |  |
| 3 | $4.7241E-01$ |  |
| 4 | $4.7010E-01$ |  |
| 5 | $4.6735E-01$ |  |
| 6 | $4.6765E-01$ |  |
| 7 | $4.6074E-01$ |  |
| 8 | $4.5642E-01$ |  |
| 9 | $4.5225E-01$ |  |
| 10 | $4.4951E-01$ |  |
| 11 | $4.4725E-01$ |  |
| 12 | $4.4522E-01$ |  |

ORIGINAL PAGE IS
OF POOR QUALITY

ORIGINAL PAGE IS
OF POOR QUALITY

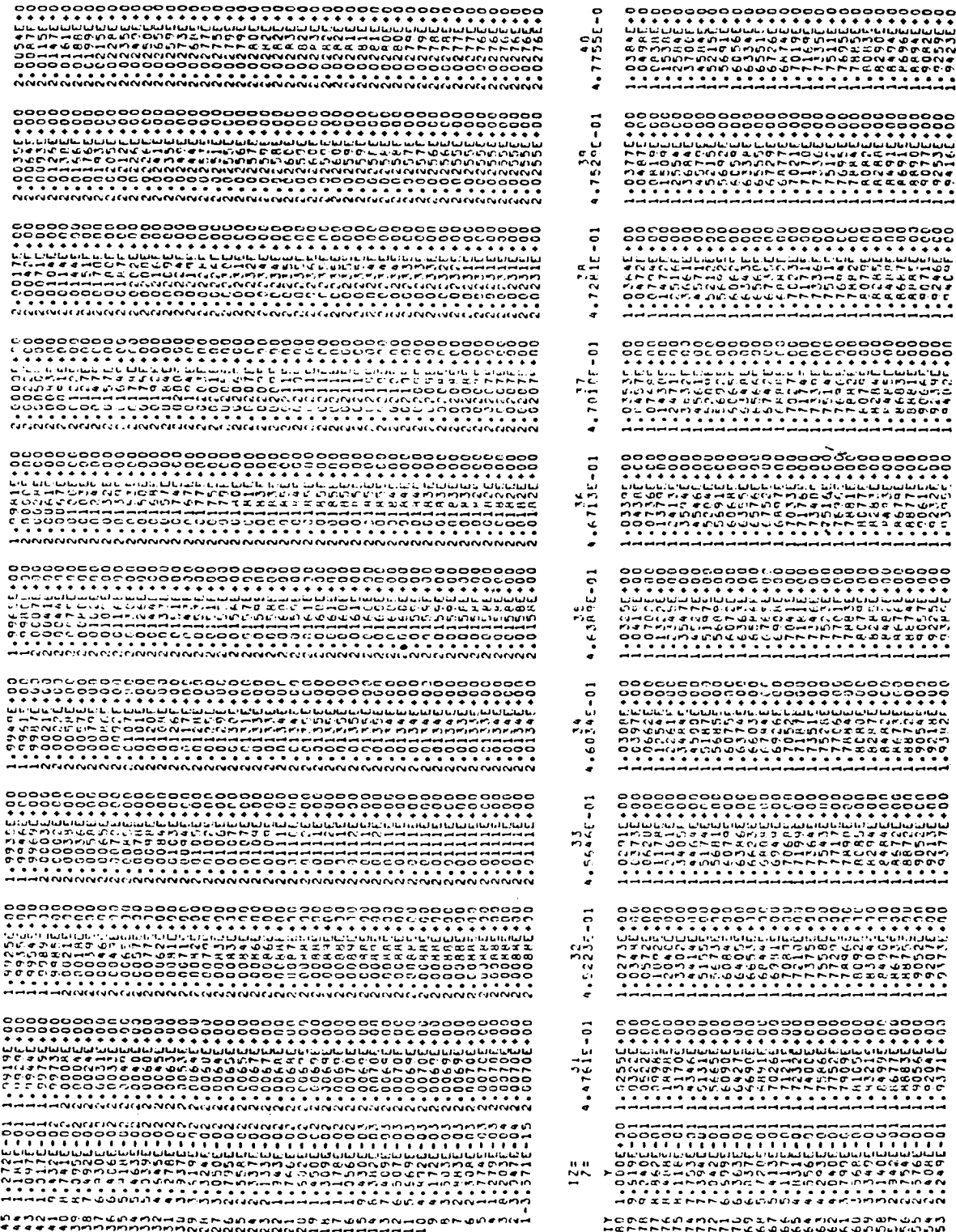
ORIGINAL PAGE IS
OF POOR QUALITY

1 STRAIGHT LOCATION X(400) = 1.7379E+00
 LEVEL = 1

CROSS PLANE DISTRIBUTION, IF PREC

| Y/Z | Z | Y | X |
|-----|------------|------------|------------|
| 1/2 | 0.0000E+00 | 2.4057E-02 | 4.0004E-02 |
| 1/2 | 9.5131E-02 | 7.1731E-02 | 7.4004E-02 |
| 1/2 | 1.0457E-01 | 1.0457E-01 | 1.0457E-01 |
| 1/2 | 1.1811E-01 | 1.4057E-01 | 1.4057E-01 |
| 1/2 | 1.3165E-01 | 1.6274E-01 | 1.6274E-01 |
| 1/2 | 1.4519E-01 | 1.8383E-01 | 1.8383E-01 |
| 1/2 | 1.5873E-01 | 2.0482E-01 | 2.0482E-01 |
| 1/2 | 1.7227E-01 | 2.2571E-01 | 2.2571E-01 |
| 1/2 | 1.8581E-01 | 2.4659E-01 | 2.4659E-01 |
| 1/2 | 1.9935E-01 | 2.6748E-01 | 2.6748E-01 |
| 1/2 | 2.1288E-01 | 2.8837E-01 | 2.8837E-01 |
| 1/2 | 2.2642E-01 | 3.0926E-01 | 3.0926E-01 |
| 1/2 | 2.4 | 3.3015E-01 | 3.3015E-01 |
| 1/2 | 2.5359E-01 | 3.5104E-01 | 3.5104E-01 |
| 1/2 | 2.6703E-01 | 3.7193E-01 | 3.7193E-01 |
| 1/2 | 2.8047E-01 | 3.9282E-01 | 3.9282E-01 |
| 1/2 | 2.9391E-01 | 4.1371E-01 | 4.1371E-01 |
| 1/2 | 3.0735E-01 | 4.3460E-01 | 4.3460E-01 |
| 1/2 | 3.2079E-01 | 4.5549E-01 | 4.5549E-01 |
| 1/2 | 3.3423E-01 | 4.7638E-01 | 4.7638E-01 |
| 1/2 | 3.4767E-01 | 4.9727E-01 | 4.9727E-01 |
| 1/2 | 3.6111E-01 | 5.1816E-01 | 5.1816E-01 |
| 1/2 | 3.7455E-01 | 5.3905E-01 | 5.3905E-01 |
| 1/2 | 3.8799E-01 | 5.5994E-01 | 5.5994E-01 |
| 1/2 | 4.0143E-01 | 5.8083E-01 | 5.8083E-01 |
| 1/2 | 4.1487E-01 | 6.0172E-01 | 6.0172E-01 |
| 1/2 | 4.2831E-01 | 6.2261E-01 | 6.2261E-01 |
| 1/2 | 4.4175E-01 | 6.4350E-01 | 6.4350E-01 |
| 1/2 | 4.5519E-01 | 6.6439E-01 | 6.6439E-01 |
| 1/2 | 4.6863E-01 | 6.8528E-01 | 6.8528E-01 |
| 1/2 | 4.8207E-01 | 7.0617E-01 | 7.0617E-01 |
| 1/2 | 4.9551E-01 | 7.2706E-01 | 7.2706E-01 |
| 1/2 | 5.0895E-01 | 7.4795E-01 | 7.4795E-01 |
| 1/2 | 5.2239E-01 | 7.6884E-01 | 7.6884E-01 |
| 1/2 | 5.3583E-01 | 7.8973E-01 | 7.8973E-01 |
| 1/2 | 5.4927E-01 | 8.1062E-01 | 8.1062E-01 |
| 1/2 | 5.6271E-01 | 8.3151E-01 | 8.3151E-01 |
| 1/2 | 5.7615E-01 | 8.5240E-01 | 8.5240E-01 |
| 1/2 | 5.8959E-01 | 8.7329E-01 | 8.7329E-01 |
| 1/2 | 6.0303E-01 | 8.9418E-01 | 8.9418E-01 |
| 1/2 | 6.1647E-01 | 9.1507E-01 | 9.1507E-01 |
| 1/2 | 6.3 | 9.3596E-01 | 9.3596E-01 |
| 1/2 | 6.4390E-01 | 9.5685E-01 | 9.5685E-01 |
| 1/2 | 6.5734E-01 | 9.7774E-01 | 9.7774E-01 |
| 1/2 | 6.7078E-01 | 9.9863E-01 | 9.9863E-01 |
| 1/2 | 6.8422E-01 | 1.01952E | 1.01952E |
| 1/2 | 6.9766E-01 | 1.04041E | 1.04041E |
| 1/2 | 7.1110E-01 | 1.06130E | 1.06130E |
| 1/2 | 7.2454E-01 | 1.08219E | 1.08219E |
| 1/2 | 7.3798E-01 | 1.10308E | 1.10308E |
| 1/2 | 7.5142E-01 | 1.12397E | 1.12397E |
| 1/2 | 7.6486E-01 | 1.14486E | 1.14486E |
| 1/2 | 7.7830E-01 | 1.16575E | 1.16575E |
| 1/2 | 7.9174E-01 | 1.18664E | 1.18664E |
| 1/2 | 8.0518E-01 | 1.20753E | 1.20753E |
| 1/2 | 8.1862E-01 | 1.22842E | 1.22842E |
| 1/2 | 8.3206E-01 | 1.24931E | 1.24931E |
| 1/2 | 8.4550E-01 | 1.26920E | 1.26920E |
| 1/2 | 8.5894E-01 | 1.28909E | 1.28909E |
| 1/2 | 8.7238E-01 | 1.30998E | 1.30998E |
| 1/2 | 8.8582E-01 | 1.33087E | 1.33087E |
| 1/2 | 9.0026E-01 | 1.35176E | 1.35176E |
| 1/2 | 9.1370E-01 | 1.37265E | 1.37265E |
| 1/2 | 9.2714E-01 | 1.39354E | 1.39354E |
| 1/2 | 9.4058E-01 | 1.41443E | 1.41443E |
| 1/2 | 9.5402E-01 | 1.43532E | 1.43532E |
| 1/2 | 9.6746E-01 | 1.45621E | 1.45621E |
| 1/2 | 9.8090E-01 | 1.47710E | 1.47710E |
| 1/2 | 9.9434E-01 | 1.49799E | 1.49799E |
| 1/2 | 1.0077E | 1.51888E | 1.51888E |
| 1/2 | 1.0211E | 1.53977E | 1.53977E |
| 1/2 | 1.0345E | 1.56066E | 1.56066E |
| 1/2 | 1.0479E | 1.58155E | 1.58155E |
| 1/2 | 1.0613E | 1.60244E | 1.60244E |
| 1/2 | 1.0747E | 1.62333E | 1.62333E |
| 1/2 | 1.0881E | 1.64422E | 1.64422E |
| 1/2 | 1.1015E | 1.66511E | 1.66511E |
| 1/2 | 1.1149E | 1.68600E | 1.68600E |
| 1/2 | 1.1283E | 1.70689E | 1.70689E |
| 1/2 | 1.1417E | 1.72778E | 1.72778E |
| 1/2 | 1.1551E | 1.74867E | 1.74867E |
| 1/2 | 1.1685E | 1.76956E | 1.76956E |
| 1/2 | 1.1819E | 1.79045E | 1.79045E |
| 1/2 | 1.1953E | 1.81134E | 1.81134E |
| 1/2 | 1.2087E | 1.83223E | 1.83223E |
| 1/2 | 1.2221E | 1.85312E | 1.85312E |
| 1/2 | 1.2355E | 1.87401E | 1.87401E |
| 1/2 | 1.2489E | 1.89490E | 1.89490E |
| 1/2 | 1.2623E | 1.91579E | 1.91579E |
| 1/2 | 1.2757E | 1.93668E | 1.93668E |
| 1/2 | 1.2891E | 1.95757E | 1.95757E |
| 1/2 | 1.3025E | 1.97846E | 1.97846E |
| 1/2 | 1.3159E | 1.99935E | 1.99935E |
| 1/2 | 1.3293E | 2.02024E | 2.02024E |
| 1/2 | 1.3427E | 2.04113E | 2.04113E |
| 1/2 | 1.3561E | 2.06202E | 2.06202E |
| 1/2 | 1.3695E | 2.08291E | 2.08291E |
| 1/2 | 1.3829E | 2.10380E | 2.10380E |
| 1/2 | 1.3963E | 2.12469E | 2.12469E |
| 1/2 | 1.4097E | 2.14558E | 2.14558E |
| 1/2 | 1.4231E | 2.16647E | 2.16647E |
| 1/2 | 1.4365E | 2.18736E | 2.18736E |
| 1/2 | 1.45 | 2.20825E | 2.20825E |
| 1/2 | 1.4699E | 2.22914E | 2.22914E |
| 1/2 | 1.4833E | 2.24903E | 2.24903E |
| 1/2 | 1.4967E | 2.26992E | 2.26992E |
| 1/2 | 1.5101E | 2.29081E | 2.29081E |
| 1/2 | 1.5235E | 2.31170E | 2.31170E |
| 1/2 | 1.5369E | 2.33259E | 2.33259E |
| 1/2 | 1.5503E | 2.35348E | 2.35348E |
| 1/2 | 1.5637E | 2.37437E | 2.37437E |
| 1/2 | 1.5771E | 2.39526E | 2.39526E |
| 1/2 | 1.5905E | 2.41615E | 2.41615E |
| 1/2 | 1.6039E | 2.43704E | 2.43704E |
| 1/2 | 1.6173E | 2.45793E | 2.45793E |
| 1/2 | 1.6307E | 2.47882E | 2.47882E |
| 1/2 | 1.6441E | 2.49971E | 2.49971E |
| 1/2 | 1.6575E | 2.52060E | 2.52060E |
| 1/2 | 1.6709E | 2.54149E | 2.54149E |
| 1/2 | 1.6843E | 2.56238E | 2.56238E |
| 1/2 | 1.6977E | 2.58327E | 2.58327E |
| 1/2 | 1.7111E | 2.60416E | 2.60416E |
| 1/2 | 1.7245E | 2.62505E | 2.62505E |
| 1/2 | 1.7379E | 2.64594E | 2.64594E |
| 1/2 | 1.7513E | 2.66683E | 2.66683E |
| 1/2 | 1.7647E | 2.68772E | 2.68772E |
| 1/2 | 1.7781E | 2.70861E | 2.70861E |
| 1/2 | 1.7915E | 2.72950E | 2.72950E |
| 1/2 | 1.8049E | 2.75039E | 2.75039E |
| 1/2 | 1.8183E | 2.77128E | 2.77128E |
| 1/2 | 1.8317E | 2.79217E | 2.79217E |
| 1/2 | 1.8451E | 2.81306E | 2.81306E |
| 1/2 | 1.8585E | 2.83395E | 2.83395E |
| 1/2 | 1.8719E | 2.85484E | 2.85484E |
| 1/2 | 1.8853E | 2.87573E | 2.87573E |
| 1/2 | 1.8987E | 2.89662E | 2.89662E |
| 1/2 | 1.9121E | 2.91751E | 2.91751E |
| 1/2 | 1.9255E | 2.93840E | 2.93840E |
| 1/2 | 1.9389E | 2.95929E | 2.95929E |
| 1/2 | 1.9523E | 2.98018E | 2.98018E |
| 1/2 | 1.9657E | 3.00107E | 3.00107E |
| 1/2 | 1.9791E | 3.02196E | 3.02196E |
| 1/2 | 1.9925E | 3.04285E | 3.04285E |
| 1/2 | 2.0059E | 3.06374E | 3.06374E |
| 1/2 | 2.0193E | 3.08463E | 3.08463E |
| 1/2 | 2.0327E | 3.10552E | 3.10552E |
| 1/2 | 2.0461E | 3.12641E | 3.12641E |
| 1/2 | 2.0595E | 3.14730E | 3.14730E |
| 1/2 | 2.0729E | 3.16819E | 3.16819E |
| 1/2 | 2.0863E | 3.18908E | 3.18908E |
| 1/2 | 2.1097E | 3.20997E | 3.20997E |
| 1/2 | 2.1231E | 3.23086E | 3.23086E |
| 1/2 | 2.1365E | 3.25175E | 3.25175E |
| 1/2 | 2.15 | 3.27264E | 3.27264E |
| 1/2 | 2.1699E | 3.29353E | 3.29353E |
| 1/2 | 2.1833E | 3.31442E | 3.31442E |
| 1/2 | 2.1967E | 3.33531E | 3.33531E |
| 1/2 | 2.2101E | 3.35620E | 3.35620E |
| 1/2 | 2.2235E | 3.37709E | 3.37709E |
| 1/2 | 2.2369E | 3.39798E | 3.39798E |
| 1/2 | 2.2503E | 3.41887E | 3.41887E |
| 1/2 | 2.2637E | 3.43976E | 3.43976E |
| 1/2 | 2.2771E | 3.46065E | 3.46065E |
| 1/2 | 2.2905E | 3.48154E | 3.48154E |
| 1/2 | 2.3039E | 3.50243E | 3.50243E |
| 1/2 | 2.3173E | 3.52332E | 3.52332E |
| 1/2 | 2.3307E | 3.54421E | 3.54421E |
| 1/2 | 2.3441E | 3.56510E | 3.56510E |
| 1/2 | 2.3575E | 3.586 | 3.586 |

**ORIGINAL PAGE IS
OF POOR QUALITY**



ORIGINAL PAGE IS
OF POOR QUALITY

**ORIGINAL PAGE IS
OF POOR QUALITY**

ORIGINAL PAGE IS
OF POOR QUALITY

The image consists of a dense, uniform grid of small black dots on a white background. The dots are arranged in a regular, repeating pattern, creating a subtle texture or noise effect. There are no other elements, text, or graphics present in the image.

$$1 \leq i \leq 71 \quad 4.99425 \cdot 10^{-01} \quad 4.99525 \cdot 10^{-01} \quad 4.99615 \cdot 10^{-01} \quad 4.99715 \cdot 10^{-01} \quad 4.9977 \cdot 10^{-01} \quad 4.99845 \cdot 10^{-01} \quad 4.99895 \cdot 10^{-01} \quad 5.00005 \cdot 10^{-01}$$

A high-resolution image showing a dense grid of binary digits (0s and 1s). The pattern is arranged to form a faint watermark of the Eiffel Tower. The tower's silhouette is visible against a background of a repeating binary code pattern.

| | | | |
|--|---|--|------------------------------|
| 1. Report No.
NASA CR-4021 | 2. Government Accession No. | 3. Recipient's Catalog No. | |
| 4. Title and Subtitle

Computation of Multi-Dimensional Viscous Supersonic Flow | | 5. Report Date

October 1986 | |
| | | 6. Performing Organization Code | |
| 7. Author(s)

R. C. Buggeln, Y. N. Kim, and H. McDonald | | 8. Performing Organization Report No.

None (E-3211) | |
| | | 10. Work Unit No.

505-62-21 | |
| 9. Performing Organization Name and Address

Scientific Research Associates, Inc.
P.O. Box 498
Glastonbury, Connecticut 06033 | | 11. Contract or Grant No.

NAS3-22027 | |
| 12. Sponsoring Agency Name and Address

National Aeronautics and Space Administration
Lewis Research Center
Cleveland, Ohio 44135 | | 13. Type of Report and Period Covered

Contractor Report
Final | |
| 15. Supplementary Notes

Project Manager, Thomas J. Benson, Internal Fluid Mechanics Division, NASA Lewis Research Center. | | 14. Sponsoring Agency Code | |
| 16. Abstract

<p>A method has been developed for two- and three-dimensional computations of viscous supersonic jet flows interacting with an external flow. The approach employs a reduced form of the Navier-Stokes equations which allows solution as an initial-boundary value problem in space, using an efficient noniterative forward marching algorithm. Numerical instability associated with forward marching algorithms for flows with embedded subsonic regions is avoided by approximation of the reduced form of the Navier-Stokes equations in the subsonic regions of the boundary layers. Supersonic and subsonic portions of the flow field are simultaneously calculated by a consistently split linearized block implicit computational algorithm. The results of computations for a series of test cases associated with supersonic jet flow is presented and compared with other calculations for axisymmetric cases. Demonstration calculations indicate that the computational technique has great promise as a tool for calculating a wide range of supersonic flow problems including jet flow. Finally, a User's Manual is presented for the computer code used to perform the calculations.</p> | | | |
| 17. Key Words (Suggested by Author(s))

Analysis
Nozzles
Supersonic
Navier-Stokes | | 18. Distribution Statement

Unclassified - unlimited
STAR Category 02 | |
| 19. Security Classif. (of this report)

Unclassified | 20. Security Classif. (of this page)

Unclassified | 21. No. of pages

192 | 22. Price*

A09 |

*For sale by the National Technical Information Service, Springfield, Virginia 22161